GNSS-PPP NAVIGATION IN OBSTRUCTED ENVIRONMENTS USING A CHIP-SCALE ATOMIC CLOCK AND CLOCK COASTING

SIHAN YANG

A THESIS SUBMITTED TO
THE FACULTY OF GRADUATE STUDIES
IN PARTIAL FULFILMENT OF THE REQUIREMENTS
FOR THE DEGREE OF
MASTERS OF SCIENCE

GRADUATE PROGRAM IN EARTH AND SPACE ENGINEERING
YORK UNIVERSITY
TORONTO, ONTARIO

SEPTEMBER 2020

Abstract

The Precise Point Positioning (PPP) measurement processing technique for Global Navigation Satellite Systems (GNSS) is applied widely for scientific applications that require sub-metre level accuracy with few obstructions. PPP is expanding into mass-market applications at the consumer level. However, the technique suffers from inherent disadvantages of GNSS-based technologies. Obstructed environments such as urban canyons downgrade the solution. The study presents a solution that requires one less satellites in such scenarios and improves the navigation solution given poor geometry by implementing a clock coasting method to PPP and using a GNSS receiver aided by an external chip-scale atomic clock (CSAC). Data were collected in both static and kinematic scenarios. Through simulation of signal obstructions, the CSAC-aided receiver with clock-coasting produced solutions at sub-metre level of accuracy, even if only 3 satellites were available. The study leads to a more robust GNSS navigation solution that performs better with fewer satellites and a poor geometry.

Acknowledgements

I would like to thank my supervisor Prof. Bisnath for his teaching and assistance during my MSc degree, my colleagues in the GNSS lab for their invaluable roles as friends and co-workers, and I would also like to thank my parents for their constant support of my goals. Finally I would also like to thank my wife for her help with everything in life.

Contents

List of Tables

List of Figures

List of Acronyms

ADEV Allan Deviation. 37

AR Ambiguity Resolution. 9

AVAR Allan Variance. 37

CPT Coherent Population Trapping. 41

ECEF Earth-Centred, Earth-Fixed. 6

GEO Geostationary Orbit. 4

GLONASS Global'nava Navigastionnaya Sputnikovaya Sistema. 2, 3

GNSS Global Navigation Satellite System. i

GPS Global Positioning System. 2

IGS International GNSS Service. 11, 16

IGSO Inclined Geosynchronous Orbit. 4

IOC Initial Operational Capacity. 2

IONEX IONosphere map EXchange format. 16

IRNSS Indian Regional Navigation Satellite System. 4

LOS Line-of-Sight. 18

MEO Medium Earth Orbit. 4

MGEX Multi-GNSS Experiment. 16

NavIC Navigation with Indian Constellation. 4

NLOS Non-Line-of-Sight. 19

PLL Phase-Locked Loop. 75

PNT Position, Navigation and Timing. i

PPP Precise Point Positioning. i

PRN Pseudorandom Noise. 2, 5, 6

QZSS Quasi-Zenith Satellite System. 4

RCM Receiver Clock Modelling. 33

RTK Real Time Kinematic. i

SBAS Satellite-Based Augmentation Systems. 5

SLS Sequential Least Square. 34

SPP Single Point Positioning. 34

SV Space Vehicles. 2

TOW Time-of-Week. 67

WAAS Wide Area Augmentation System. 5

Chapter 1

Introduction to GNSS and Research Overview

Global Navigation Satellite System (GNSS) refers to a constellation system of satellites providing signals which provides a Position, Navigation and Timing (PNT) signals for civilian or military use. The solution requires processing of various observations through data filtering, error mitigation and parameter estimation. The position solution has typically an accuracy of a few metres. The solution is optimised using either differential techniques, requiring extra infrastructures such as Real Time Kinematic (RTK), or point positioning such as Precise Point Positioning (PPP).

In the last few years the importance of GNSS has been emphasised by the emergence of such new applications of drone tracking, autonomous driving, precise agriculture etc. Researchers and engineers utilised a range of GNSS software and hardware to adjust the technology to better serve their industries (Bisnath and Gao, 2009).

1.1 Overview of GNSS

Since the introduction of the first GNSS constellation in the 1980s, many countries and organisations have invested in their own satellite navigation systems. Currently there are four global constellations and two major regional constellations available for civilian use. The section will provide an overview of their status as well as technological aspects.

1.1.1 Navigation Satellite Systems in the World

The U.S. launched the first prototype Global Positioning System (GPS) satellite in 1978, succeeding its predecessor the U.S. Transit System. GPS reached Initial Operational Capacity (IOC) in 1993. Each of the satellites transmit signals in L-band on L1 (1575.52 MHz), L2 (1227.60 MHz) and newer GPS satellites on L5 (1176.45 MHz) (Langley, Teunissen, and Montenbruck, 2017). The frequencies are modulated various ranging codes. While some of these codes are commonly used in civilian applications, such as L1C/A, L2C or L5, there are also encrypted military code not available for commercial use. All GNSS signals have the characteristic modulation of the carrier with Pseudorandom Noise (PRN) code. A PRN code is continuously repeated at intervals and serves as a a timing signal and an identifier of the satellite, so that the receiver is able to recognise and distinguish the individual satellite, or Space Vehicles (SV). The signal is also modulated with a low-rate broadcast navigation message that specifies information about the SV's orbit, as well as the timing offset for the SV's clock with respect to GPS Time scale.

The USSR developed its own system, Global'nava Navigastionnaya Sputnikovaya

Sistema (GLONASS), or literally "Global Navigation Satellite System" in English in 1982 and the system operated under similar principles to GPS. The capacity of the system declined after the collapse of the Soviet Union. However, Russia took over the maintenance and upgrades as the second generation of GLONASS-M launched in 2003 and the third generation of GLONASS-K launched in 2011.

The Galileo system is developed as a joint initiative of the European Commission (EC) and the European Space Agency (ESA). The first Galileo test satellite was launched in 2005, but the first two In-orbit Validation (IOV) satellites were launched in 2011. The system is expected to reach full operational capability by 2020 and a newer generation of Galileo satellites will be operational in 2025.

The BeiDou Satellite System of China, commonly abbreviated as 'BeiDou' or 'BDS', named after Big Dipper, was initially a small regional navigation system that became operational in early 2000s. The system is developed collectively by a number of research and engineering groups in China, most notably lead by the China Academy of Space Technology (CAST), primarily funded by the State Council of China. After failure of negotiation to take part in the European Galileo system, the BDS project initiated its second phase of regional support (BDS-2) over East Asia in 2004 and completed the phase in 2012. The third phase BDS-3, which is expanded to a global constellation became fully operational in June 2020.

Table 1.1 provides a summary of the four GNSS systems to date. The systems are traditionally divided into space, control and user segments. The space segment consists of the constellation of SVs in orbits. The control segments consists of maintenance operation of the system by monitoring and uploading necessary navigation data to the SVs from ground stations around the globe. The user segment is defined by the receiver devices using signals to produce a PNT solution.

Table 1.1: A summary of the 4 operational GNSS in 2020

Constellation	Orbit	Full Operational Capacity	Frequencies Transmitted
GPS	MEO	1995	L1 1575.42 Mhz
			L2 1227.60 Mhz
			L5 1176.45 Mhz
GLONASS	MEO	1995/2010(Restored)	L1 1602.00 Mhz
			L2 1246.00 Mhz
			L5 1292.025 Mhz
Galileo	MEO	2020	E1 1575.42 Mhz
			E5a 1176.45 Mhz
			E5b 1207.14 Mhz
			E6 1278.75 Mhz
BeiDou	MEO,IGSO,GEO	2020	B1 1561.098 Mhz
			B2 1207.14 Mhz
			B3 1268.52 Mhz

Apart from the four current global constellations, there exist a few notable regional systems. The Quasi-Zenith Satellite System (QZSS) developed by Japan launched its first satellite in 2010. The system became operational in 2018 covering Japan, parts of East Asia and Australia. India developed the Indian Regional Navigation Satellite System (IRNSS), which was renamed Navigation with Indian Constellation (NavIC) in 2016. The system provides both public signals for commercial use and restricted service to encrypted devices.

GNSS can be augmented by Satellite-Based Augmentation Systems (SBAS), which utilize geostationary communication satellites to provide differential corrections and integrity checks to users as a service. SBAS in North America is primarily provided by the Wide Area Augmentation System (WAAS).

1.1.2 Estimation of Positional Variables

GNSS signals travelling from constellations are in the form of an electro-magnetic wave in the L-band, ranging from 1-2 GHz at the speed of light. The difference of the time of transmission, in the time frame of the satellite, and the time of receiving, in the time frame of the receiver is recorded as τ_r^s. The observation of signals transmitted from the satellites allows three basic types of observations. Each observation type is associated with an observation equation, where the three-dimensional positions of the user are variables. For each type of observation, a set of observation equations are used to solve the variables. Since in most cases there are more equations than the number of unknown variables, estimation techniques such as least-square estimation or Kalman Filters are used. In positioning applications, the most commonly used observables are pseudoranges and carrier-phase observations.

Pseudorange Observables

The primary measurement is code modulation, or pseudorange measurement. Once a GNSS satellite is acquired, the receiver can regenerate the characteristic Pseudorandom

Noise (PRN) sequence locally. The locally generated sequence is continuously compared to received signals for an eventual match. At this point, we say a satellite is tracked by the GNSS receiver. A time difference τ_r^s representing the time taken for a signal to travel from satellite to receiver can now be computed.

The time difference τ_r^s is multiplied by the speed of light in vacuum c to compute the geometric range between the receiver and the satellite, denoted $\rho_r^s(t)$. On the other hand, the geometric range can be written as the spatial distance usually in an Earth-Centred, Earth-Fixed (ECEF) coordinate frame:

$$\begin{aligned}\rho_r^s =& ||\boldsymbol{r}_r(t) - \boldsymbol{r}^s(t-\tau_r^s)|| = c\tau_r^s \\ =& |(x(t) - X(t-\tau_r^s)^2 + (y(t) - Y(t-\tau_r^s)^2 + (z(t) - Z(t-\tau_r^s)^2)|^{\frac{1}{2}}\end{aligned} \tag{1.1}$$

In equation 1.1, spatial coordinates of the SV are denoted in capital letters X, Y, Z, whereas x, y, z denote the receiver coordinates. Numbering each satellite as 1,2,3...n, we have a system of range observations to solve the three Cartesian variables.

$$\begin{aligned}\rho_1 =& [(X_1 - x)^2 + (Y_1 - y)^2 + (Z_1 - z)^2]^{\frac{1}{2}} \\ \rho_2 =& [(X_2 - x)^2 + (Y_2 - y)^2 + (Z_2 - z)^2]^{\frac{1}{2}} \\ \rho_3 =& [(X_3 - x)^2 + (Y_3 - y)^2 + (Z_3 - z)^2]^{\frac{1}{2}} \\ & \dots \\ \rho_n =& [(X_n - x)^2 + (Y_n - y)^2 + (Z_n - z)^2]^{\frac{1}{2}}\end{aligned} \tag{1.2}$$

The solution to system 1.2 can be acquired from linearisation and estimation for each epoch. An epoch is the timestamp at which the receiver records the observations.

In GNSS processing, we use a slightly more sophisticated term pseudorange $p_t^s(t)$ to imply the mis-synchronisation of the receiver clock and the satellite clock. The relation between the pseudorange and geometric range, and also a simplistic form of the pseudorange observation equation is given by

$$p_t^s(t) = \rho_r^s + c(\delta t_r - \delta t^s) \tag{1.3}$$

where two timing errors δt_r and δt^s refer to the clock error in the receiver and the satellite, respectively. The reason for emphasising on timing errors is that the relative scale of the errors versus the speed of light, and the fact that the receiver clock and the satellite clock are mis-synchronised due to error sources, clock performance or relativity. In short, a millisecond of timing error leads to a ranging error of ~300 km.

The two clock errors are treated differently. The satellite clock error δt^s is updated regularly from ground stations while its offsets and drifts are thus determined and included in the navigation message. The receiver is able to deduce the error term from local computations. The satellites are also equipped with state-of-art space-grade atomic clocks that are more stable. Therefore, the term is commonly computed and compensated for during error estimation process.

However, the receiver clock errors δt_r, are much larger. As it will be explained in later chapters, most GNSS receivers' clock error leads to errors of at least several metres over a 10-second period. Depending on the way a receiver treats its timing errors, the value could be much higher. Therefore, the term is designed to be part of the unknowns as the fourth variable along with spatial variables x, y, z, condensed into a state vector $\boldsymbol{x}$

$$\boldsymbol{x} = \begin{bmatrix} x \\ y \\ z \\ \delta t_r \end{bmatrix} \tag{1.4}$$

Carrier Phase observables

Carrier phase measurement refers to the accumulated phase measured at the receiver. Instead of ranges, the receiver tries to continuously determine the phase of each measurement. Using this approach, the measurement of ranges is more precise. Carrier phase measurement requires continuous tracking of satellite signals. Many factors can cause cycle slips, namely the discontinuities in carrier phase measurement that lead to loss of current count of accumulated cycles. Harsh environments, multipath effects and ionospheric scintillation and more could all lead to cycle slips.

The observation equation for carrier phase measurement is parameterized in a similar way to the pseudorange equation (Teunissen, 2017):

$$\Phi^s_{r,L1}(t) = \rho^s_r(t) + c(\delta t_r - \delta t^s) + \lambda_{L1} N^s_{r,L1} \tag{1.5}$$

In addition to variables listed in the pseudorange equation, here we have the wavelength-scaled integer ambiguity on L1 carrier-phase $\lambda_{L1} N^s_{r,L1}$.

A key problem in solving the carrier-phase equation lies in solving the integer ambiguity of $N^s_{r,L1}$, the exact number of cycles since the initial signal acquisition. The integer remains constant as long as tracking lock is maintained. It remains as a key difficulty in precise positioning as convergence period for the computation usually takes tens of minutes. Generally, a float solution is obtained first, ignoring the integer term in the equation. Then an estimated value of the integer ambiguity is derived from an Ambiguity Resolution (AR) algorithm. Finally, the solution is fixed by validation through assessment based on functional model, stochastic model or algorithm used.

Doppler Shift Observations

The relative motion between satellite and receiver causes a Doppler shift in received frequency. The measurement can be used to deduce velocity and is also used in the initial tracking loop for the receiver hardware for adjustment. Unlike carrier-phase measurement, Doppler measurement only requires samples of signals and do not require a signal lock.

1.1.3 Estimation of Errors

PPP processing requires the application of additional corrections to the pseudorange and carrier phase measurements since un-differenced observations do not cancel out errors. The additional corrections are highly important to achieve few cm-dm level accuracy.

Atmospheric Errors

To enable accurate positioning and timing applications, we need to counter the refraction of electromagnetic waves in troposphere and ionosphere (Hobiger and Jakowski, 2017).

1. Tropospheric delay – Both code and carrier phase measurements are affected by tropospheric delays in the same way. The delay is caused by the wet and dry (hydrostatic) components and modelled at the zenith angle and scaled by an appropriate mapping function to any elevation angle (Hobiger and Jakowski, 2017) . Therefore the tropospheric delay can be modelled first by a separation of variables (Choy, 2009):

$$d_{trop} = M_{dry} d_{dry} + M_{wet} d_{wet} \tag{1.6}$$

where the M_{dry}, M_{wet} denote the mapping functions and d_{dry}, d_{wet} denote the zenith path delays (ZPD). In the York PPP software, the hydrostatic ZPD (d_{dry}) is obtained using the model from (Davis et al., 1985) and wet ZPD (d_{wet}) is obtained using the Hopfield model.

2. Ionospheric delay – The high density of electrons influences the propagation of the electromagnetic waves. Ionosphere delay can be defined as being inversely proportional to the square of the transmission frequency. Thus, dual-frequency GNSS receivers can measure and remove the ionospheric effect by forming the dual-frequency, ionosphere-free linear combination. Single-frequency GNSS users rely on an external ionospheric product or model to mitigate the ionospheric delay as there is no second frequency to form the ionosphere-free linear combination.

In more basic positioning algorithms, only atmospheric errors are estimated using models without external input of atmospheric data. However in PPP, the following errors are also estimated to bring error down to centimetre level or less (Banville et al., 2014). Atmospheric errors are also estimated either by setting it as a variable, or by using more sophisticated atmospheric models such as IONEX products (Schaer and Gurtner, 1998).

Antenna phase centre offset and variation

1. Receiver antenna – The electrical phase centre is not aligned with the physical centre of mass of the antenna and causes an error. The variation of the phase centre depends on the changing direction of incoming GNSS satellite signals, causing positioning error up to 10 cm in the vertical component (Mader, 1999).

2. Satellite antenna – There is a separation between the GNSS satellite centre of mass and the electronic phase centre of its antenna. Models used by International GNSS Service (IGS) community for satellite orbit modelling refer to the satellite centre of mass (Kouba, 2009).

Other Error Sources

In the PPP algorithm, to improve the positioning accuracy to cm-dm level, a few other errors are modelled in the engine (Kouba and Héroux, 2001).

1. Phase wind-up: The relative orientation of the transmission and the receiver antennas is important because signals emitted by GNSS satellites are circular polarised. It affects carrier phase measurements only with an error around 10 cm.

2. Relativistic effects: As the precision of measurement reaches nanosecond, special relativistic effects must be considered. They include: the Sagnac effect, periodic clock error and fixed frequency offset effect. These errors can account to 10 m, but can be modelled accurately using navigation messages.

3. Solid earth tides: The earth is not 'rigid' and is pliable enough to respond to the same gravitational forces that generate the ocean tides. This contributes errors around 20-cm level.

4. Ocean loading: Ocean loading is the deformation of the sea floor and adjacent land responding to the redistribution of seawater which takes place during the ocean tide, causing accuracy loss of a few centimetres (Kouba and Héroux, 2001).

5. Polar tides: Polar tides are caused by the motion of the Earth's spin axis w.r.t its crust. The accyracy loss usually don't exceed centimetre-level.

6. Differential Code Bias (DCB): difference between code observations such as P1-C1 bias (Montenbruck, Hauschild, and Steigenberger, 2014). The effect of a code bias could reach the metre-level.

7. Receiver noise: The receiver noise is modelled as white noise. For high-end geodetic receivers, the effects are usually negligible to less than millimetre level.

8. Multipath: Multipath is the error caused by reflection of signals by nearby objects such as buildings, trees, cars etc. More details about multipath in the presented

experiments will be given in later chapters (Ward, Betz, and Hegarty, 2017 ; Musso et al., 2005).

Dilution of Precision

A way to evaluate geometric effect on the navigation solution is by calculating DOPs. The proof for DOP computation with 4 satellites is given here in detail as it relates to the clock coasting algorithm used in this research. In the most common least square estimation process, the linearized navigation equations are given by:

$$A\boldsymbol{x} = \boldsymbol{\rho} \tag{1.7}$$

where $\boldsymbol{x}$ is the four dimensional position and time correction vector,$\boldsymbol{\rho}$ is the pseudorange residual vector and A is the four dimensional design matrix:

$$\boldsymbol{x} = \begin{bmatrix} x \\ y \\ z \\ \delta t \end{bmatrix} \qquad \boldsymbol{\rho} = \begin{bmatrix} \rho_1 \\ \rho_2 \\ \rho_3 \\ \rho_4 \end{bmatrix} \qquad A = \begin{bmatrix} \frac{\partial \rho_1}{\partial x} & \frac{\partial \rho_1}{\partial y} & \frac{\partial \rho_1}{\partial z} & 1 \\ \frac{\partial \rho_2}{\partial x} & \frac{\partial \rho_2}{\partial y} & \frac{\partial \rho_2}{\partial z} & 1 \\ \frac{\partial \rho_3}{\partial x} & \frac{\partial \rho_3}{\partial y} & \frac{\partial \rho_3}{\partial z} & 1 \\ \frac{\partial \rho_4}{\partial x} & \frac{\partial \rho_4}{\partial y} & \frac{\partial \rho_4}{\partial z} & 1 \end{bmatrix} = \begin{bmatrix} \alpha_{1x} & \alpha_{1y} & \alpha_{1z} & 1 \\ \alpha_{2x} & \alpha_{2y} & \alpha_{2z} & 1 \\ \alpha_{3x} & \alpha_{3y} & \alpha_{3z} & 1 \\ \alpha_{4x} & \alpha_{4y} & \alpha_{4z} & 1 \end{bmatrix}$$

Equation 1.7 can be solved directly assuming the design matrix is invertible:

$$\boldsymbol{x} = A^{-1}\boldsymbol{\rho} \tag{1.8}$$

Let the errors in the pseudorange be ϵ, the estimation of the solution vector $\hat{\boldsymbol{x}}$, then equation 1.8 can be re-written as:

$$\hat{\boldsymbol{x}} = A^{-1}(\boldsymbol{\rho} + \boldsymbol{\epsilon}) \tag{1.9}$$

The covariance matrix of user position and clock bias error is denoted by $C_{\boldsymbol{x}}$, and can be written as

$$\begin{aligned} C_{\hat{\boldsymbol{x}}} &= E\langle \hat{\boldsymbol{x}}\hat{\boldsymbol{x}}^T \rangle - E\langle \boldsymbol{x}\boldsymbol{x}^T \rangle \\ &= E\langle A^{-1}(\boldsymbol{\rho} + \boldsymbol{\epsilon})(\boldsymbol{\rho} + \boldsymbol{\epsilon})^T {A^{-1}}^T \rangle - E\langle A^{-1}\boldsymbol{\rho}\boldsymbol{\rho}^T {A^{-1}}^T \rangle \\ &= \hat{\boldsymbol{A}}^{-1}(E\langle \boldsymbol{\rho}\boldsymbol{\rho}^T \rangle + 2E\langle \boldsymbol{\rho}\boldsymbol{\epsilon}^{\boldsymbol{T}} \rangle + E\langle \boldsymbol{\epsilon}\boldsymbol{\epsilon}^T \rangle - E\langle \boldsymbol{\rho}\boldsymbol{\rho}^T \rangle) A^{-1} \\ &= \sigma_\rho^2 ({A^{-1}}^T A^{-1})^{-1} \end{aligned} \tag{1.10}$$

It has the form of

$$C_{\hat{\boldsymbol{x}}} = \sigma_\rho^2 \begin{bmatrix} V_{xx} & \dots & \dots & \dots \\ \dots & V_{yy} & \dots & \dots \\ \dots & \dots & V_{zz} & \dots \\ \dots & \dots & \dots & V_{tt} \end{bmatrix} = \sigma_\rho^2 V_4 \tag{1.11}$$

where V_{ii} are diagonal terms of the matrix V_4. The geometric dilution of precision ($GDOP_4$) is defined as

$$GDOP_4 \equiv \sqrt{Tr(V_4)} = \sqrt{V_{xx} + V_{yy} + V_{zz} + V_{tt}}/\sigma_\rho \tag{1.12}$$

which leads to the definition of position, horizontal, vertical and time dilution of precision ($PDOP_4$, $HDOP_4$, $VDOP_4$, and $TDOP_4$), let e,n,u be the 'east', 'north', 'up' axis in the local tangent plane system,

$$PDOP_4 \equiv \sqrt{V_{xx} + V_{yy} + V_{zz}} / \sigma_\rho \tag{1.13}$$

$$HDOP_4 \equiv \sqrt{V_{ee} + V_{nn}} / \sigma_\rho \tag{1.14}$$

$$VDOP_4 \equiv \sqrt{V_{uu}} / \sigma_\rho \tag{1.15}$$

$$TDOP_4 \equiv \sqrt{V_{tt}} / \sigma_\rho \tag{1.16}$$

This concludes the proof for DOPs equations in traditional four-satellite settings. The term is commonly used to specify the error propagation as a mathematical effect of navigation satellite geometry on positional measurement precision.

1.1.4 Overview of Precise Point Positioning

PPP is a processing technique that utilises multiple frequencies of observation data, both pseudoranges and carrier-phase measurements, as well as precise orbital and clock products provided by various institutions (Kouba and Héroux, 2001). Compared to differential techniques, PPP requires no differencing of observers, therefore it does not require construction of additional infrastructures. In many applications where infrastructure is scarce or expensive, such an advantage makes PPP a economical viable. PPP requires only a single receiver and precise data from product providers. PPP offers accuracy at the centimetre-level and such accuracy can now be achieved in some recent low-cost receivers (Aggrey et al., 2019).

York PPP Engine

The York GNSS PPP software is a modular and scalable processor used in the GNSS Laboratory, York University. The program is written in C++ with complimentary MATLAB codes for plotting and result analysis. In its post-processing mode, the software reads an observation file in Receiver Independent Exchange Format (RINEX) format, processes the file according to parameters set by user using a sequential least squares estimator and produces a navigation solution, residuals and other optional parameters. It is capable of processing L1/L2/L5 frequencies and GREC (GPS, GLONASS, Galileo, BeiDou) constellations. Precise product from International GNSS Service (IGS) or Multi-GNSS Experiment (MGEX) can be used. Additional optional corrections include differential code bias and IONEX (IONosphere map EXchange format) file.

Observation Equation in York PPP

Dual-frequency PPP is based on forming ionosphere-free linear combinations of the code and carrier-phase measurements (Wells et al., 1986). However, one could also utilise slant ionospheric delay as an alternative. Conventionally, the un-differenced observation equation can be expressed in the engine as (Aggrey, 2014):

$$P_{L_i}^{GPS} = \rho^i + c(\partial t^s - \partial t_r) + d_{trop} + d_{ion,L_i} + b_{P_{r_i}}^{L^i} + b_P^{L^i,S_j} + d_{multi(P_{L_i})} + \epsilon(P_{L_i}^{GPS}) \quad (1.17)$$

$$\Phi_{L_i}^{GPS} = \rho^i + c(\partial t^s - \partial t_r) + d_{trop} + d_{ion,L_i} + b_{\Phi_{r_i}}^{L^i} + b_\Phi^{L^i,S_j} + \lambda_{L_i}, N_{L_i} + d_{multi(\Phi_{L_i})} + \epsilon(P_{L_i}^{GPS}) \quad (1.18)$$

The terms are:

- $P_{L_i}^{GPS}$ - Pseudorange measurement on L1 or L5 (m)
- $\Phi_{L_i}^{GPS}$ - Carrier-phase measurement on L1 or L5 (m)
- ρ^i - Geometric range (m)
- c - Speed of light (m/s)
- ∂t^s - Satellite clock error (sec)
- ∂t_r - Receiver clock offset (sec)
- d_{trop} - Tropospheric delay (m)
- d_{ion,L_i} - Ionospheric delay on L1 or L5 (m)
- $b_{P_{r_i}}^{L^i}, b_{\Phi_{r_i}}^{L^i}$ - Receiver equipment bias for pseudorange and carrier-phase measurements, respectively (m)
- $b_P^{L^i,S_j}, b_\Phi^{L^i,S_j}$ - Satellite equipment bias for pseudorange and carrier-phase measurements, respectively (m)
- λ_{L_i} - Wavelength of L1 or L2 carrier waves (m)
- N_{L_i} - Unknown cycle ambiguity term on L1 or L2 carrier-phases (cycles)
- $d_{multi(P_{L_i})}, d_{multi(\Phi_{L_i})}$ - Pseudorange/Carrier-phase multipath on L1 or L2 (m)
- $\epsilon(P_{L_i}^{GPS}), \epsilon(\Phi_{L_i}^{GPS})$ - Pseudorange/Carrier-phase measurement noise (m)

By linearising observation equations one can derive estimates of unknown parameters through a least-square estimation process.

1.2 GNSS Application in Obstructed Environments

The wide-use of GNSS technology in consumer markets present new challenges in obstructed, especially urban environments. As a relatively prevalent and low-cost positioning technique, GNSS is gaining momentum today in novel applications. However, obstructed environments challenge GNSS use in multiple ways.

GNSS Disruptions in Obstructed Environments

The framework of GNSS is designed around open-sky usage. However, as GNSS is widely used as a robust PNT solution, it is strongly demanded in obstructed environment such as urban areas. A number of disruptions arise from obstructions that degrades positioning performance. Such challenges includes but are not limited to low visibility of satellites, reflection and attenuation of signals as well as interference (Ward, Betz, and Hegarty, 2017 ; Zhu et al., 2018).

In urban environments, where the GNSS application is usually assumed as kinematic, the surroundings of user are in constant change. Buildings and larger vehicles can effectively block Line-of-Sight (LOS) to satellites, resulting in a reduced number of visible satellites. In a deep urban canyon with buildings surrounding the user, only satellites at high elevations are visible, so geometry becomes poor. If the user travels along one side of the road, a common scenario for driving and walking, the geometry will also suffer from an uneven distribution of satellites overhead. Compared to vehicles, pedestrians are expected to suffer more from poor geometry along the cross direction on streets (Wang, Groves, and Ziebart, 2012). This is due to pedestrians walk closer to the sides of buildings in most streets.

Another important disruption is caused by the reflection of signals. The reflection of signals can either becomes multipath errors if the satellite is still visible, or becomes a Non-Line-of-Sight (NLOS) reception if the satellite is not visible as shown in Figure 1.1 and Figure 1.2. Multipath is the reception of multiple reflected or diffracted replicas of the desired signal, along with the direct path signal (Ward, Betz, and Hegarty, 2017). Multipath signals are always delayed as it always takes a longer path. Multipath errors have been extensively studied, and a number of measures to detect and reduce multipath effect have been presented from both antenna/receiver design to post-processing techniques and integration of more sensors (Zhu et al., 2018). A special type of error from reflection of signals comes from an NLOS observation. The error introduced from an NLOS observation can be varied from tens of metres to kilometres depending on the size and distance of the structure the signal reflected on. Studies have also been conducted to predict NLOS observations through mapping of surroundings either by cameras, or by using map data (Groves et al., 2013).

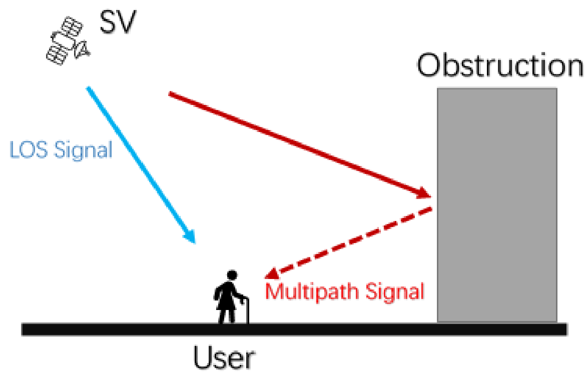

Figure 1.1: Illustration of a multipath signal from a LOS satellite

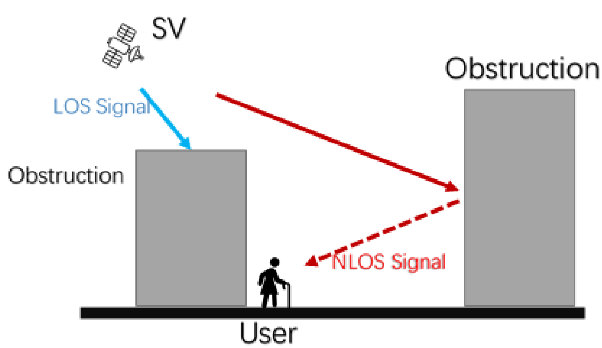

Figure 1.2: Illustration of a multipath signal from an NLOS satellite

Signals can also be attenuated in obstructed environments, most commonly due to vegetation. Cities often have lines of trees planted on sides of roads as barriers and also greenery. These trees and other vegetation cause small-scale multipaths, refraction of signals, and attenuation. Signal impacts from vegetation is more difficult to be characterised as the effect varies from the type of vegetation, moisture, and foliage (Ward, Betz, and Hegarty, 2017).

Obstructed environment can be categorised in an increasing order in terms of median signal attenuation in decibels. Such order can be open, rural, sub-urban, urban and in-building. Each of type can be further categorised as light, moderate or heavy depending on the density of relevant obstructions (Bullock and King, 2017). Using York University in Toronto as an example, the area to the north of York University, where most of the data collection is conducted in this research, consists of mostly wide-open driveways with short buildings relatively far from the roads, and can then be categorised as a sub-urban-light scenario. Driving inside the campus, where buildings have usually several floors, and with trees scattered around, the scenario can be categorised as an urban-moderate. The parking lot served as the starting and ending point of each data collection is surround by trees, while the scenario is open-sky within the lot, the entrance and exit of the parking lot is best categorised as rural-heavy due to a high density of tall vegetation. However, as data collection will show in later chapters, this way of categorisation requires further adjustment to PNT applications in most urban areas. Real-world urban areas are not uniform. An underpass in a rural area will cause more disruption in short periods than most urban canyons.

Requirement for PNT Solution in Emerging Applications

As GNSS is becoming used more extensively in emerging applications in recent years, a number of studies worldwide have been conducted to address the difficulties and challenges in navigating in obstructed environment, with specific focuses on urban canyons. Many of those emerging applications, such as autonomous vehicles, unmanned aerial vehicle (UAV) tracking, or navigation for the blind are safety-of-life applications. These applications bring a higher requirement in PNT performance in terms of accuracy, integrity, continuity, and availability (Zhu et al., 2018). These factors are impaired in urban environments from the disruptions mentioned earlier.

Accuracy is a statistical metric to determine how close the navigation solution is from a reference of the 'true' solution. While a number of metrics for accuracy exist, often it is measured as a percentile of cumulative distribution. One common way to measure the accuracy of position is to assume Gaussian distribution of pseudorange errors, and measure the error magnitude that 95% of errors fall within (Hegarty et al., 2017). The accuracy of GNSS solution in obstructed environments is challenged by reduced number of satellites, reflection of signals, and attenuation of signals as previously mentioned.

The definition of integrity follows closely to definition of accuracy. It is a measure of trust in the correctness of solution produced by the system, and capability of the system itself to provide timely warnings to the user, known as alerts (Hegarty et al., 2017). The concept of GNSS integrity is drawing more attention as GNSS solution began to be used in legal liability applications in traffic. As a GNSS solution suffers from the reduction of accuracy from the described reasons, the complex resultant effect on solution due to environment needs to be correctly categorised and integrated. The user's system should be able to recognise the type of obstructed environment and act accordingly. An example of such type could be a mountainous road where most satellite on one side of the user are not visible, leaving only the other side of satellites available. While the receiver may be able to compute a solution, the solution is likely to be biased towards the obstructed side due to geometry and limited satellite signal reception.

Another factor is the continuity of the GNSS solution in an obstructed environment. Continuity is defined as "...the probability that the specified system performance will be maintained for the duration of a phase of operation, presuming that the system was available at the beginning of that phase of operation" (Hegarty et al., 2017). Safety-of-life applications require the system to be so reliable that a solution within designed parameters can be generated in the environment it is designed for. In obstructed environment, the combined effects of the environment reduce the number of satellites processed by GNSS engine due to either loss of tracking on the receiver-end, or rejection on the processing-end. The former is caused by losing LOS due to obstruction, while the latter is more likely to be caused by NLOS observations, multipath, or attenuation of signals.

Availability of a navigation system is the percentage of time that the services of the system are usable (Hegarty et al., 2017). Availability is an indication of the ability of the system to provide a usable navigation service within a specified coverage area. Availability can be viewed as a combined effect of accuracy, integrity, and continuity. In the early deployment stage of GPS, the availability of GNSS was limited due to inability to track enough satellites in many geographical areas. Today, due to the expansion of GNSS, the availability of a solution is no longer restrained by the number of satellites. However in obstructed environments, the availability is again hampered from the disruptions mentioned above.

1.3 Problem Statement

In post-processing of GNSS data from urban areas, the accuracy of solution is impaired due to extra error sources. Poor geometry and accuracy results in more possibilities that challenges integrity. Continuity is impacted from the lower number of processed satellites as a result of less visible satellites due to LOS obstructions, less tracked satellites due to attenuation of signals, and more rejections in processing stage due to higher errors. All these factors lead to a weaker availability of GNSS solution in urban environments. Works has done on multiple fronts to tackle one or more of these disruptions to make GNSS technology more suitable with emerging applications in obstructed environment.

This study will provide a novel approach by introducing a new external timing sensor of a more precise clock to PPP technique that will enhance the availability of GNSS in obstructed environments. The PPP technique is inherently superior in obstructed environment, as the algorithm in the software is able to utilise precise data products to better filter out poorer observations, and therefore provides a better accuracy. The precise clock is able to assist on multiple fronts from satellite tracking speed on receiver side, to post-processing on user side. Although some mechanisms are not available for modification within the receiver's hardware design, the receiver is expected to perform better under a more stable external clock, to improve the accuracy of solution. The clock coasting technique, which is the main focus of this research, allows a three-satellite solution using SLS estimation, while only introducing errors at sub-metre level, and also improves the solution when the geometry is poor due to obstructions. Thus, not only the accuracy is improved in obstructed environments, but also integrity as poor geometry will show less impact on solution accuracy and continuity as a three-satellite solution is now available for a duration up to tens of minutes. The integration presents a more robust GNSS solution to mitigate disruptions in obstructed environments and, specifically, in urban canyons.

1.4 Thesis Objectives

The thesis aims to provide a more robust GNSS solution in urban environment using a combination of a more precise external clock and PPP augmentation with the clock coasting technique. Clock-specific knowledge was studied and analysed for the requirement and caveats in real-world applications. Then using a geodetic receiver, the receiver was interfaced with the clock and a few options of interfacing were explored. Using static tests, the performance of the clock bias was analysed and compared with traditional GNSS receiver clock, proving its superiority in terms of stability. Based on the findings, kinematic datasets were collected. Simulated urban canyons and other challenging scenarios were implemented in order to test the system's improvement in terms of accuracy, continuity, availability and resilience.

Chapter 2

Research Context and Novelty of the Work

Since the introduction of GPS, global research communities have been working on research spanning multiple fields to improve the technology and to extend its applications. This research focuses on improving GNSS navigation solution using an external clock and PPP augmentation in obstructed environments. This chapter provides a survey on the topic of integrating GNSS receiver with external clocks, the specific use of Chip-Scale Atomic Clocks and receiver clock modelling approach. Upon summarising the existing work in the area, the novelty of this research is presented.

2.1 Early Work on GNSS with a Precise Clock

In the 1980s the U.S. government allowed civil use of GPS. However, compared to having at least 30 GPS satellites in orbits today with addition of other GNSS constellations, there were only about a dozen active satellites in the 1980s, and the number rose to 20 by the 1990s. The GPS constellation at the time resulted in periods of substantial outages over a number of geographical areas a few times each day. Researchers anticipated three-satellite GPS coverage, sometimes along with poor geometry. Ideas were proposed to tackle the outages and improve navigation solution during outages. A key paper with which the research follows closely was the 1983 work by Mark A. Sturza, titled "GPS Navigation Using Three Satellites and a Precise Clock". In the paper, Sturza proposed to accomplish three-satellite GPS navigation by equipping the user with a precise clock (Sturza, 1983). The precise clock provides timing stability for the user to ignore the single variable of receiver clock error during a three-satellite periods, so that a navigation solution can still be produced. Later the method is referred to as "clock coasting" in texts (Knable and Kalafus, 1984). The paper discussed impacts from a three-satellite situation, presented a new formula for DOPs calculation in three-satellite scenario without estimating the receiver clock error, and finally showed experimental results on the geometry of three-satellite scenario.

In the three-satellite clock coasting method,the linearized navigation equations are given by

$$\boldsymbol{\rho} = B\boldsymbol{x} + \boldsymbol{b}(t) \tag{2.1}$$

where

$$\boldsymbol{x} = \begin{bmatrix} \delta_x \\ \delta_y \\ \delta_z \end{bmatrix} \quad \boldsymbol{\rho} = \begin{bmatrix} \rho_1 \\ \rho_2 \\ \rho_3 \end{bmatrix} \quad \boldsymbol{b}(t) = b(t) \begin{bmatrix} 1 \\ 1 \\ 1 \end{bmatrix} \quad B = \begin{bmatrix} \alpha_{1x} & \alpha_{1y} & \alpha_{1z} \\ \alpha_{2x} & \alpha_{2y} & \alpha_{2z} \\ \alpha_{3x} & \alpha_{3y} & \alpha_{3z} \end{bmatrix} \tag{2.2}$$

and scalar $b(t)$ is the clock bias at time t.

Following the previous proof, one can again derive the position correction vector as a function of pseudorange residual

$$\boldsymbol{x} = B^{-1}(\boldsymbol{\rho} - \boldsymbol{b}(t)) \tag{2.3}$$

and similarly, let the clock bias variance be σ_b^2,

$$C_{\hat{\boldsymbol{x}}} = B^{-1}(\sigma_\rho^2 I_3 + \sigma_b^2 I_3){B^{-1}}^T = \sigma_\rho^2[(B^T B)^{-1} + \frac{\sigma_b^2}{\sigma_\rho^2} B^{-1}{B^{-1}}^T] = \sigma_\rho^2 V_3 \tag{2.4}$$

Then we can derive the $PDOP_3$ using its definition:

$$\begin{aligned} PDOP_3 &\equiv \sqrt{Tr(V_3)} \\ &= \sqrt{Tr((B^T B)^{-1} + \frac{\sigma_b^2}{\sigma_\rho^2} B^{-1}{B^{-1}}^T)} \\ &= \sqrt{V_{xx} + V_{yy} + V_{zz}}/\sigma_\rho \end{aligned} \tag{2.5}$$

In the same manner as we can define $HDOP_3$ and $VDOP_3$ in their local coordinates.

In his work, Sturza (1983) showed that with a precise clock, the three-satellite navigation can not only be achieved, but also resulted in a better 'geometry' than four-satellites standard GPS positioning. His work proved clock coasting to be viable, and in fact using a precise clock as an extra sensor that replaces a satellite in certain situations will result in improved navigation solution. However, at that time, there was no atomic clock that portable to give the solution a very meaningful application beyond theoretical discussion.

Early experiments by Sturza (1983) showed during 25 minutes of signal outage, having three satellites and a precise clock are more valuable than having an additional satellite. Figure 2.1 shows having a good quartz crystal oscillator (QXO) clock or a Rb atomic clock will give a better solution than having one more satellite in the three-satellite scenario. It is worth noting that it has been decades since the experiment and the clock technology has been much upgraded. Newer atomic clocks, even the chip-scale ones are superior in their frequency stability in minutes or longer.

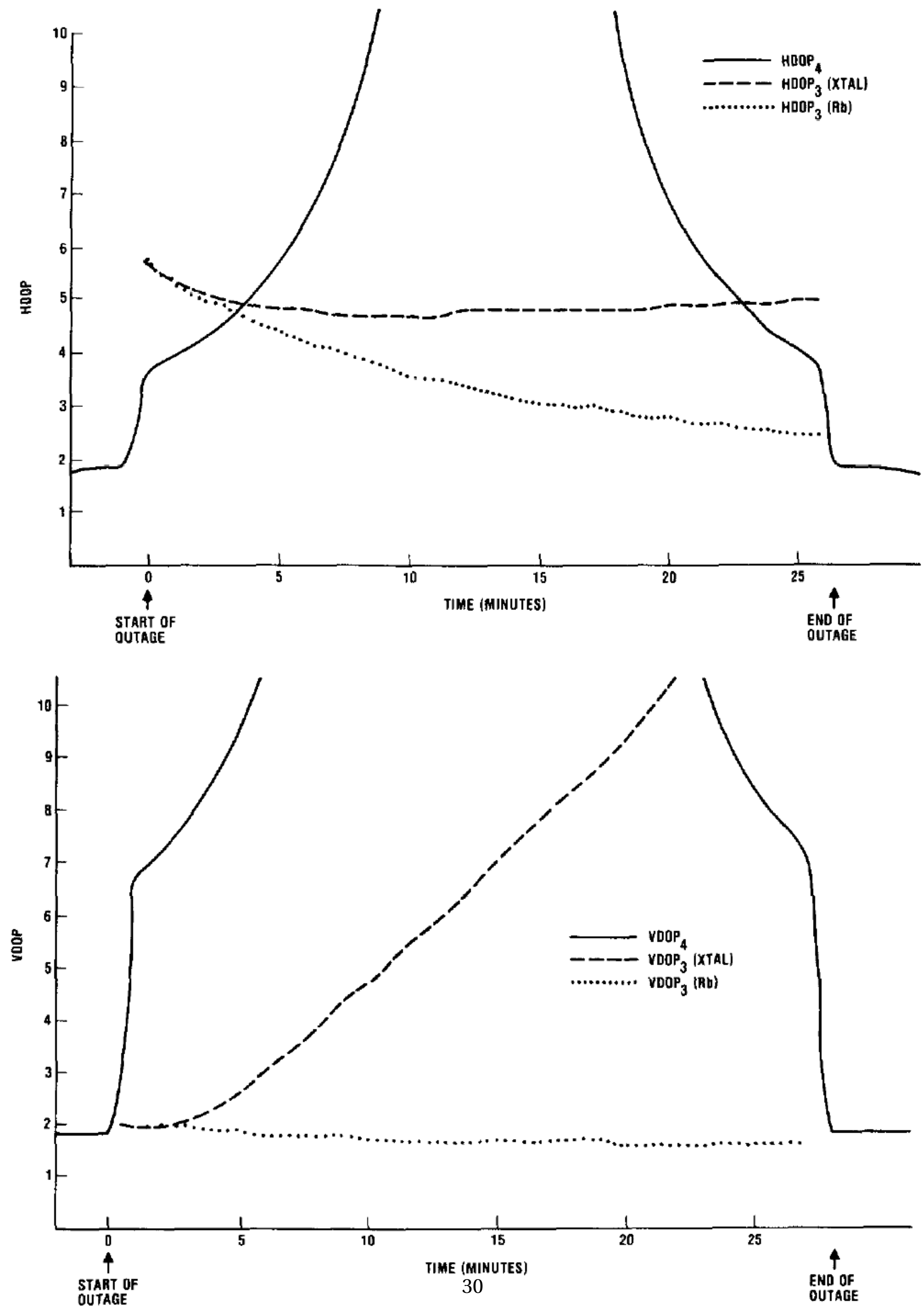

Figure 2.1: Effects on $HDOP$ (top) and $VDOP$ (bottom) of clock coasting during an outage (Sturza, 1983)

Today, a number of portable precise clock technologies are available. The most typical technology used in GNSS are the Quartz Crystal Oscillators (QXOs) (Langley, Teunissen, and Montenbruck, 2017). Oscillators are cut from crystals in different shape, size and orientation. All these factors within crystalline structure affect the properties of the oscillator. Using different techniques to mitigate environmental factors on a variety of crystal shapes lead to a few categories of quartz crystal oscillators. Temperature-Compensated Crystal Oscillators (TCXOs) are most widely used in GNSS receivers due to their low costs and small scale.

A few more precise external clock options are available today. Oven-Controlled Crystal Oscillators (OCXOs) provide a much more robust frequency stability than TCXOs. However, they are more expensive (> 1000 USD), and consumes much more power of hundreds of milli-watts. More recently Chip-Scale Atomic Clocks (CSACs) are developed using either Cs or Rb. CSACs has a generally more stable frequency curve than OCXOs and consumes much less power (120 mW) although it is more expensive at thousands of U.S. dollars.

2.2 Use of Chip-Scale Atomic Clocks in GNSS

The introduction of CSAC since early 2010s gave a new birth to the idea of clock coasting. Ramlall et al. (2011) was among the first groups to implement the idea of clock coasting using CSAC. Following closely to the idea of three-satellite GNSS navigation, their paper explored the clock-aided navigation, predicted clock bias using Kalman Filter and least squares estimation, and compared the results using simulation. Their result shows with an atomic clock, the standard deviation in positional errors are at 11.1 m - 13.8 m in a static obstructed scenario, where SVs above 50 degrees of elevation are blocked over a data collection of 2 hours and 50 minutes. Using a quartz clock, the positioning errors are over 100 m (Ramlall, Streeter, and Schnecker, 2011). Furthermore, their Kalman filter approach for clock bias showed less errors of 11.1 m versus 12.6 m from least squares. In the same dataset without obstruction, the navigation solution is more precise for the CSAC-aided receiver with errors all less than 10 m. Their work was based on simulation and provided theoretical proof for the effectiveness of CSAC-aided GNSS.

More practical work involving CSAC was carried out by a few other groups as the hardware became increasingly available in mid-2010s, most noticeably Fernandez et al (2016). In several published studies on the topic, the group provided a hands-on guide for interfacing CSAC with existing GNSS receivers, and conducted data collection in several settings using publicly available GNSS post-processing software (Calero and Fernandez, 2015; Fernandez, Calero, and Eulia Pares, 2016, 2017). The group produced a faster way to discipline the CSAC depending on temperature. Normally, the process will take three times the disciplinary constant, and for the case of CSAC disciplined to a GNSS receiver, this disciplining usually require a few hours. With manual adjustment according to environmental temperatures, the time is reduced to less than an hour. In term of navigation solution, the group showed a superior positioning performance for the CSAC-aided receiver in both static and kinematic settings, where in the more detailed static test, a receiver with CSAC achieved a standard deviation error of 1.25 m versus 2.11 m with on-board TCXO clock, using a geodetic receiver on short time periods.

Lin Ma et al. (2015) presented a deep-coupled integration of CSAC and GNSS research which gave robust experimental support to theories of achieving better DOPs by introducing the clock as an extra sensor. Their weighted linear optimal estimation method produced results with only three satellites available in a kinematic test over a course of 300s of outage. The average standard deviation in horizontal error in the 300 seconds before outage, with four visible satellite was 13.2 m, whereas the error in a 300-second outage was only increased to 16.1 m. Furthermore, their experiment showed using a CSAC, the errors in the vertical direction is significantly reduced, and with lesser satellites, the advantage of CSAC became more obvious. With 8 visible satellites during 100 seconds of experiment, the receiver with CSAC showed a standard deviation in vertical error of 7.7 m and 8.3 m with 4 satellites. The receiver without CSAC showed errors of 13.0 m and 28.4 m, respectively (Ma et al., 2015). The result showed significant improvement in vertical errors, and allowed three-satellite solutions.

2.3 Receiver Clock Modelling

Krawinkel et al. (2018) argued by using a more stable external clock, the bias behaviour of external clock can be modelled.The physically meaningful prediction of the clock behaviour is possible over intervals in which the integrated clock noise is smaller than that of the GNSS observations in use (Weinbach and Schön, 2011 ; Krawinkel, 2018). Such approach is referred to as Receiver Clock Modelling (RCM). Their work involved characterisation of frequency behaviour of several CSAC models and tuned Kalman Filter according to the individual characteristic of the clocks, hereby also achieved three-satellite solution.

In the RCM approach, the frequency characteristics of the clock model is carefully analysed using a highly advanced atomic clock to acquire raw data from the CSACs. The CSACs' phase data are converted to frequency data, gaps and outliers in measurement are addressed. Using the advanced atomic clock as reference, the raw data provides an Allan Deviation (ADEV) plot of each CSAC model against averaging time. Through Fourier Analysis, the respective h_i coefficient of their fractional frequency deviations are computed. Then a Kalman Filter approach for the clock error is implemented, using the computed h_i coefficients to tune each Q matrix. Similarly, an Sequential Least Square (SLS) approach can also implemented for the clock error modelling.

Kinematic results have shown the RCM approach improved the Single Point Positioning (SPP) performance in precision and accuracy, reliability, integrity, continuity and availability. Positioning precision and accuracy is improved especially in the vertical direction. By disabling tracked satellites, leaving only three satellites in view, the positioning performance of a three-satellite solution using RCM is also examined. The RCM approach was proven to provide a three-satellite solution when the traditional approach cannot. However, the result shows errors during the three-satellite periods jumped to several metres, instead of less than 2 metres in the experiments. In the following kinematic experiments, the RCM approach has shown significant improvement in vertical accuracy by reducing the errors to below 10 m.

2.4 Novelty of the PPP + Clock Coasting Approach

Various work has been done in the field of integrating GNSS and an external clock. However, this research presents a new perspective, and addressed the challenges in urban GNSS navigation in a more realistic approach, meaning easier to implement and practice than RCM. A prototype using low-cost receivers and antenna had shown the idea is viable and produced kinematic results with horizontal accuracy down to a 0.37 m in an open-sky environment with some simulated obstructions (Yang and Bisnath, 2020)

First of all, none of the works had utilised precise approaches such as PPP. With the additional corrections in PPP the solution by itself without additional clock already reaches sub-metre level. Connecting an external clock alone may not further improve the solution. RCM showed promising prospects in improving vertical errors. However, with PPP the vertical errors can already be reduced to the centimetre-level, as will be shown in this research. In this case, the advantage of an external clock in terms of accuracy will become less useful. Instead, this work will utilise the already existing PPP, and focus on improving its performance in realistic, obstructed scenarios with the clock.

Secondly, the work selects clock coasting instead of receiver clock modelling. The reason is that receiver clock modelling assumes receiver clock noise to be smaller than that of GNSS observations. This relation is true for pseudorange measurements, but not true for carrier-phase measurements extensively used in PPP processing. Furthermore, the RCM approach requires intensive analysis on clock's behaviour using expensive hardware. This study aims to provide a cost-effective, mass-market-friendly prototype to integrate the external clock. Therefore, RCM does not meet the criteria.

Lastly, the work involves more rigorous data collection under realistic scenarios, and it provides more scenarios that will challenge the system in obstructed environments. The mentioned works have shown the possibility of three-satellite solutions. This work relates to the earlier ideas of improving solutions also in poor geometry, and test the system under various situations. In the age of four GNSS operational constellations, the major challenge in urban GNSS is no longer the number of visible satellites, but rather to improve the overall availability of solution in the most challenging geometries and harsher rejections. This study will focus most on urban canyons.

Chapter 3

Chip-Scale Atomic Clocks as a Timing Sensor in Clock Coasting Algorithm

3.1 Overview of Clock Stability

Early works in the field of categorising frequency and stability of clocks was done in the 1960s and 1970s (Barnes et al., 1971 ; Barnes and Allan, 1966). An oscillator's performance is measured by the deviation of its actual frequency from the nominal value. The stability of the oscillator is used to describe the closeness of its actual frequency to the nominal value over a certain period of time, often denoted τ. A typical measure for the stability is called the Allan Deviation (ADEV) or its variance version Allan Variance (AVAR). A rigorous definition will be given later.

Fundamentally, an oscillator gives out a periodic voltage signal, at time t:

$$V(t) = (V_0 + \epsilon(t)) \sin\big(2\pi\nu_0 t + \phi(t)\big) \tag{3.1}$$

where V_0 is the nominal voltage amplitude and ν_0 the nominal frequency. The errors or fluctuations of amplitude and frequency described by the term $\epsilon(t)$ and the term $\phi(t)$ as functions of time. While observing the oscillator signal, frequency is key and not the amplitude. Therefore, for the subsequent discussion the amplitude term is ignored. Taking the time derivative of the sine term produces angular frequency $\omega(t)$

$$\omega(t) = \frac{\mathrm{d}}{\mathrm{d}t}[2\pi\nu_0 + \phi(t)] \tag{3.2}$$

and its instantaneous frequency can be given as:

$$\nu(t) = \frac{\omega(t)}{2\pi} = \nu_0 + \frac{1}{2\pi}\frac{\mathrm{d}\phi}{\mathrm{d}t} \tag{3.3}$$

As a way to compare different oscillators regardless of their nominal frequencies, we define an important term, fractional frequency, $y(t)$ as

$$y(t) = \frac{\nu(t) - \nu_0}{\nu_0} = \frac{1}{2\pi\nu_0}\frac{\mathrm{d}\phi}{\mathrm{d}t} \tag{3.4}$$

The fractional frequency is a unitless quantity serving as the basis for frequency stability comparisons. The phase (time) deviation $x(t)$ is obtained by integrating the fractional frequency deviation over a period of time, i.e.,

$$x(t) = \int_0^t y(t')dt' = \frac{\phi(t)}{2\pi\nu_0} \tag{3.5}$$

Generally the time error of a clock can be expressed as (Beard and Senior, 2017)

$$x(t) = x_0 + y_0 t + \frac{1}{2}at^2 + \int_0^\tau E(t')dt' + \epsilon(t) \tag{3.6}$$

where x_0 represents the time offset or synchronisation error at $t = 0$; y_0 represents a constant frequency offset; a represents a constant frequency drift, also known as the clock ageing rate; $E(t)$ is the fractional frequency offset due to environmental effects, such as temperature, vibration, etc. Finally, $\epsilon(t)$ represents the random deviations of the clock's error. To characterise the behaviour of $\epsilon(t)$ over an averaging time τ, the time average of time change, at time stamp $i+1$, and the time-averaged fractional frequency $\bar{y}$ is

$$\bar{y}_i = \frac{x_{i+1} - x_i}{\tau} = \frac{1}{\tau}\int_{t_i}^{t_i+\tau} y(t)dt \tag{3.7}$$

The 2-sample variance of the time-averaged fractional frequency is defined as the Allan Variance for an averaging time τ as (Beard and Senior, 2017):

$$\sigma_y^2(\tau) = \langle\frac{(\bar{y}_{k+1} - \bar{y}_k)^2}{2}\rangle \tag{3.8}$$

Here, it is assumed the measurements are adjacent, $\{t_1, t_2, ..., t_i, t_{i+1} ... t_n\}$ a partition of the total time period. If dead time (timestamps without measurements) exists in the measurement, we can no longer take Allan variance as the result will be biased. Allan variance is also not sensitive to the overall frequency offset y_0. Using the developed ADEV as a tool to characterise the random deviations over time, equation 3.6 can now be re-written using $\sigma_y^2(\tau)$ as:

$$x(t) = x_0 + y_0 t + \frac{1}{2}at^2 + \int_0^{\tau} E(t')dt' + \tau\sigma_y(\tau) \tag{3.9}$$

3.2 Chip-scale Atomic Clocks

Atomic clocks provide the most advanced and stable oscillator frequency up to date. Traditionally atomic clocks are expensive, massive and power-consuming. In GNSS processing, they were most widely used in satellites. However, recent advances allow atomic clocks to reduce in size, cost and power, while keeping their superior stability.

3.2.1 Principle of Operation

Atomic clocks are oscillators that uses a hyperfine transition frequency of atoms' EM spectrum. Hyperfine structures (Figure 3.1) are the discrete shifts and splittings in the discrete energy levels of atoms, molecules or ions resulted from nuclear dipole/quadruple moments (Griffiths and Schroeter, 2018). The hyperfine structure transition frequency of some isotopes of particular elements, such as Cs-133 or Rb-87 can be used as a basis of atomic clocks due to their structure. In fact the SI second is defined as 9,192,631,770 cycles of such transition of Cs-133 isotope.

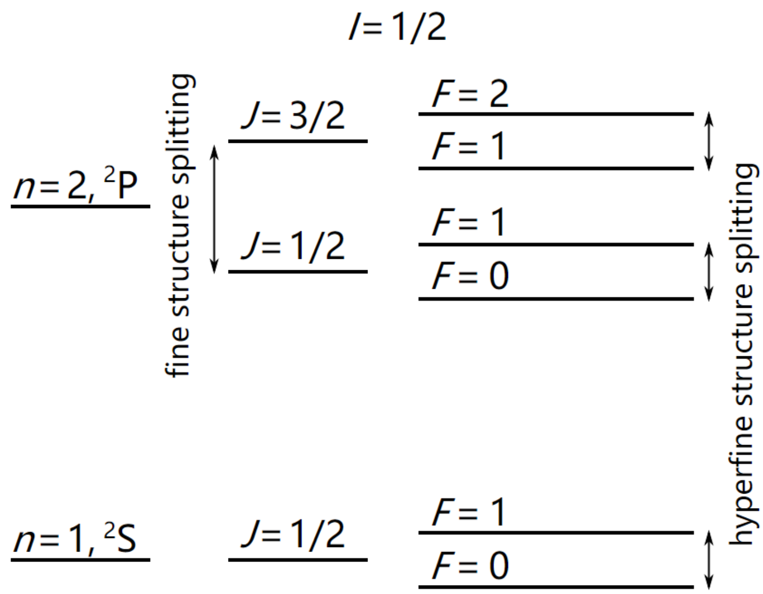

Figure 3.1: Example of the hyperfine structure in a Hydrogen atom. Source: *https://commons.wikimedia.org*

Recent innovations in multiple disciplines has contributed to the miniaturisation of atomic clocks (Microsemi, 2016). The CSAC used in our experiment employs Coherent Population Trapping (CPT) as an alternative to traditional interrogation techniques (Lutwak et al., 2002). An illustration of CSAC operation is shown in Figure 3.2. The built-in TCXO provides the principle Radio-Frequency (RF) output buffered by the CMOS. The frequency of TCXO output is constantly corrected using the ground state hyperfine frequency of the Cs atom in the physics package through the loop filter. The microwave synthesizer generates a frequency of 4596.cX Mhz, tuned by a micro processor to resolution in 1×10^{-12}. The tuning process can be controlled by the user for manual or automatic calibration to another reference. With the recent innovations, the CSACs achieves a small volume of 16 cm^3 and a low power consumption of <140 mW. The CSAC can be mounted to small hand-held devices with battery power, and in the field of GNSS may serve as a great addition to existing low-cost receivers.

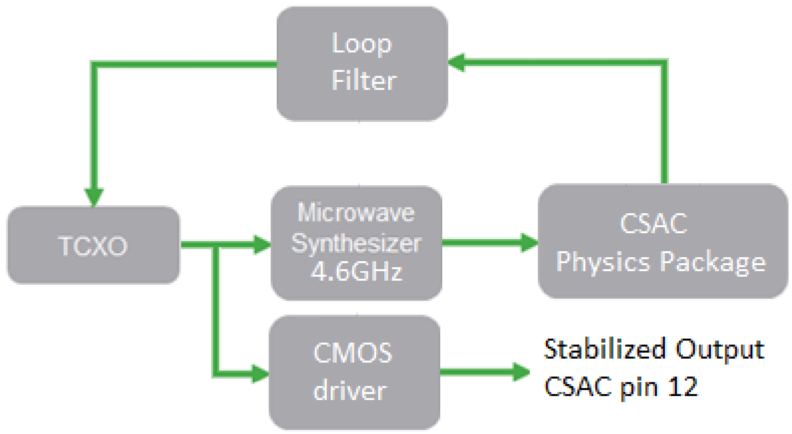

Figure 3.2: Diagram of CSAC operational principle (Microsemi, 2017a)

The 'atomic' component is enclosed in the CSAC physics package which contains a tiny silicon resonance cell filled with gaseous Cs, a vertical cavity surface-emitting laser (VCSEL) is used to excite the atoms, and a photo detector as the sensor for the photons passed through the tube (Lutwak et al., 2004). The laser illuminates Cs atoms in the resonance cell with polarised EM waves. The Cs atoms are excited to a non-scattering coherent superposition state. It is essential for the centre stack of the VCSEL, photodiode and the resonance cell to stabilised in at a temperature between 85 to 95 Celsius. Therefore, the centre stack is thermally isolated from the ambient environment through a vacuum packaging mechanical suspension system. The photo detector senses the laser passed through the resonance cell and obtains a resonance line. A precise resonance line is crucial to the stability of the clock compared to a wide or blurry line. To achieve a precise and narrow line, the polarisation of laser must be stable. Figure 3.3 provides and example illustration if the physics package (Lutwak et al., 2004).

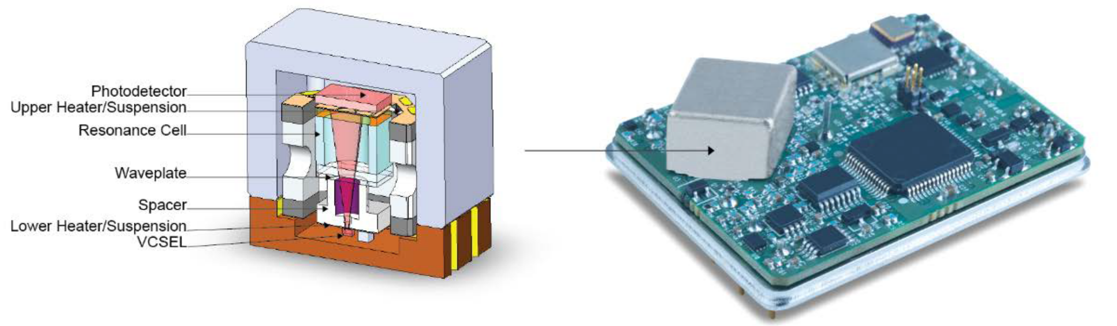

Figure 3.3: Illustration of CSAC physics package and its appearance in the chip (Lutwak et al., 2004)

The microwave synthesizer of the 4.6 GHz voltage-controlled oscillator is phase-locked to a 10 MHz TCXO. The microwave output is applied to the laser and fine-tunes the laser according to the response measured from atoms. The fine-tuning is controlled by a digital signal processor, with the goal of achieving a precise resonance line. During the start-up sequence, the processor controls the CSAC to complete acquisition of the resonance line, stabilise the temperature of the physics package and fine-tune the resonance behaviour using a microwave synthesizer. Once the whole process is finished, the clock is "locked". The frequency of the TCXO is constantly compared to and corrected to the Cs hyperfine frequency. The comparison drastically improves the TCXO's stability, as well as the environmental sensitivity. Finally, the TCXO outputs a 10 MHz RF signal.

3.2.2 CSAC Environmental and ageing Factors

As stated in the previous chapter, the requirement for a precise, narrow lock is crucial to obtain stable clock behaviour. The complexity and physical nature of the physics package also means it is more prone to environmental factors than most electronics, specifically, temperature change and vibrations. In addition, the ageing of various part of the CSAC, such as thermal isolation and laser will decrease the clock's performance in the long term.

Environmental Temperature

The temperature inside the Cs resonance tube is isolated using the combination of a vacuum chamber, suspension system and heater. The thermal isolation system limits the CSAC's operational temperature range. For the model used, the limit is from -10 °C to 70 °C. Prior to a technical upgrade, the CSAC model was only able to operate from -10 °C to 35 °C. Operating outside the specified parameters may lead to loss of lock. If a CSAC loses lock during its operation, frequency errors will be introduced, leading to time errors as shown in Figure 3.4. The plots give a quantitative prediction of receiver clock errors should a loss-of-lock occurs. During the roughly 70 seconds of the time without lock, the clock produces a maximum phase error of $t \times 10^{-8}$ seconds, or an equivalent ranging error of 15 metres in the worst-case scenario (Microsemi, 2018).

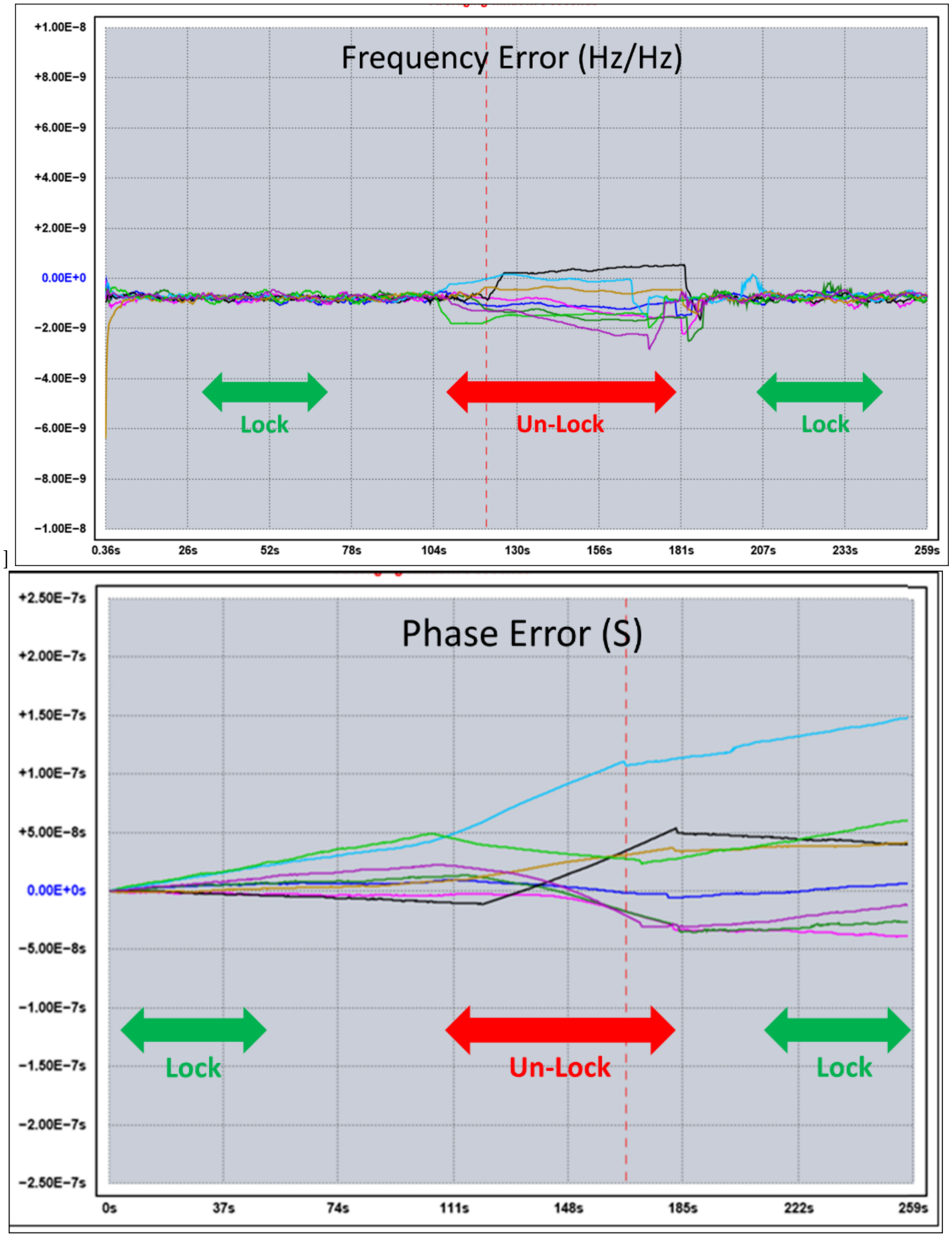

Figure 3.4: Example of frequency (top) and phase (bottom) errors after a loss of lock (Microsemi, 2018)

In a manufacturer experiment, two identical CSACs were tested against an OCXO clock, where the oscillators are kept at a high temperature of 50 °C for more than an hour then cooled to -10 °C in 12 minutes, then rapidly heated back to the initial temperature after 2 hours. 3.5 shows the rapid increase in frequency error during cooling down. But with temperature stabilised, CSACs stabilised as well, albeit with performance worse than that in high temperature. Similar behaviour can be observed from the OCXO clock; however, it is more susceptible to temperature changes, as its frequency error reaches four times or more than the CSAC. It is also noticeable that the CSAC shows individual characteristics as a result of individual VCSEL characteristics. A plot of frequency response after these rapid temperature change provided by Microsemi is shown in Figure 3.5. Table 3.1 provides the performance statistics.

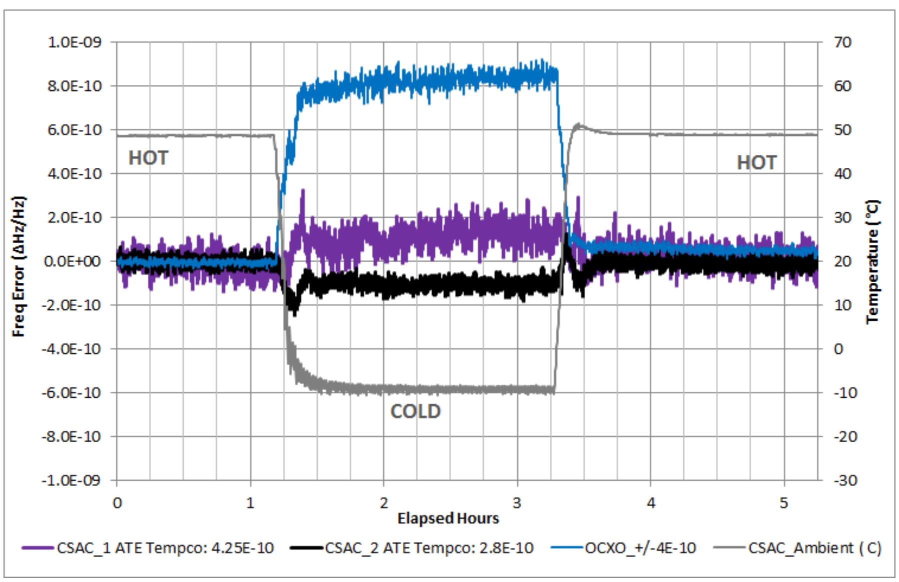

Figure 3.5: Plot of frequency responses after rapid temperature change (Microsemi, 2018)

Oscillator	2 Hours	3 Hours	5 Hours
OCXO	2 µs	5 µs	6.5 µs
CSAC 1	0.1 µs	0.7 µs	1.1 µs
CSAC 2	–0.2 µs	–0.8 µs	–0.9 µs

Table 3.1: Table of accumulated time errors after rapid temperature change (Microsemi, 2018)

After the rapid change in temperature, the CSACs have each accumulated a time error of 1.1 μs and = 0.9 μs over 5 hours, compared to the OCXO's time error of 6.5 μs.

In addition, the manufacturer's test also shows that a frequency offset of 5×10^{10} Hz leads to 10.5 μs of time error at the end of experiment. The test concludes that the initial frequency offset is much more substantial the temperature-induced effects as shown in Figure 3.6. The importance of the initial frequency offset also means good disciplining is necessary for CSAC to minimise frequency errors and thus optimise its performance.

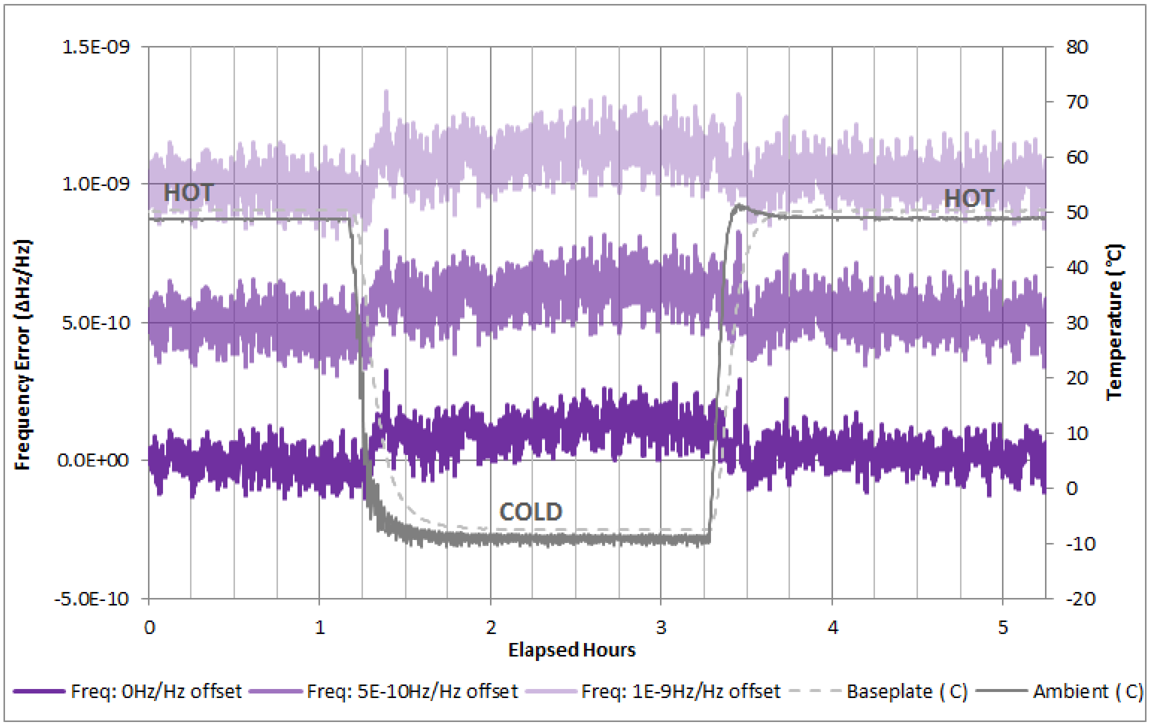

Figure 3.6: Frequency errors given initial frequency offsets (Microsemi, 2018)

For practical use of a CSAC the CSAC-aided GNSS receiver application, it is expected that low temperatures below -10 °C in a number of geographical areas in winter, and also rapid temperature change when the user goes outdoors from a heated building. When a loss-of-lock occurs, the frequency of the CSAC will become unstable and no longer usable for either clock coasting or RCM. Fortunately, a loss-of-lock can be detected by the clock itself so that the system can adjust to it. The minimum temperature of -10 °C presents a challenge, but product upgrades in CSAC are already making progress in reducing it to a lower temperature.

Vibration

Vibration is usually experienced by the clock during transportation, maintenance or operational use. For example, a CSAC on-board a moving vehicle will experience vibration. A manufacturer example is provided in Figure 3.7. The following test results were provided by Microsemi as a reference to the effect of vibration on the clocks' stability (Microsemi, 2014).

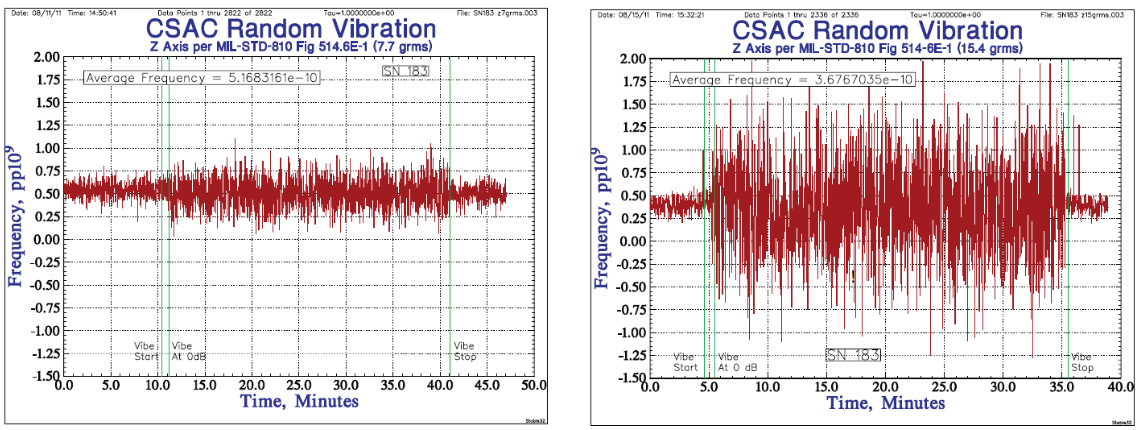

Figure 3.7: Plot of frequency errors under random vibration (Microsemi, 2014)

Figure 3.8 illustrates the frequency accuracy for a CSAC under random vibration along its Z-axis. The clock becomes more unstable when vibration becomes stronger at 15.4 grms. More testing shows that the CSACs suffers from highest performance lost during a strong vibration along Z-axis, causing its ADEV to decrease from the 10^{-12} range to 10^{-11} when $\tau = 100$s , and from the 10^{-11} range to 10^{-10} when $\tau = 1$s.

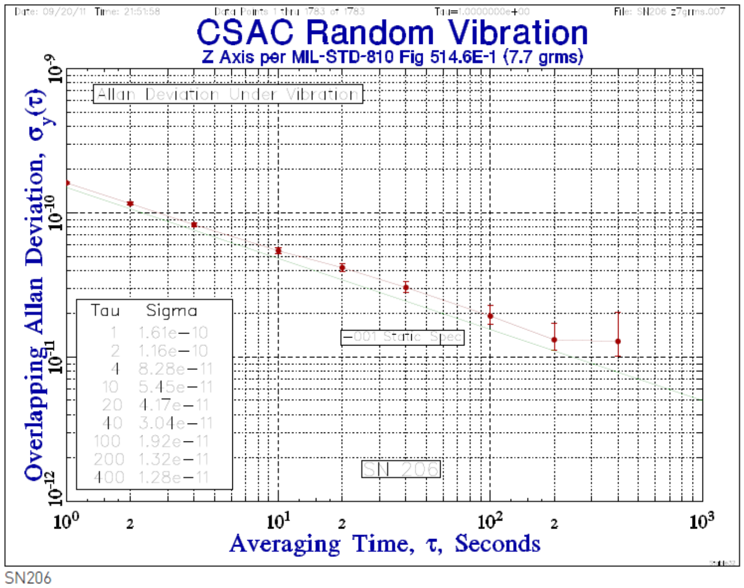

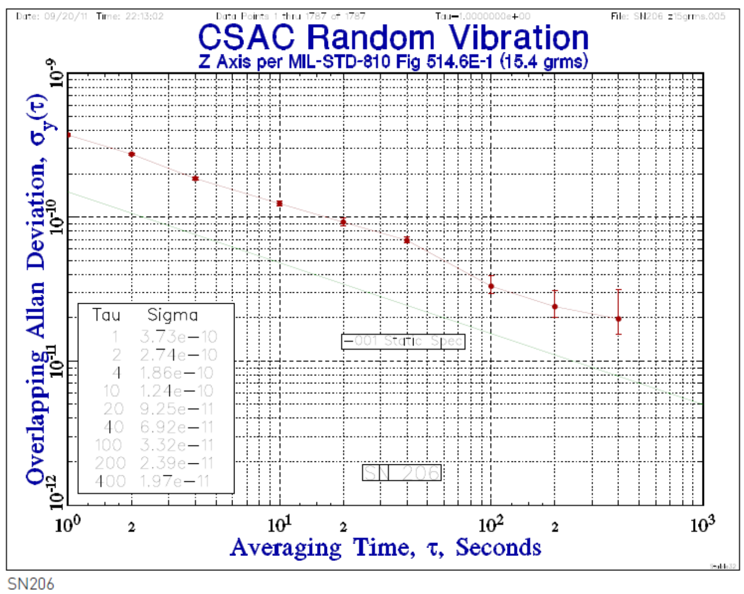

Figure 3.8: Plot of Allan deviation under random vibration (Microsemi, 2014)

In addition, the experiment has also shown that out of the 4 CSACs tested, all four survived (non-operational) a 500 g shock test, while one survived a 2000 g shock test (Microsemi, 2014) .

Vibration tests show that the changes to frequency due to vibration is not significant compared to environmental temperature. Our usage of CSAC-aided receiver are most likely used in vehicles where vibration is at 1-3 grms (Fei et al., 2010).

Ageing

The CSAC model suffers from ageing like most clocks. ageing is the term used to describe an inherent frequency drift when observed over a long duration. Figure 3.9 shows the effect of ageing on a tested CSAC. It can be seen that the ageing effect tends to show negative frequency offset in the first few months, then begin randomly variate over the next few years. It is worth noting that the physical deterioration of the physics package contributes much to the ageing effect. Therefore the actual ageing pattern differs from clock to clock.

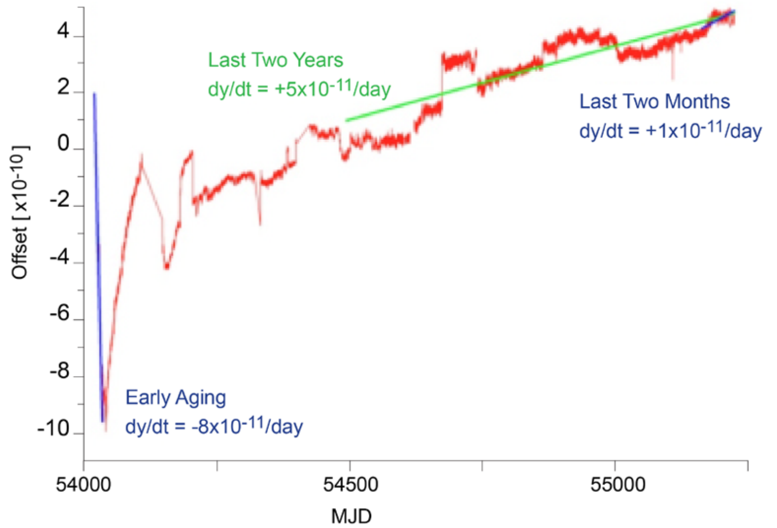

Figure 3.9: Plot of frequency offsets of a CSAC over three years (Microsemi, 2016)

The manufacturer claims the ageing rate should be less than 9×10^{-10} per month. In the extreme cases show in Figure 3.10, one sample shows the same ageing rate as the claimed maximum, while the other sample demonstrated exemplary performance comparable to that of a Rb atomic clock (Microsemi, 2016).

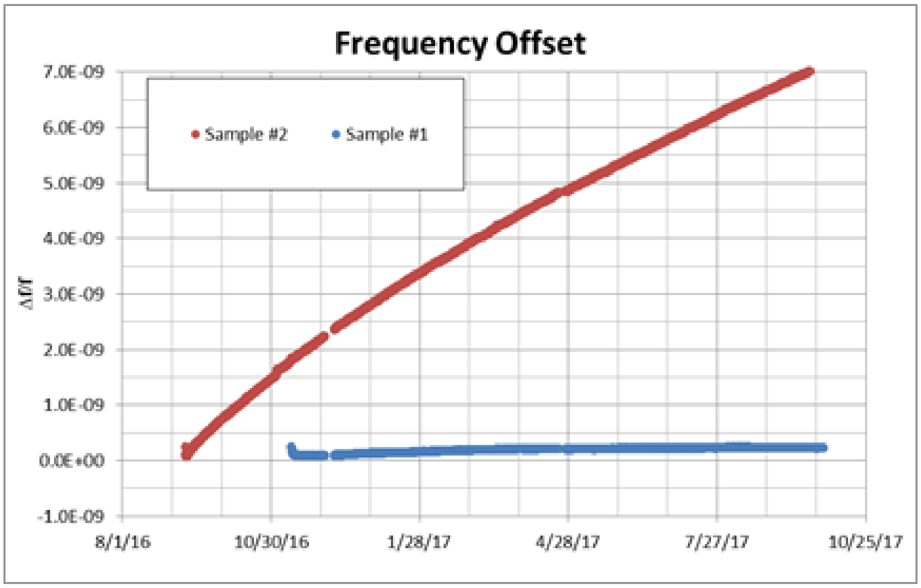

Figure 3.10: Two extreme cases of CSAC ageing over 10+ months (Microsemi, 2017b)

Ageing primarily affects our work in terms of disciplining. Its frequency drift will become apparent in the long-term as steering values (to be explained) shows a pattern as time passes. However in the short-term for clock coasting, it can be assumed that the changes is negligible.

The effects from the three error sources show the practicality of a CSAC-aided GNSS receiver for most day-to-day applications. It also shows how different each clock could behave. Each of the clock may show vastly different characteristics due to temperature, vibration or ageing. Such properties make CSAC behaviour difficult to predict with a generalized model. The individual characteristics of each clock makes mass use of clock modelling more difficult and certainly more costly, as clock modelling requires detailed characterisation of each clock. The process requires state-of-the-art hardware, a superior atomic clock, and time invested to generate a good model. For most applications we expect a simple and direct approach for the system, that the hardware is easily replaceable and software universal. Clock coasting simply relies on the inherent stability of CSACs. Interchanging clock hardware requires no change in software parameters. It does not require extensive modelling and testing for individual clocks. The behaviour under identical software is predictable. It is noteworthy that all the mentioned effects are universal to oscillators. QXOs such as OCXOs and TCXOs tend to suffer more from ageing and temperature change. While it is considered as a future work to implement OCXOs for a more cost-effective solution, this work aims to build a prototype and choosing CSACs is the more rational choice.

3.3 CSAC Disciplining

Despite the superiority of the CSAC over TCXO clocks in terms of short-term stability, the CSAC still suffers from physical limitations of being susceptible to environmental factors and ageing factors. In addition, CSACs have inherent drifts as all clocks. To enhance the performance of a CSAC, a common procedure called 'disciplining' is used, in which the clock constantly tries to steer itself to an external superior source of oscillation. Good disciplining, such as a CSAC being disciplined by a Rubidium/Caesium atomic clock enhances the CSAC's performance while the CSAC's performance, will downgrade if it is disciplined by an inferior source over a certain time constant τ to be found using ADEV plots.

3.3.1 Disciplining a CSAC to a GNSS receiver

Figure 3.11 shows the ADEV comparison between a few typical clock types. CSAC appears to be more stable than GPS clock when $\tau < 6000$ s. However, over a longer term, the GNSS receiver clock becomes more stable as a result of periodic synchronisation with GPS satellite time. Such behaviour of the two types of the clocks promotes a scheme of operation where in a shorter term the CSAC acts as a replacement of the receiver TCXO, but meanwhile the TCXO clock disciplines the CSAC over a longer periods, so that the CSAC is more stable in the longer terms.

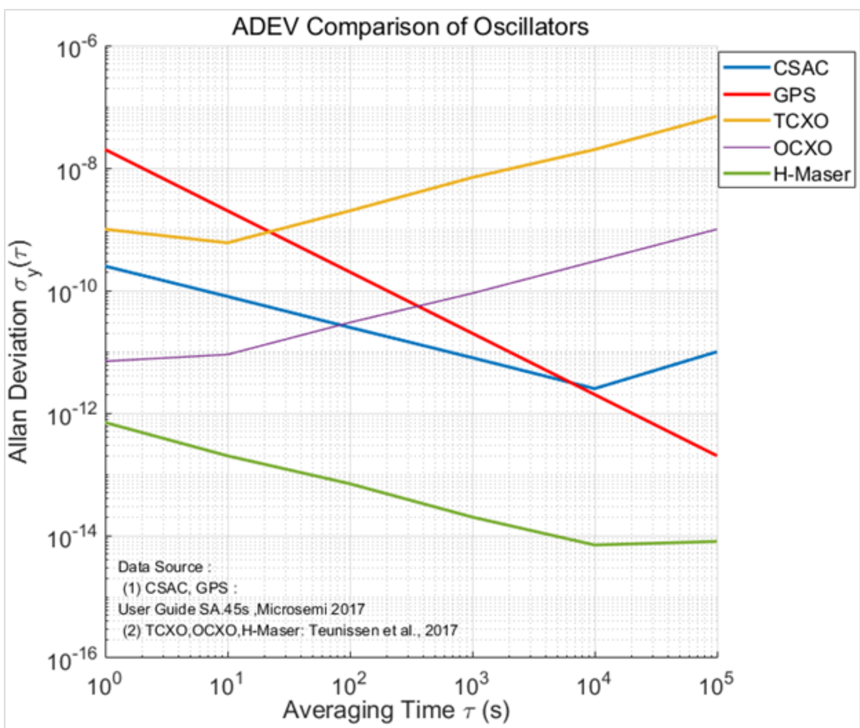

Figure 3.11: Allan deviation comparison between CSAC, GPS and other clocks

In Figure 3.12, both the GNSS receiver and CSAC are controlled by a PC through

USB/serial connections. The CSAC outputs its 10 MHz time signal to the GNSS receiver, while the receiver also provides its own 1 part-per-seconds time signal to the CSAC for disciplining. The disciplining process is controlled through commands from the PC. While disciplining, the CSAC will try to steer itself so that the phase difference can be reduced below a phase threshold constant, denoted as t_m, over a specified averaging time τ. The CSAC employs a steering algorithm to adjust the CSAC's microwave synthesizer through a numerically represented steering value, in units of pp 10^{-12}. The algorithm simultaneously steers both phase and frequency to the external reference.

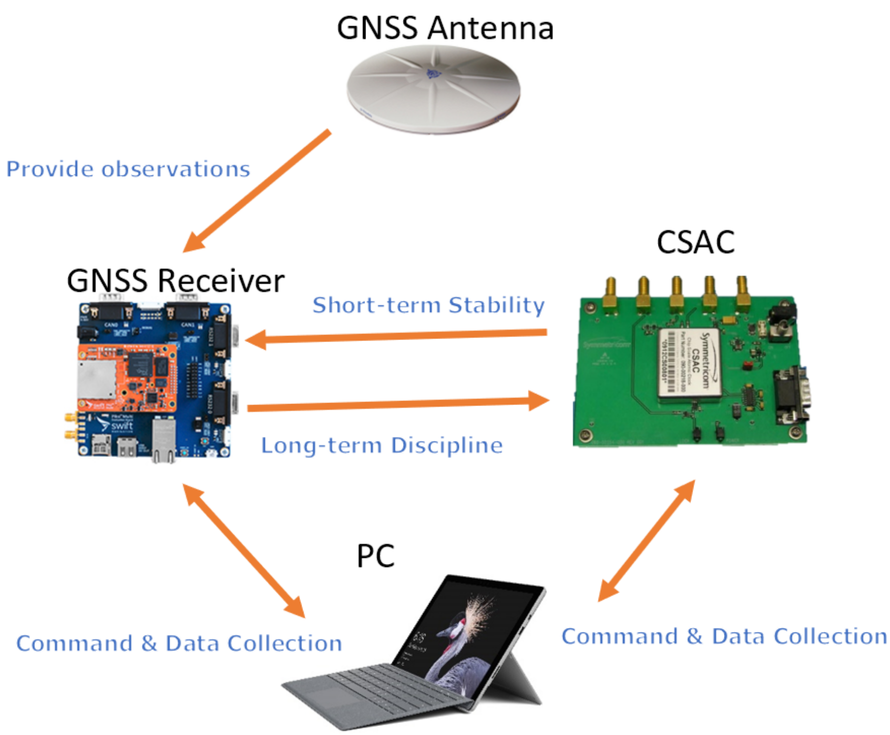

Figure 3.12: Schematics of a prototype CSAC-aided GNSS setup

The selection of τ is crucial. When the CSAC is disciplined to a GNSS receiver, the value of τ should not be less than 6000 s, otherwise we will be steering the CSAC to an inferior source. The larger the τ , the more time it will take for the CSAC to complete the disciplining process. By default, the disciplining phase threshold is set to $t_m = 20\,ns$. The value can be changed in the CSAC's NVRAM to allow a more or less strict disciplining. An example screenshot of output from CSAC is shown in Figure 3.13. When disciplined to a less stable source, such as a GNSS receiver clock, the phase threshold is typically set higher than the default value. In the thesis, it usually takes 4-5 times τ to discipline the CSAC to a Piksi Multi GNSS receiver for $t_m = 60\,ns$. The CSAC failed to discipline itself to the receiver when t_m was set to $20\,ns$. If the so external oscillator is too poor or shows erratic behaviour, the CSAC will not be able to discipline successfully and may cause diverging behaviour in its steering values.

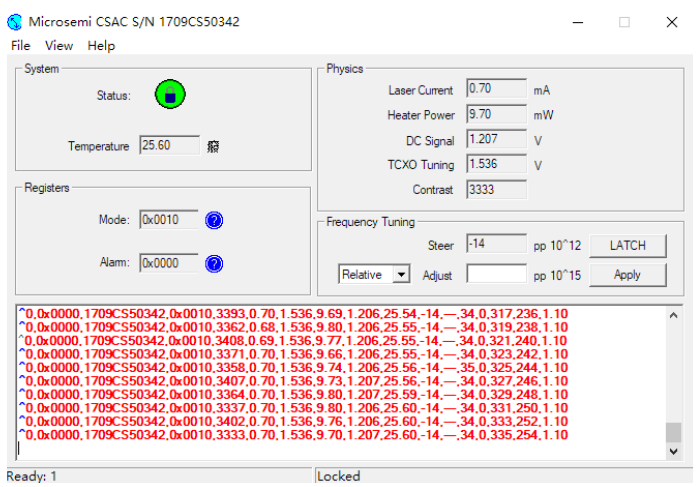

Figure 3.13: Example of CSAC output during a disciplining process

Figure 3.14 shows the behaviour of clock steering value and phase deviation from the external source during disciplining to a GNSS receiver. The averaging time τ was set to 6000 s, and DISC-OK threshold was set to $t_m = 60\,ns$. The CSAC began steering from its initial frequency to the reference clock and finally stabilised at a steering value of approximately -380.

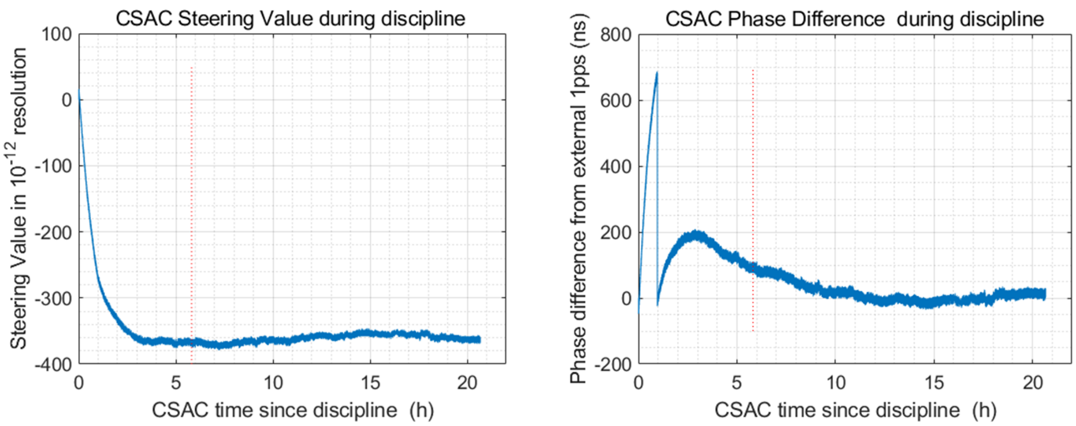

Figure 3.14: Experimental results of disciplining a CSAC to a GNSS receiver. The steering values (left) and phase deviations (right) are shown, with the red dashed line indicating a DISC-OK status.

By repeatedly sending the telemetry commands (!^[CRLF]) from the PC, the CSAC reports its own health, operational parameters, steering value, and phase difference measurement from the external frequency source, if available. While steering itself during disciplining, the CSAC continues to act as a frequency source, sending time signals to the receiver. If, for any reasons, the external signal from the receiver becomes unavailable during disciplining, the CSAC enters 'holdover' mode, maintaining the last steered frequency and waiting for the external signal to come back. However, if the subsequent external frequency has drifted significantly in phase ($> 1\,\mu s$) during the outage, the CSAC will reinitialise the disciplining process.

The steering value is located in the volatile memory of the CSAC. This means after each power cycle, the previous steering value will be lost and the clock will lock onto a frequency during start-up, which may vary due to hardware environment and ageing. The user may choose to 'LATCH' the steering value into the CSAC permanently, so that the CSAC will automatically steer itself by the amount during each start-up. However it is only encouraged to latch the steering value when the clock is referenced to a superior source, as there is no way to retrieve previously latched values. It is also worth noting that the NVRAM of the CSAC has less than 20,000 times of writing limit during its lifetime. Each latching contributes one writing operation and if we constantly latch a new value for the clock, the clock will break permanently in several hours. Some other commands, such as turning on/off discipline mode, setting τ or t_m will also write the NVRAM. It is imperative for any CSAC-receiver interfacing operations to minimise such actions as much as possible.

Chapter 4

Software and Hardware Implementation of a CSAC-aided GNSS Receiver

This chapter presents detailed experimental methodologies used in the thesis leading to experiments and results. The chapter starts with an overview of the clock coasting algorithm implementation in the York GNSS PPP engine. Then, it proceeds on the hardware assembly and interfacing prior to experiments.

4.1 Clock Coasting Technique in PPP

This work chooses PPP over other processing techniques as it aims to provide a mass-market friendly solution in urban PNT. Differential techniques such as RTKs require infrastructure to be built which require financial investment in prior and certain costs to maintain. However, PPP does not require any additional infrastructures, and with the recent development in multi-constellation, multi-frequency receivers, PPP is getting closer to RTK-level of accuracy with low-cost hardware (Aggrey et al., 2019). What PPP does require is the internet access to satellite product servers for real-time processing, but today with booming 5G expansion and already well-built communication infrastructures around the globe, even in rural areas, PPP does not introduce any additional costs. Existing infrastructures would be sufficient to support PPP in most part of the world.

The software implementation of this research is primarily on introducing clock coasting to PPP algorithms. Clock coasting in this research follows closely to the work done by Sturza in 1983, and is automatically enabled when the PPP engine detects a situation where the solution may be compromised due to environmental obstructions, and clock coasting could result in a better solution. A simple flow-chart for the implementation of clock coasting in the YorkU PPP C++ code is described in Figure 4.1:

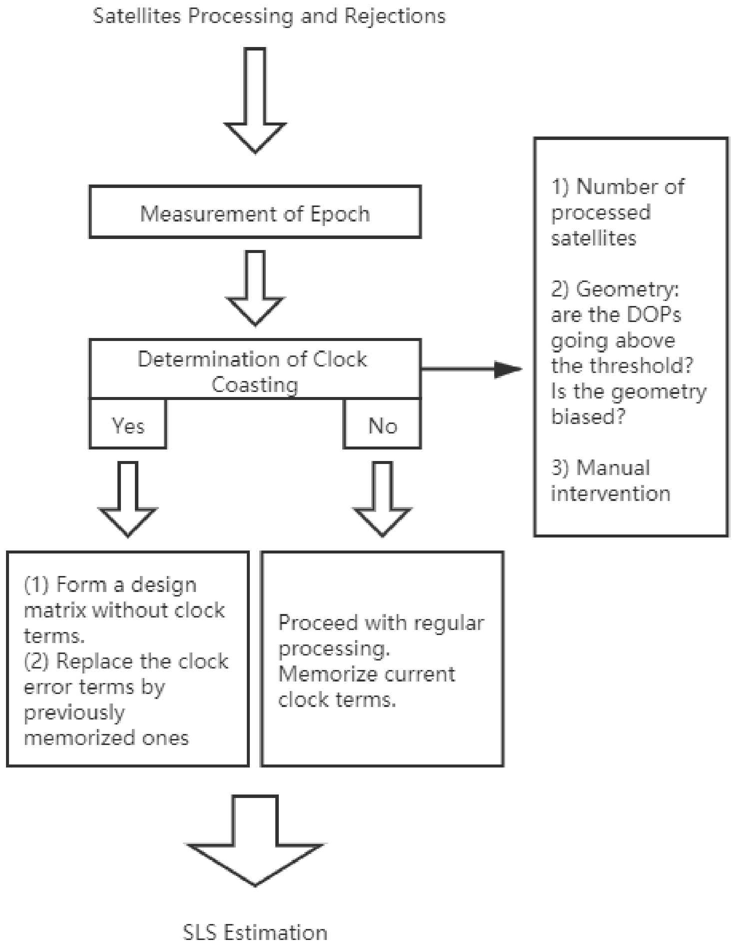

Figure 4.1: Illustration of clock coasting flowchart

A function designed to determine if clock coasting should be used in the current epoch is placed right after the rejection of satellites which failed quality tests. The function is not intelligent by itself, but rather outputs a Boolean using established parameters. Two factors come into play in the process: (1) If the number of satellites is enough for the computation of the current epoch; (2) If the geometry is likely to be poor, or the accuracy in receiver clock error too high. In addition, a manual switch can be used to activate the clock coasting algorithm for specific epochs or GPS time stamps.

As is known, if there are only three satellites available in an epoch, traditional PPP will not be able to produce a point solution. York GNSS PPP Engine estimates wet Zenith Tropospheric Delays (ZTD) as a part of the state vector. A state vector in the engine is given as :

$$\boldsymbol{x} = \begin{bmatrix} x \\ y \\ z \\ \epsilon_{ztd,wet} \\ \dots \\ \delta_{t,GPS_Code} \\ \delta_{t,GLO_Code} \\ \delta_{t,BDS2_Code} \\ \delta_{t,GAL_Code} \\ \delta_{t,BDS3_Code} \\ \dots \\ \delta_{t,GPS_Phase} \end{bmatrix} \tag{4.1}$$

The code and phase clock errors are separately modelled as white noises and estimated for each constellation. Additional terms involves corrections unrelated to and not used in this project. With clock coasting, both code and phase clock terms are eliminated from processing and are replaced by the most recent 'good' clock states assumed to have high accuracies. Relevant terms from the design matrix are taken out, requiring less observations.

Furthermore, if the engine determines the DOPs of the previous epoch were above a certain threshold, indicating poor geometry, it will also enable clock coasting for the current epoch. A special case is when the satellites are limited to one side of receiver, such as a car travelling below a cliff or a pedestrian standing next to a tall building. In such a case, even if there are enough satellites to give a solution, the poor geometry results in a high error in the cross-street direction. Clock coasting will also improve the solution in this scenario. Currently, the determination process has plenty of room for improvement, as more research can be done to explore how solution is compromised depending on environmental factors. C/N_o values of observations can also be taken into consideration.

If the output from the determination function is false, then the normal estimation process takes place. In addition, the receiver clock error of the current epoch will be memorized to be used in the next epoch if required. If the output from the determination function is true, then the estimation process is altered by deleting the receiver clock error term in the design matrix, reducing the rank of design matrix. Thus the solution can now be generated using one less satellite. However the algorithm does not mean the receiver clock error is not estimated, but rather, the clock error term inherited from the last 'good' epoch is used. The algorithm also means the longer clock coasting lasts, the less accurate the solution will be come as the clock drifts. It is still possible quantify the error introduced by the receiver clock by predicting receiver clock errors using established data. Such approach requires a stable clock and as shown in Chapter 5, is not possible using on-board TCXO clocks, which fluctuates randomly. It also leaves room for a separate prediction algorithm for the receiver clock error, such as RCM.

4.2 CSAC-Receiver Two-way Augmentation

The study primarily employs NovAtel OEM729 geodetic GNSS receiver development kits. The OEM729 model is highly customisable and the development kits allow a number of input/output channels simultaneously. The augmentation requires a two-way process of communication between CSAC and receiver.

4.2.1 CSAC to Receiver - Providing Timing Signals

An illustration of the development board used for CSAC along with its interfaces is shown in Figure 4.2. From CSAC to receiver, the CSAC provides precise timing signals in 10 MHz format to the receiver. The CSAC output is an RF, CMOS 0VDC to 3.3VDC waveform. A high-speed buffer on the CSAC evaluation board converts the CMOS output to an AC-coupled output capable of delivering 10 dBm to a 50 load. The process is fairly automated and does not require additional action on the CSAC's part.

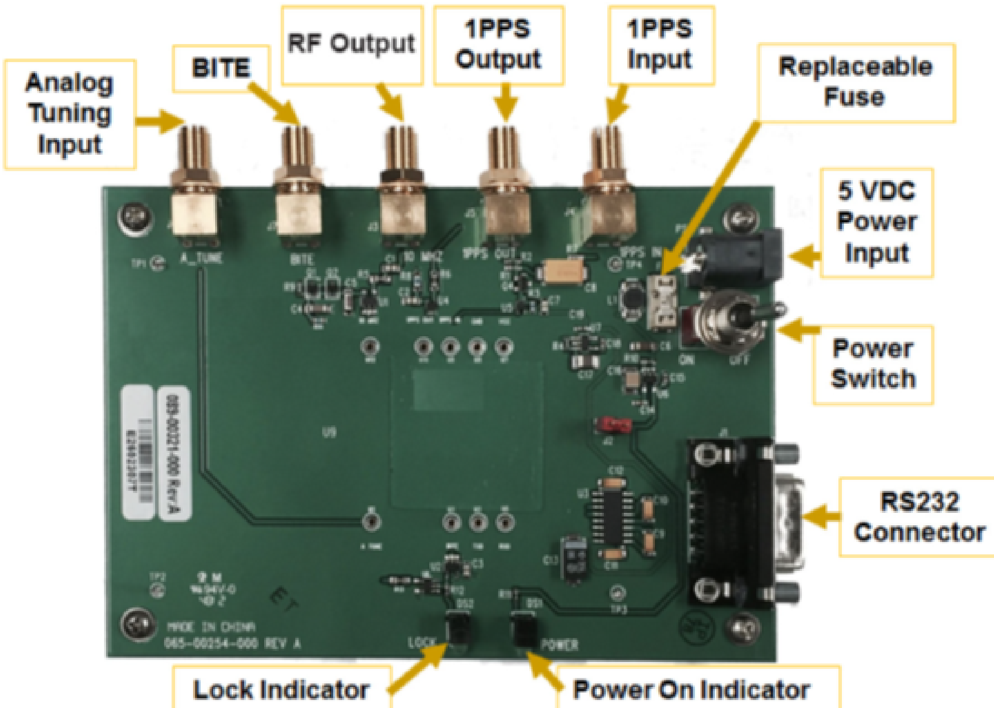

Figure 4.2: Illustration CSAC development board from User Manual (Microsemi, 2017a)

Action is required for the receiver to properly adjust to the external timing signals. A set of essential parameters must be determined prior to data collection as those parameters will affect experimental outcome. To understand the process,the internal process of the GNSS receiver's timing synchronisation must be first explained.

Receiver time synchronisation with GPS time only occur when the receiver locks onto the first satellite. The process is done by decoding the navigation message which is transmitted via individual subframes. Each subframe is 300 bits in length. With the 50 Hz data bit rate a new subframe is transmitted every six seconds. The transmit time of the next subframe is encoded in each of the subframes, in units of seconds in GPS

Time-of-Week (TOW). With the first subframe decoded, the receiver will approximate the current clock offset. The approximation is not accurate, and the calibrated time is designated as COARSE, as it is a rough calculation biased on the approximate propagation time from the satellite signal to the receiver. The accuracy of the receiver time is expected to be within 30 milliseconds of GPS Time.

When at least four satellites are acquired, a more accurate estimate of the receiver clock offset is calculated. The calibrated time within the receiver is now designated as FINE. Fine time accuracy is a function of the GPS constellation status and is influenced by external receiver RF delay. The time accuracy is specified as 20 ns (1 sigma) with internal compensation. When several receivers are used simultaneously, a receiver can transfer its already 'warmed-up' timing to 'cold' receivers using 1 pps input and output.

When an external oscillator is connected and enabled using the EXTERNALCLOCK command through the console, the approximation process is taken over by a Kalman filter within the receiver. The user will have to specify three ADEV coefficients, namely h_0, h_{-1}, and h_{-2} of their external clock in order for the Kalman Filter to properly approximate clock dynamics. The receiver has built-in values for typical TCXO, OCXO, Rb or Cs external clock. Real clocks, especially CSACs will likely have different ADEV coefficients than the built-in ones. For this research, values provided on the Microsemi SA.45s datasheets are used. To further improve the accuracy of the values and adjust to the ageing effect on the clock, one could measure the coefficients using a frequency spectrum analyser or a more precise atomic clock. Since processing is done using raw data collection afterwards, the internal clock modelling mostly affects the signal acquisition/tracking stage.

Another option is to let the external clock steer the internal TCXO clock through the CLOCKADJUST command. By turning on CLOCKADJUST, the timing process is again taken over by the internal TCXO steering to the external CSAC. The behaviour of clock offset will be similar to that of the external clock in the long term. However, it is more prone to short-term instabilities due to the TCXO.

4.2.2 Receiver to CSAC - Long-term Disciplining

A CSAC has an internal drift that leads to frequency offsets in a longer term. This drift is compensated through periodic discipline from a more stable clock so that the CSAC can adjust its own frequency output and improve performance. In our case, the calibration is done by steering the CSAC to the GNSS receiver, which has a stable tracking of four or more satellite in an open area.

An illustration of the development board for OEM7 series is shown in Figure 4.3. From receiver to CSAC, a 1 PPS signal is sent to the 1 PPS IN port. It is worth noting that in this research, a 1PPS signal is not directly accessible from the OEM729 development kit. As a work-around, the EVENT-OUT output is used instead. The EVENT-OUT output is configured to output a square pulse of 20 ns every single second, and is synchronised with the internal oscillator.

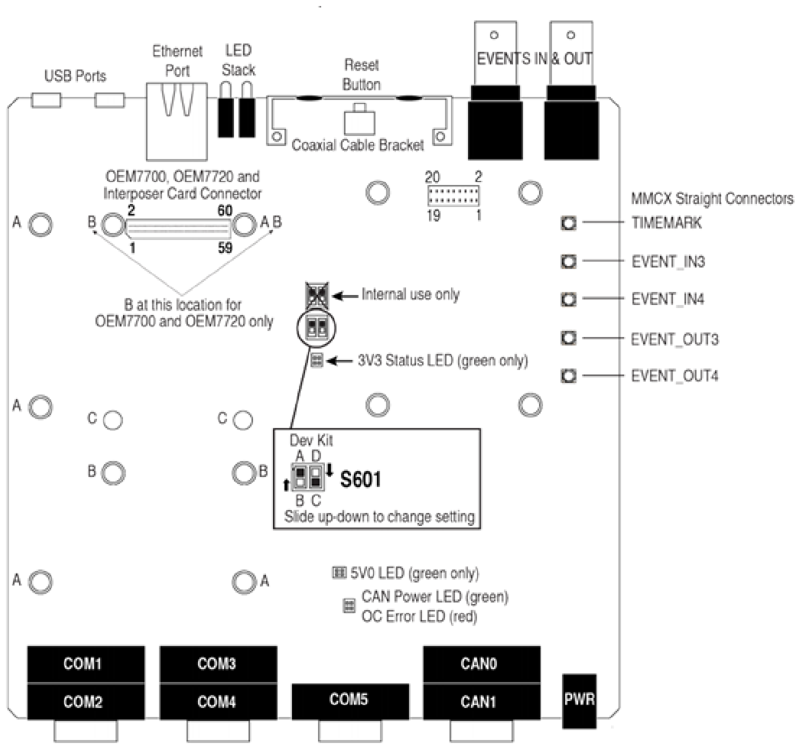

Figure 4.3: Illustration NovAtel OEM7 development board from User Manual (NovAtel, 2019)

The CSAC enters discipline mode under command console input, and proceeds with the disciplining process as detailed earlier. Disciplining should not be turned on when the system is in use, as the GNSS receiver's clock output will be affected by the quality of observation and measurement. If the quality of GNSS receiver's clock output is disrupted, the time to completed discipline will be prolonged. If the disruption causes radical change in output, the CSAC may try to match the radical signal causing discipline algorithm to fail. In the experiments of the thesis, if the signal given to the CSAC is not stable and constantly disrupted due to antenna connection problem, the steering values will fluctuate and unable to find an approximate range to lock on. The system under disciplining will also not be able to produce an improved solution as the CSAC will be in constant self-adjustment to match the external signal. And solutions using a CSAC in discipline mode will not show improvement.

A positive note: For for many applications, the final steering value from the disciplining of CSAC follows the ageing pattern of the CSAC; meaning that the final steering value from today's disciplining will not deviate much from yesterday's. E.g. in the thesis the steering value on March 08, 2020 and March 15, 2020 were found to be -260×10^{-12} per part versus -264×10^{-12} per parts. Therefore the system is not required to perform a discipline on a regular basis.

Chapter 5

CSAC-aided GNSS PPP: Methodologies, Experiments, Results and Discussion

This chapter presents to experimental procedures used to produce datasets, which in turn led to a series of result in static and kinematic tests. Elevation masks of various duration and strength were used to simulate obstructed urban environments in which clock coasting algorithm is tested. The results were analysed and discussed.

5.1 Experimental Set-up and Research Questions

The schematic of the experiments are shown in Figure 5.1. A prototype system of the CSAC-aided GNSS receiver was built using NovAtel OEM729 GNSS receiver and Microsemi SA.45s CSAC, which has key parameters extracted from official documents in Table 5.1. Both are installed in their development kits and integrated as described in Chapter 5. Experiments were conducted to answer a series of questions of the system's performance both in generic environments, and also in obstructed environments. To compare the results, two identical OEM729 receivers were used: One receiver was connected with the SA.45s CSAC and was referred to as 'Receiver A'. A stock OEM729 receiver without any further modification was used alongside the CSAC-aided receiver, and referred to as 'Receiver B'. Both receivers shared the same antenna for all experiments. The signal from the antenna was routed to both receivers using a high-performance GNSS signal splitter. Two identical cables were used to connect the receivers to the signal splitter. And finally both Receiver A, B, and the CSAC were connected and controlled by a PC.

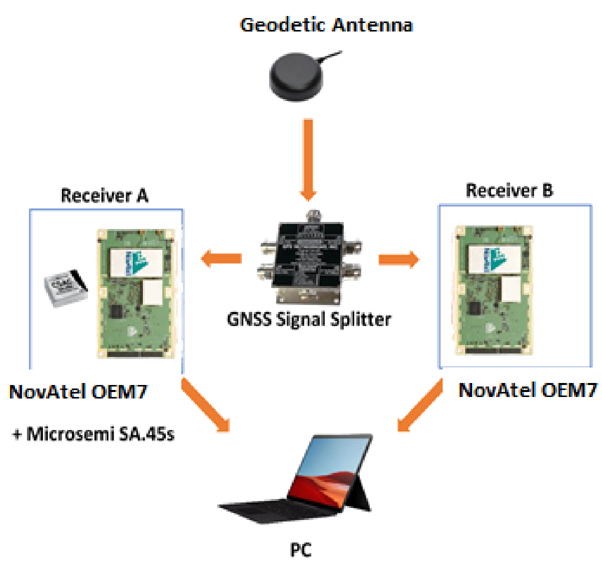

Figure 5.1: Schematics Receiver A and B used in experiments

Table 5.1: Parameters of Microsemi SA.45s CSAC (Microsemi, 2017a)

Properties	Parameters
Power Consumption	<120 mW
Volume	<17 cc
Weight	<35 g
Operating Temperature	-10°C to 70°C
Warm-up Time	<180 s

The questions being addressed with the experiments and their purpose are:

1. How good is the static GNSS-PPP solution with CSAC (with no obstructions)? This basic experiment would provide more insight on the receiver-clock interaction mechanism and represent a base line for the following kinematic environments test. Improved solution with CSAC is expected according to literature, but how much improvements will be there in PPP?

2. How good is the solution in an 'open-sky' environment with CSAC? Some of real-world scenarios would also be in more rural or suburban settings. Are any improvement using CSAC, or perhaps any downsides? Furthermore, a number of cited studies indicate improved solution quality in the vertical direction. With the accuracy of PPP already within centimetres in the vertical direction, can the CSAC make any improvements too.

3. How much error is introduced when clock coasting is applied? For different durations and types of path (curved or straight), data would be analysed. In a rather

extreme case, what if the clock coasting is turned on throughout a data collection? Error of a few metres were expected when the clock coasting was applied for TCXO, and decimetres for CSAC during a few seconds. The error is also expected to grow as the clock coasting is prolonged.

4. How effective is clock coasting in obstructed environments? Using software simulations, obstructed environments can be simulated. A number of scenarios are already mentioned in earlier chapters. The effect on navigation solution when geometry was compromised was investigated. Using our existing data collected, the navigation solution with the obstructions can be compared to those without obstructions. The scenarios we are interested include:

    - An urban canyon in which multiple satellites are obstructed for different duration from tens of seconds to minutes. Poorer geometry, and a worse navigation performance in the canyon is expected. However, with clock coasting, the solution should be improved.
    - A deep urban canyon that is more challenging to the processing. A poor geometry, with lower availability of solution due to satellite LOS signal loss is expected. However, with clock coasting the solution should be available also during the three-satellite periods.
    - A biased obstructed environment such as a pedestrian walking next to a skyscraper or a car driving below a cliff. A biased solution in the cross-street direction at metres level is expected. It also expected that the additional timing sensor and clock coasting would improve solution and reduce bias. This

scenario is referred to as the ’cliff scenario’.

The performance of clock coasting would be examined in the scenarios as well. The scenarios are designed to bring real-life challenges to the system, and to test not only if the system works well, but also the limits of the system at this current stage of development.

5. What are the limits of the current CSAC-aided GNSS receiver prototype? What future work, or integration can be done to address these limits, and what are the prospects for improvements?

5.2 Static Data Collections and Results

A static experiment to compare receiver A and B was conducted on Feb 26, 2020 or DOY (Day-of-Year) 58. The data were collected within the GNSS lab using a geodetic-grade antenna from the rooftop of the Petrie Science and Engineering Building, York University, Toronto, Canada. The data collection lasted over 17.5 hours with both receivers collecting data simultaneously. The reference solution was collected beforehand in earlier experiments using 24 hour of data from a TOPCON geodetic receiver, and was processed using NovAtel Inertial Explorer in PPP mode.

5.2.1 Satellite Tracking and Geometry

The use of an external clock may improve the GNSS receiver’s correlator synchronisation due to the reduction of the Phase-Locked Loop (PLL) bandwidth (Fernandez, Calero, and Eulia Pares, 2016). The actual process is very much controlled by the internal design of the receiver. Therefore it is necessary to examine the tracking performance of the receivers before proceeding with kinematic road tests. The GDOP and number of satellites processed through the YorkU GNSS PPP engine are plotted in Figure 5.2. The plots show the receivers do not track the same set of satellites all the time. There were occasions where a single satellite was not simultaneously tracked by both receivers.

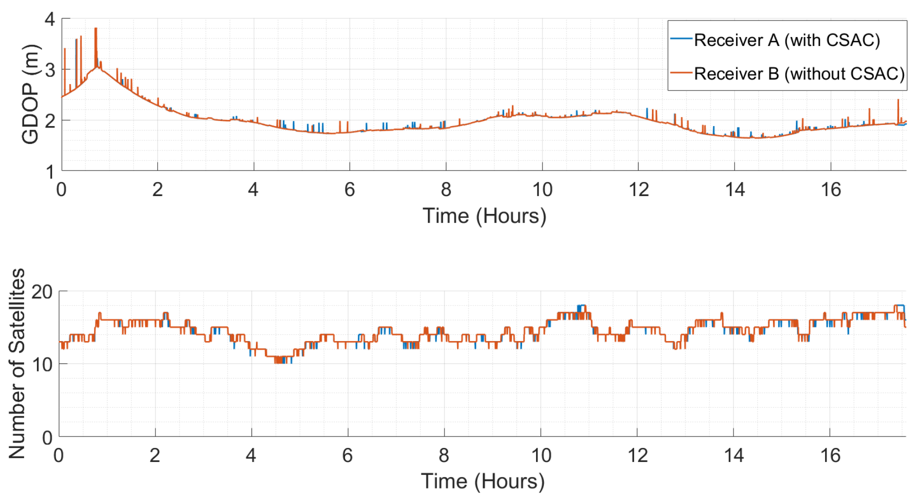

Figure 5.2: Geometric dilution of precision (above) and number of processed satellites (below)

5.2.2 Positioning Results

The errors in the north, east and up directions are shown in Figure 5.3. The result shows both receivers are able to converge to the antenna position in the centimetre level. Using an accustomed convergence threshold of 10 cm, receiver A converges in 641 s in the east direction, and a similar 658 s for receiver B without CSAC. In the north direction, receiver A converges in 2375 s, whereas receiver B takes 1892 s. In the vertical direction, neither receivers are able to maintain an error below 10 cm in the first 9 hours. The rms (root-mean-square) errors are also calculated for both receivers. In the north direction, receiver A shows an error of 26 cm, and receiver B shows an error of 25 cm. In the east direction, receiver A shows an error of 30 cm, and 24 cm for receiver B. In the horizontal directions, the receivers show very similar and precise result with difference in at most centimetre level. Since this is the level of precision we expect from our PPP program, there is no clear improvement is found. In the vertical direction, receiver A shows an rms error 6 cm, and receiver B shows an rms error of 5 cm.

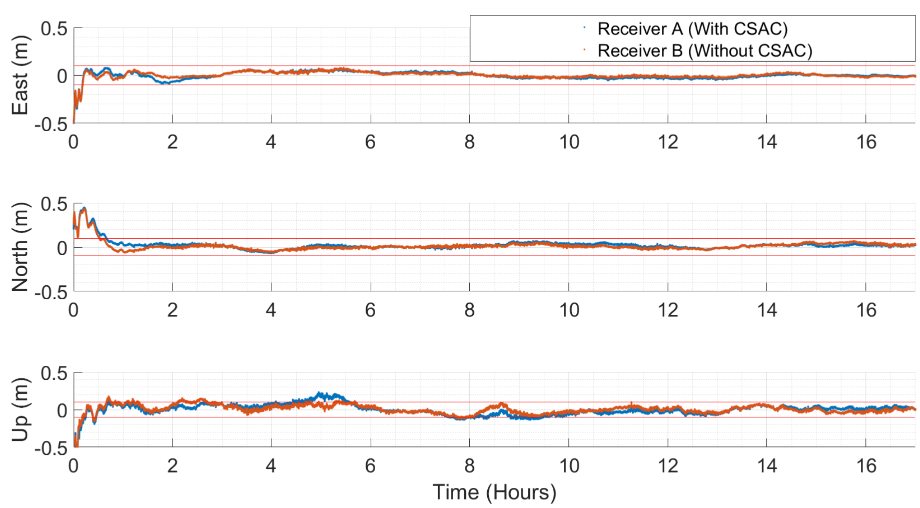

Figure 5.3: East, north and up directional errors with the red solid line indicating a convergence threshold of 10 cm.

5.2.3 Discussion

Our experiment did not show a clear improvement of using the CSAC as external clock in static PPP processing. To eliminate the possible errors due to our PPP engine, the data is further tested using the Inertial Explorer software. Both receivers show identical 0.6 cm of rms error in the north direction, 1.8 cm in the east direction and 4.0 cm in the vertical direction. The result suggests the improvement from a CSAC in the open-sky, static setting is negligible in PPP processing. However, with kinematic processing, and especially when three-satellite solution is involved, the situation changes dramatically.

These results are expected because of (1) the high number of satellites available throughout the static data collection; (2) standard PPP processing using geodetic hardware in a static situation. The advantage of using a precise external clock provides no improvements in such situations.

5.3 Kinematic Data Collections and Results

The configuration was further tested in kinematic experiments. A similar setup to the static experiments was installed on a vehicle, with a NovAtel NOV850 antenna fixed on the top of the car. Both receivers and the CSAC were powered by a UPS, with limited power coming from the car. A base station using the TOPCON receiver and antenna was set up on the rooftop of Petrie Building. The base station provided an RTK solution as a post-processing reference to the PPP solution. The details of the rover and base stations are explained in Table 5.2.

	Rover Station	Base Station
Receiver	NovAtel OEM729	Topcon NET-G3A
Antenna	NovAtel NOV850	SwiftNav Geodetic Antenna
Constellation	GPS, GLONASS, Galileo, BeiDou	GPS, GLONASS
Rate of Logging	5 Hz	1 Hz
RTK Positional Accuracy (Static)	1 cm + 1 ppm	0.003m + 0.05ppm (Horizontal) 0.005m + 0.05ppm (Vertical)

Table 5.2: Parametres of the receivers used

Several 30-minute datasets were collected by driving in the suburban area close to the university campus. The drives involve passing short buildings of no more than four stories high, heavy traffic including trucks, some foliage in certain parts, and underpasses. The routes were chosen deliberately to examine the performance of the system, while keeping a trustworthy reference solution.

5.3.1 Interfacing Modes of Clock-Receiver Interaction

In each dataset, various configuration of clock modelling and clock adjustment modes were used to find an optimal receiver-clock operational scheme. The configuration involves the mode of operation for the clock and the receiver, as well as the modelling data used in the receiver. Three different configurations of interfacing the clock with the receiver were tested as shown in Table 5.3.

1. Mode 1: Both receiver and the disciplined CSAC were in their default mode of operation. The receiver relied on the timing input from the CSAC without adjusting

	Receiver	CSAC
Mode 1	Default	Default
Mode 2	CLOCKADJUST on	Default
Mode 3	Default	Disciplining

Table 5.3: Modes of clock-receiver interfacing used in the work

its own frequency. The receiver clock error showed drifts over a longer periods, but it was more stable than the TCXO clock in the short-term. A plot of receiver clock error estimation over time is shown in Figure 5.4, showing a drift of about 350 m over 24 hours.

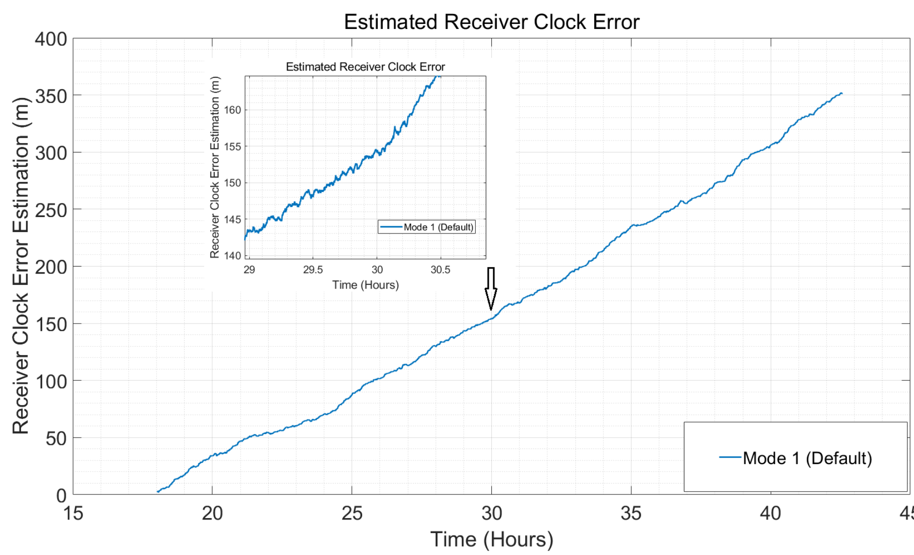

Figure 5.4: Plot of receiver clock error estimation on DOY 60, 2020 in static, open-sky environment. X-axis refers to hour of the day.

2. Mode 2: The CLOCKADJUST command was turned on for the receiver, meaning the receiver would try to steer its own clock to the CSAC's frequency. The receiver steered its own timing frequency to the external clocks'. In a longer term a similar

drift to mode 1 appeared as shown in Figure 5.5, causing an accumulated receiver clock error of 75 seconds over 18 hours. Over a shorter term of two hours, Mode 2 appeared to show a stronger random pattern rather than a linear pattern observed in Mode 1.

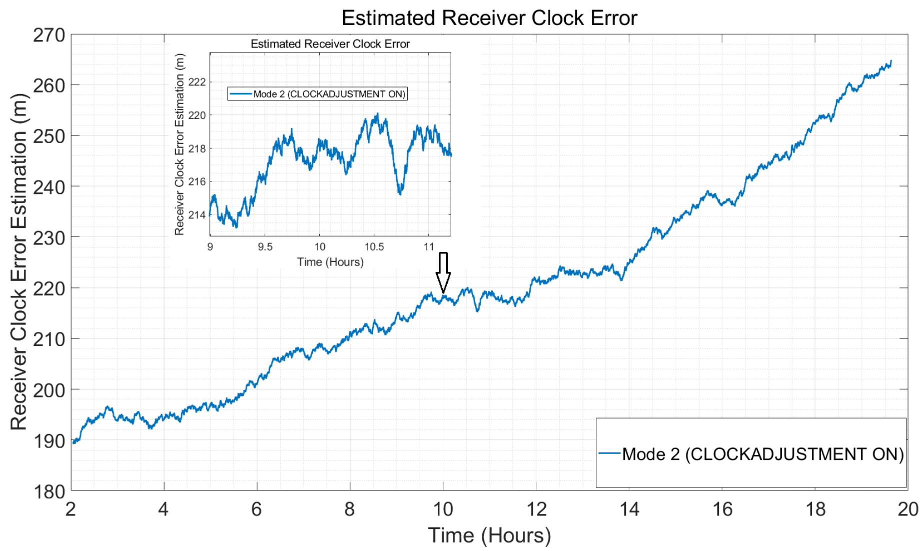

Figure 5.5: Plot of receiver clock error estimation on DOY 58, 2020 in static, open-sky environment. X-axis refers to hour of the day.

3. Mode 3: The clock was being disciplined to the receiver, it was trying to constantly adjust its output frequency, leading to unstable or fluctuating frequency changes at times. A sudden shift in the timing frequency would cause the receiver to lose track of satellites. The end result was the receiver clock errors shown in Figure 5.6 which is very similar to the TCXO's output shown in Figure 5.7. Therefore it is concluded that the clock should be running as it is without interference while the system is in use.

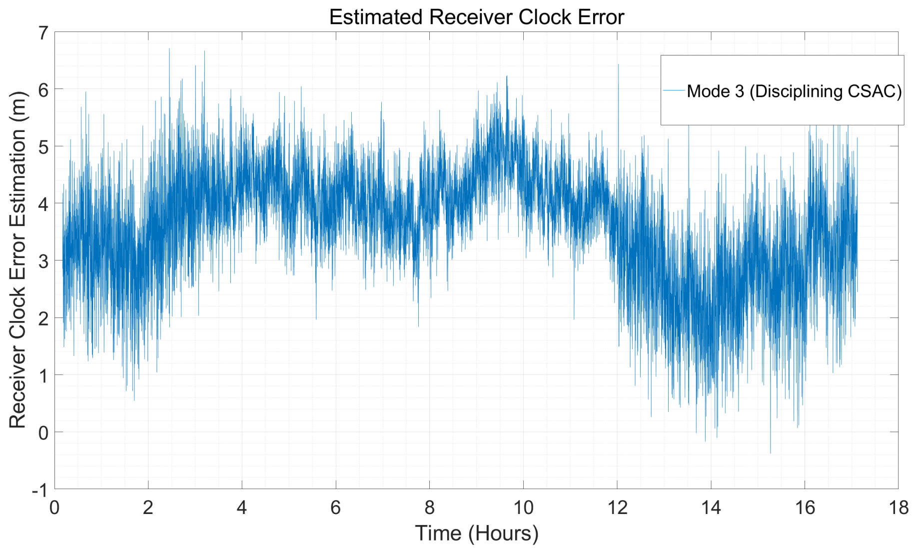

Figure 5.6: Plot of receiver clock error estimation on DOY 66, 2020 in static, open-sky environment. X-axis refers to hour of the day.

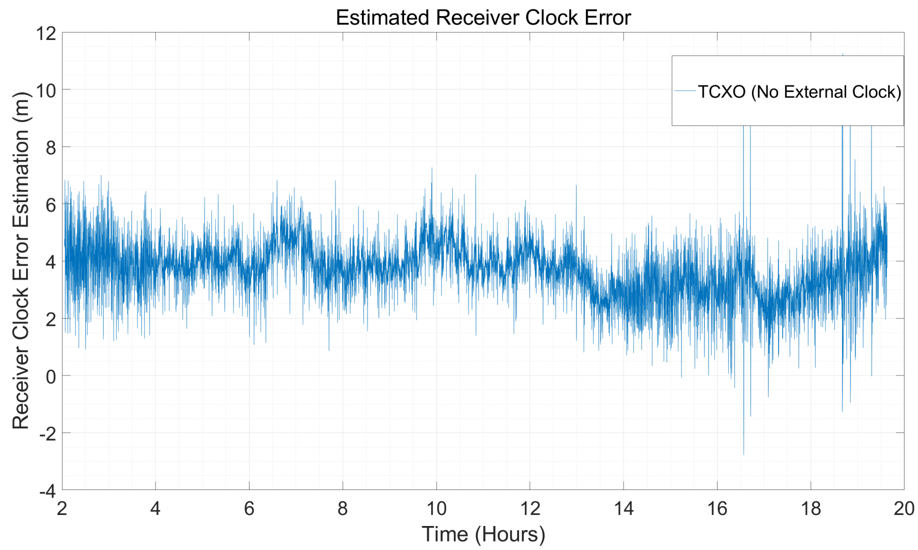

Figure 5.7: Plot of TCXO receiver clock error estimation on DOY 58, 2020 in static, open-sky environment. X-axis refers to hour of the day.

To quantitatively characterize the performance of the clock-receiver interfacing configurations, 1000 sample intervals of length 10, 100, 1000, and 10000 s were picked randomly for each experiment. The standard deviation for each interval was computed, and the mean values of the calculated standard deviations were computed. The reason of picking random intervals is that in mode 1 and 2, the clock error estimations show some trend but not stationarity, meaning that if an underlying function is removed, the solution will show stationarity just like the case in mode 3 and TCXO. The modelling of the clock drifts is not in the scope of the research. Mean standard deviation is shown in Table 5.4. The result shows an advantage in short terms (10 s and 100 s) timing stability for mode 1 and 2. The larger errors for those modes in longer terms may also be reduced to lower levels if the drifting effect is addressed. The histograms show a dominant portion of mean standard deviations fall in sub-metre range for mode 1 and 2 in short terms, whereas for the TCXO clock, outliers of several metres occur much more frequently.

	mean std in cm (10 s samples)	mean std in cm (10^2 s samples)	mean std in cm (10^3 s samples)	mean std in cm (10^4 s samples)
Mode 1	7	23	128	1136
Mode 2	7	21	70	350
Mode 3	26	56	62	71
TCXO	28	63	73	79

Table 5.4: Mean values of standard deviations over random intervals

The clock coasting algorithm relies on the timing stability over the periods it is used. The conclusion from analysing receiver clock errors show a clear advantage for clock coasting algorithm in mode 1 and 2. Mode 2 also shows smaller clock drifts over time due to the receiver's time update from GPS Time. Therefore, kinematic experiments were carried out using mode 2, where the clock was pre-disciplined and ran in normal operation during the data collection, and the receiver had turned on the CLOCKADJUST switch to utilize both the external CSAC and GPS Time updates. The statistics also provide some insights into the quantitative performance of the clock coasting algorithm we may expect. The result shows, even without further modelling of clock drifts, we can expect errors introduced by clock coasting to be within the sub-metre level for durations about 10 s to 100 s. Without the CSAC, using the on-board TCXO clock is expected to produce errors close to metres level for the same duration, and higher fluctuation of errors is expected due to the less stability of TCXO.

5.3.2 General Kinematic Result

In the dataset, the car is driven close to the York campus in a largely suburban area over a duration of 25 minutes on March 09, 2020 (DOY 69). The path taken during the experiment is shown in Figure 5.8:

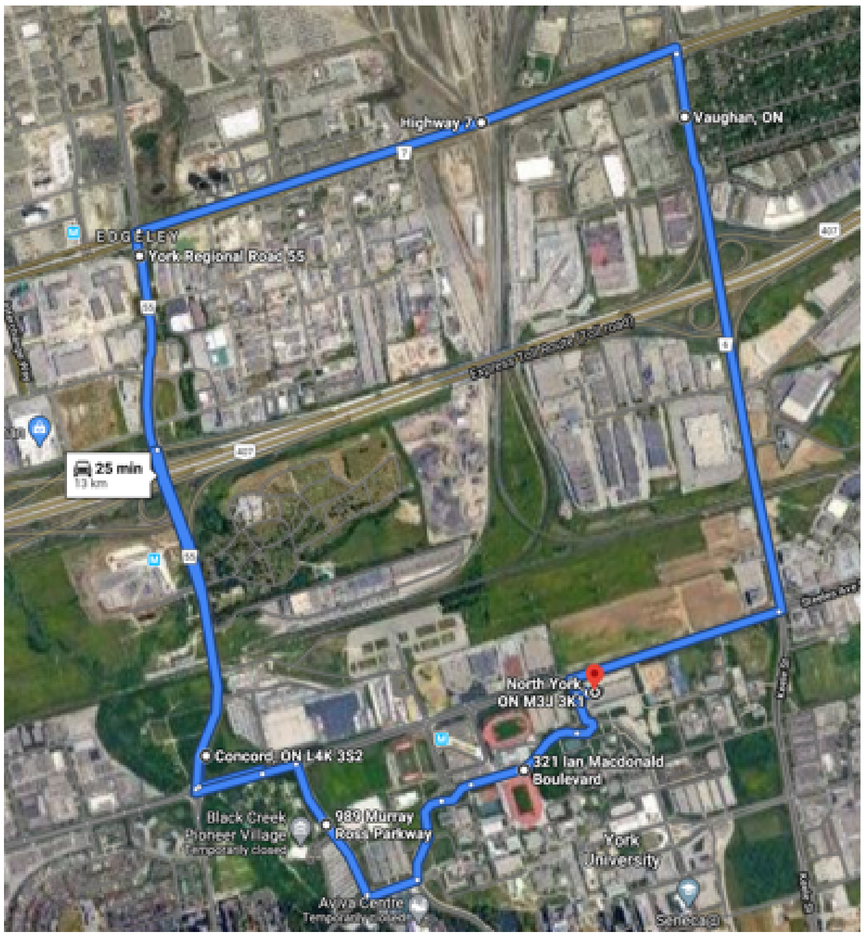

Figure 5.8: Path taken for the kinematic experiment

In Figure 5.9, the GDOPs and number of processed satellites through all epochs are plotted. The tracked satellites that were able to be processed are not identical for the two receivers. There were occasions where one receiver performs better by one satellite, and sometimes the other way around. Generally, the two receivers were tracking the same satellites.

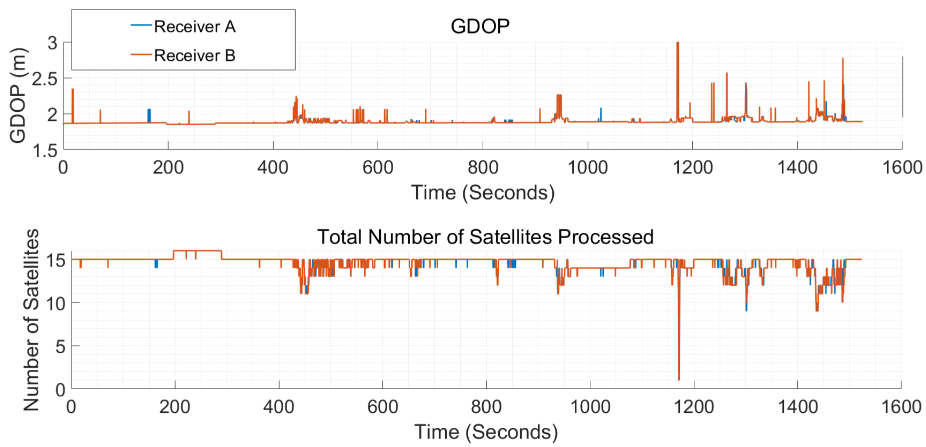

Figure 5.9: Plot of geometric dilution of precision (above) and number of satellites processed through the engine (below).

In the first weaker outage from 425 s to 500 s, two heavy trucks were recorded to pass the test vehicle on both sides, leaving 3-4 less for processing. The outage caused the quality of observation to drop, resulting in increased errors and fewer satellites processed. As shown in Figure 5.10, Receiver A was able to keep track of more satellites most of the time and 9 fewer occurrences are recorded for the lowest number of 11 satellites for receiver A. A similar pattern is also observed in the brief but strong outage around 1150 s due to a small underpass. Figure 5.11 shows the faster tracking recovery for receiver A post-outage.

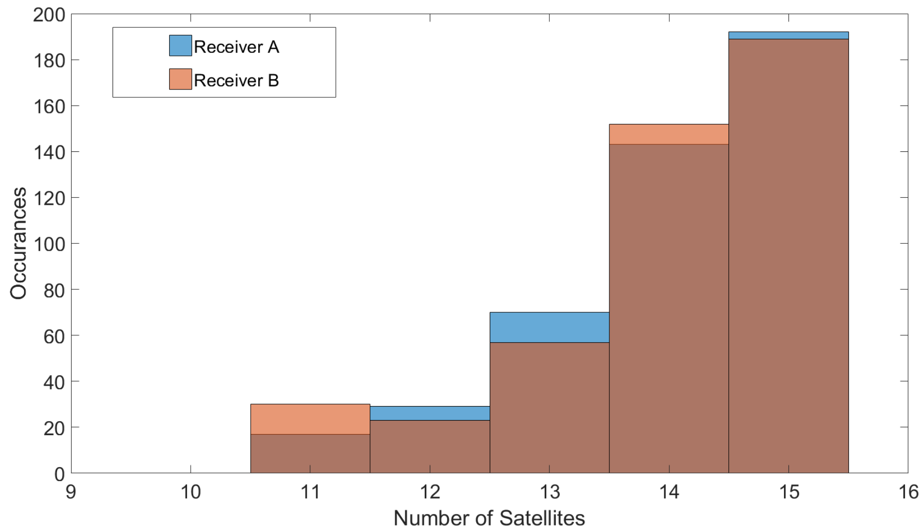

Figure 5.10: Histogram of processed SVs during the first outage (trucks)

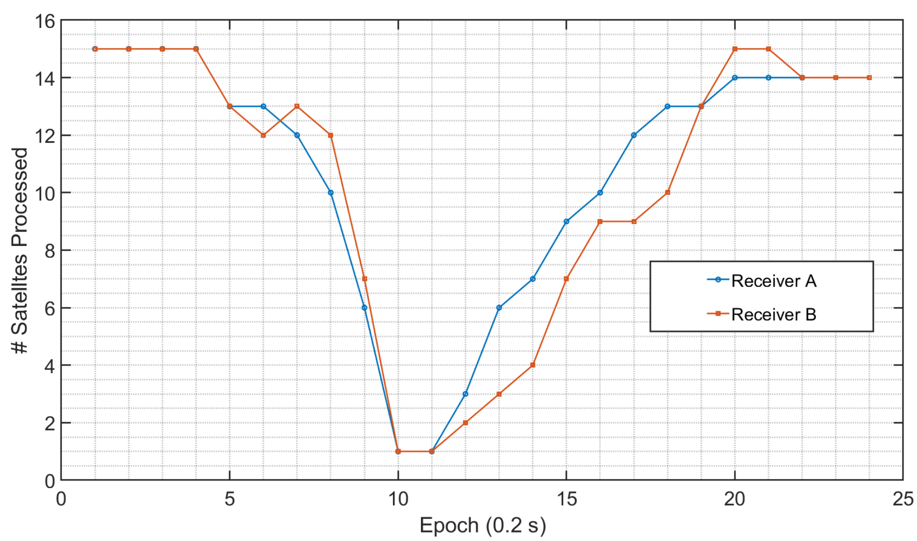

Figure 5.11: Processed SVs during the second outage (underpass)

Horizontal and vertical errors were computed using the reference RTK solution on a epoch-to-epoch basis, where the solution at identical timestamps were compared. Epochs where a reference solution was not available was skipped. Horizontal errors are plotted in Figure 5.12. Throughout the experiment, receiver A showed an rms error of 33 cm, and receiver B shows an rms error of a slightly higher 35 cm. Receiver A has an standard deviation (std) in horizontal errors of 19 cm versus 17 cm for receiver B. The performance for both receivers is highly similar, reinforcing the previous conclusion from the static data collection. Figure 5.13 shows the absolute vertical errors for both receivers. Receiver A shows a lesser rms vertical error of 26 cm versus 30 cm for receiver B. During the underpass, receiver A showed a peak of vertical error of 4.4 m, but for receiver B, the peak reaches 6.2 m. Similar to the static experiment, the improvement in normal processing is not clear.

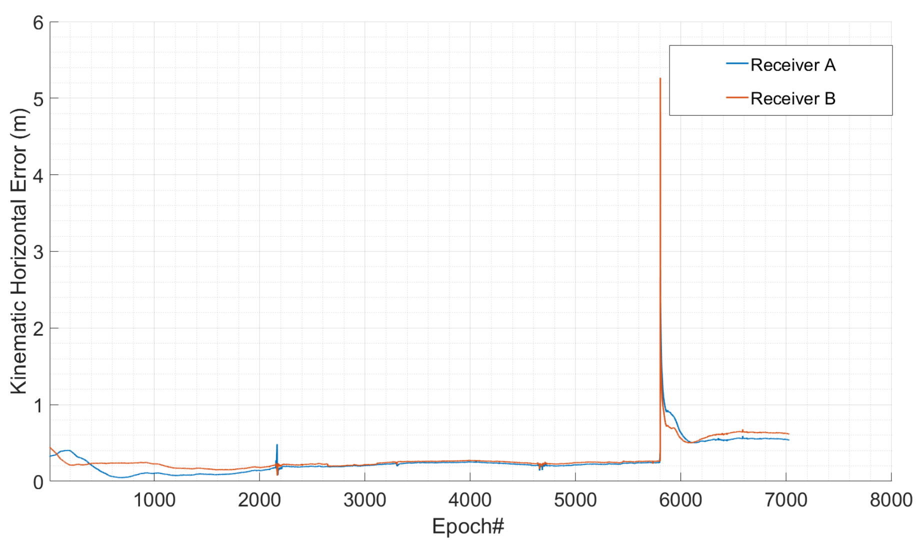

Figure 5.12: Horizontal errors in kinematic test

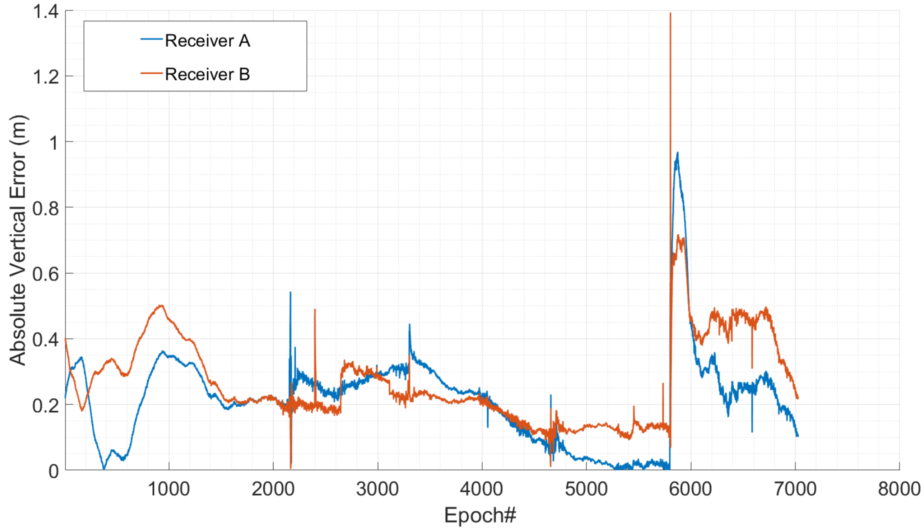

Figure 5.13: Absolute vertical errors in kinematic test

The result from the dataset shows no clear improvement for the two receivers. The reason for the result is also expected due to similar reasons for the static tests. Clock coasting was not enabled, and the advantage of a more stable clock was not utilized. However, the static and kinematic tests provided a baseline for the simulated obstructed scenario to come.

5.4 Simulation of Obstructions

A key methodology in this work is to simulate urban canyons in the real data previously collected using elevation masks. Such simulations allow for controllable, customisable and comparable environments with actual measurements. Simulated obstructions can be controlled so that a certain set of satellites can be chosen for the processing, such as a combination of 1 GPS, 1 Galileo and 1 GLONASS satellite. In real-world environments, such combinations are difficult to randomly achieve. The masks generated and developed for simulation can be customised with arbitrary direction in terms of azimuth angles or duration and strength to define buildings of different size. Without a better reference solution than the RTK solution at hands, simulation secures a trustworthy reference solution for comparison. However, our reference solution is not perfect either, as shown in the last section, natural obstructions caused outages of several epochs, and severe outages such as underpasses compromise the convergence afterwards.

The drawback of defining software masks to simulate obstructions is that it does not simulate reflected signals, including NLOS signals and multipath, nor foliage attenuation. These introduced errors affect the availability of solutions in different ways than blocking LOS alone. However, studies have been done on detecting multipath errors using CSAC as well (Preston and Bevly, 2014) by correlating the spikes in timing bias and number of SVs.

5.4.1 Short Urban Simulation

The first simulation involved short masks of 30 s in duration. Two masks of different size were implemented onto the dataset at the entrance to the residential area at epoch 9050, or 1810 s. The smaller mask blocked all satellites in 280° of azimuth angle below an elevation angle of 35°. The larger mask blocked all satellite below 55° of elevation angle. The result on geometry and number of satellites processed is shown in Figure 5.14. The larger mask halved the number of processed satellites to an average of 10 and caused slight reduction in GDOP. With the larger mask the number of satellites dropped to an average of 5, and 2 epochs contained only three satellites.

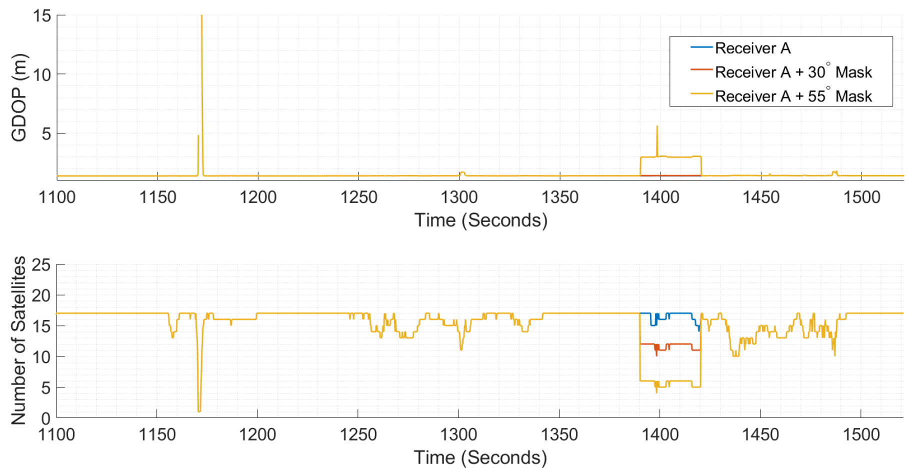

Figure 5.14: Plot of geometric dilution of precision (above) and number of satellites processed through the engine (below) in short urban simulation

The horizontal and vertical errors are computed for the first scenario with a 35° mask. Horizontal and vertical errors of receiver A for the duration of the mask is shown in Figure 5.15 and Figure 5.16 respectively. The plots for receiver B are shown in Figure 5.17 and Figure 5.18. A comparison of statistics for the duration of the mask is provided in Table 5.5. The result suggests a slightly improvement in performance for receiver A using clock coasting in the tested environment. However for receiver B, the error from clock coasting is too large and degrades the result. The vertical solution is over a metre worse than the solution without clock coasting, as is expected, the vertical component to be most prone to additional receiver clock errors.

Receiver/Errors in cm	rmse (horizontal)	$\sigma_{horizontal}$	rmse (vertical)	$\sigma_{vertical}$
Receiver A	36	1	7	4
Receiver A + CC	36	1	16	8
Receiver B	42	1	13	5
Receiver B + CC	70	20	172	166

Table 5.5: Error statistics for Receiver A and B in the 30 s, 35° mask, epoch 9050-9200

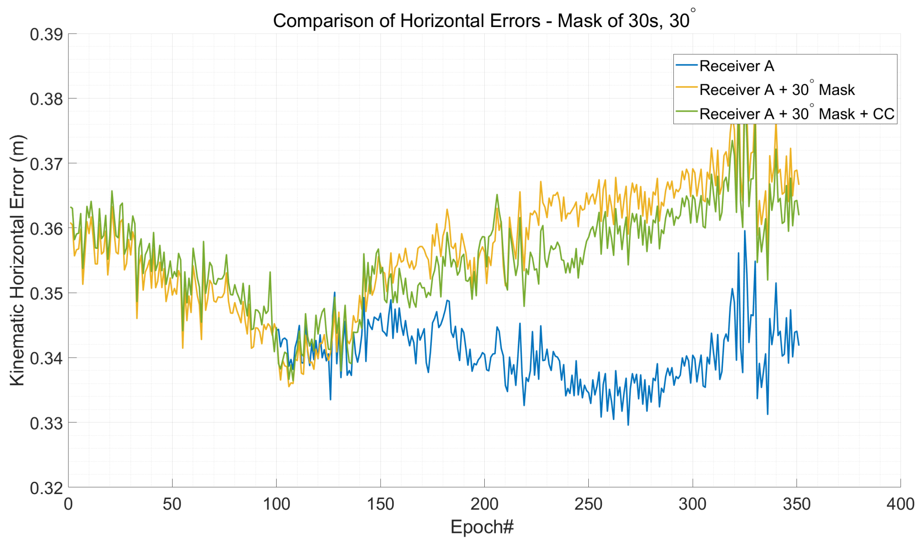

Figure 5.15: Horizontal errors in with a short, 35° mask, Receiver A

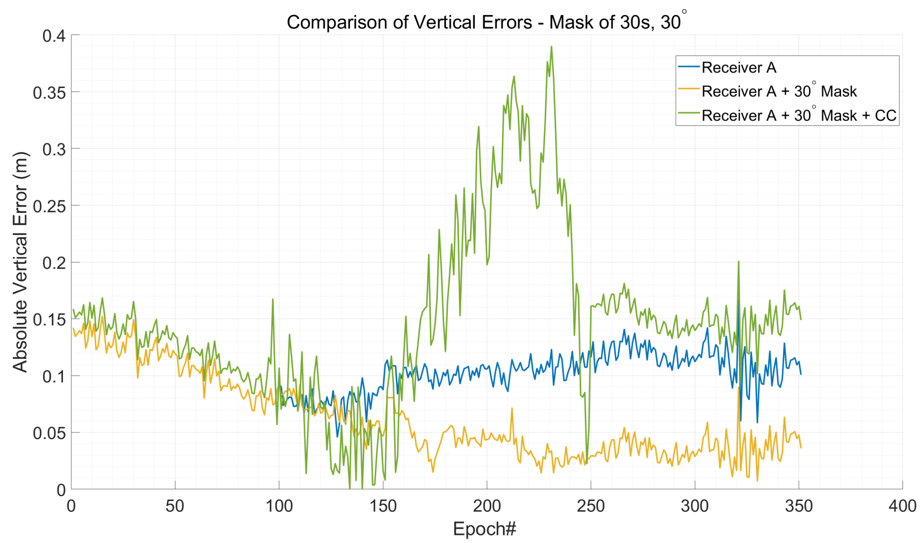

Figure 5.16: Absolute vertical errors with a short, 35° mask, Receiver A

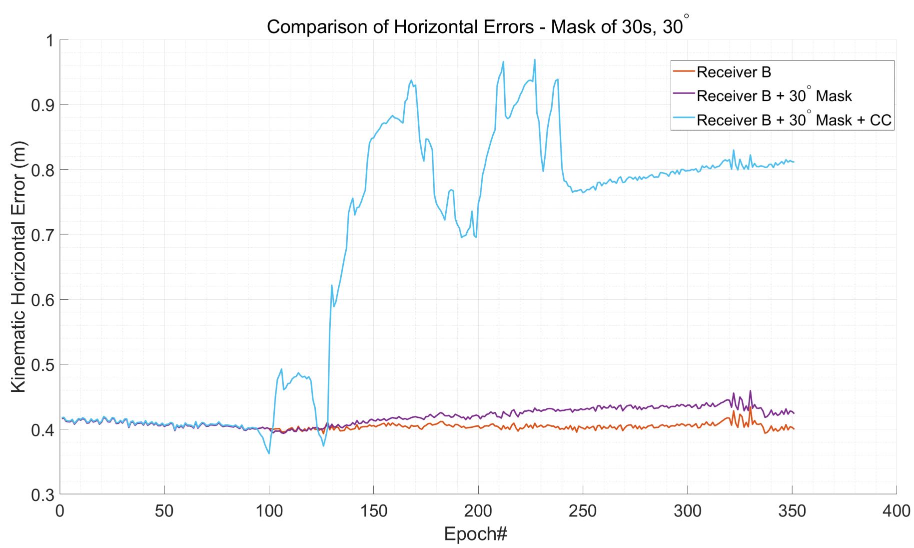

Figure 5.17: Horizontal errors in with a short, 35° mask, Receiver B

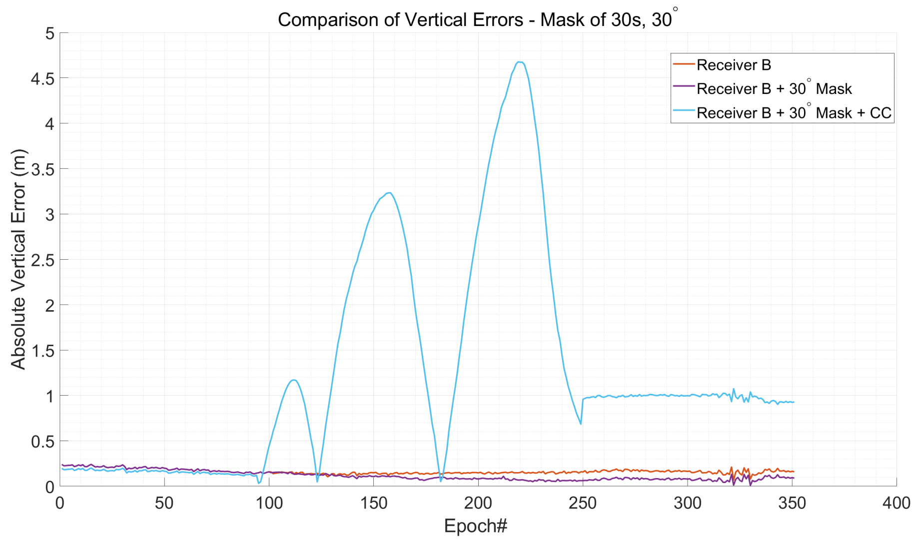

Figure 5.18: Absolute vertical errors in with a short, 35° mask, Receiver B

As the smaller mask preserved geometry (less GDOP change) we expect no improvement from the clock coasting algorithm. If so, then the next question is: whether implementing clock coasting in a 'good' geometry has a negative impact on positioning accuracy. The result shows, as expected, clock coasting with Receiver A (with CSAC) performs very similarly to the original solution without clock coasting in the horizontal direction. However, additional vertical errors were observed in the vertical direction. Receiver B suffered a reduction in accuracy in both horizontal and vertical directions. The result meets expectation as Receiver A has a much greater timing stability, and timing errors has a stronger correlation with vertical accuracy. The result also suggests while it is possible to do clock coasting with a TCXO clock, the compromise in solution will be in metres instead of centimetres. A drawback of clock coasting was also observed. Although the newly introduced errors were low with a CSAC, it took a few minutes after clock coasting for the solution to converge back to its original one. Before the re-convergence,

Receiver/Errors in cm	rmse (horizontal)	$\sigma_{horizontal}$	rmse (vertical)	$\sigma_{vertical}$
Receiver A	43	9	45	41
Receiver A + CC	37	4	17	8
Receiver B	48	9	37	36
Receiver B + CC	80	49	150	49

Table 5.6: Error statistics for Receiver A and B in the 30 s, 55° mask, epoch 9050-9200

an additional error of a few centimetres can still be observed.

A stronger mask was implemented in the same part of the dataset by blocking all satellites below 55° of elevation angle. With the larger mask, an urban-heavy situation was simulated, and the geometry was further compromised. Due to three-satellite epochs and poor geometry, spikes of errors in range of several metres can be found during the masked period. Statistics for the experiment can be found in 5.6. Clock coasting brought the error down to the sub-metre level in both horizontal and vertical directions for Receiver A as shown in Figure 5.19 and Figure 5.20. For Receiver B, the clock coasting performance is better than the original masked solution in the horizontal direction, but worse in the vertical direction, indicating a higher receiver clock error shown in Figure 5.21 and Figure 5.22.

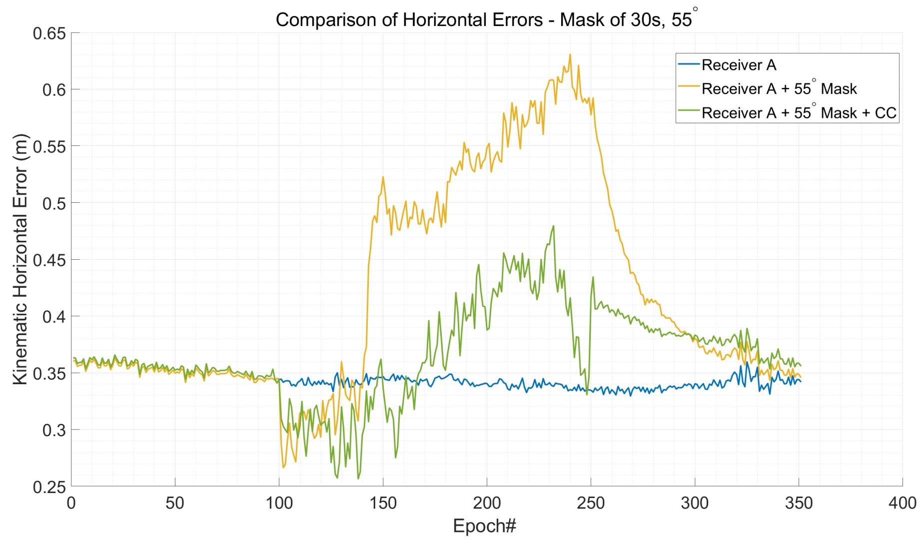

Figure 5.19: Horizontal errors in with a short, 55° mask, Receiver A

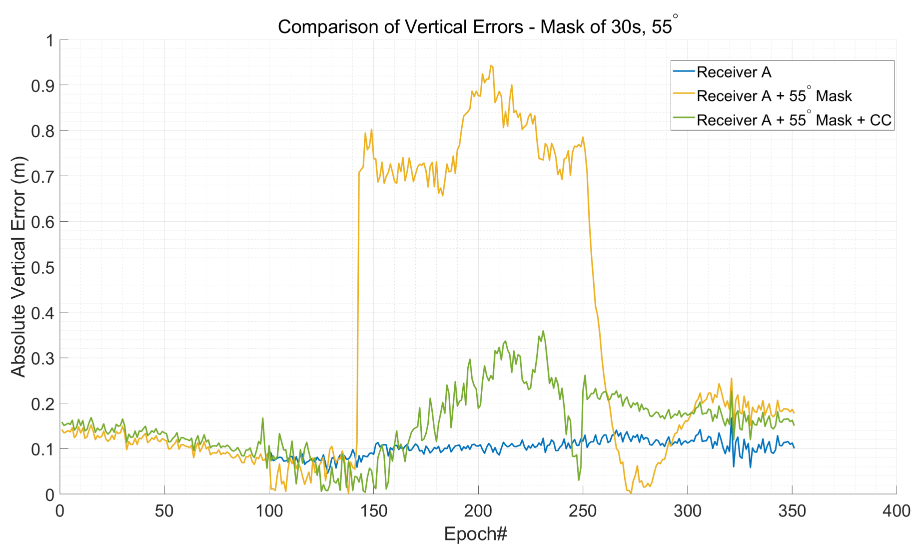

Figure 5.20: Absolute vertical errors in with a short, 55° mask, Receiver A

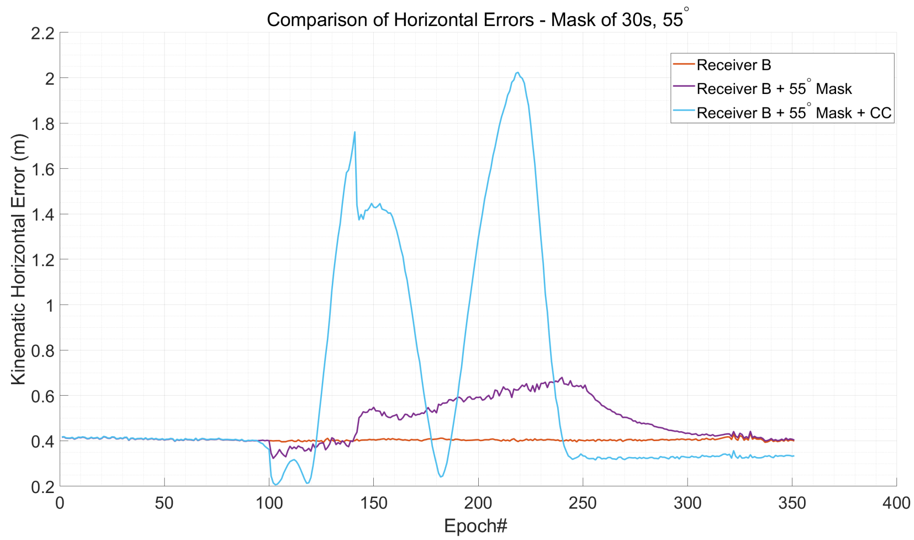

Figure 5.21: Horizontal errors in with a short, 55° mask, Receiver B

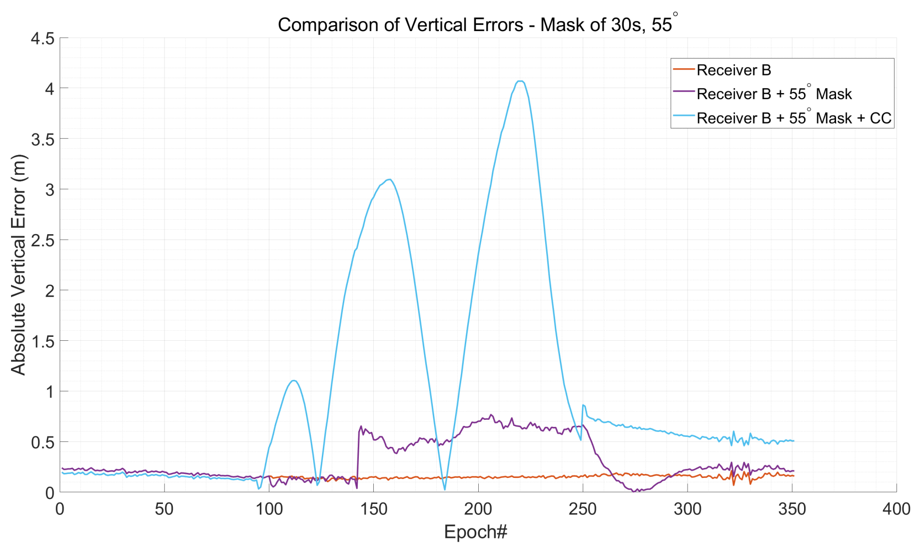

Figure 5.22: Absolute vertical errors in with a short, 55° mask, Receiver B

In the short urban simulations, masks of 35° and 55° were implemented to reduce the number of visible satellites as well as worsen geometry. With the 55° mask, Receiver A with CSAC showed an improved accuracy in both horizontal and vertical directions. Receiver B showed a large error as expected, as the negative effect from the clock coasting overshadowed the effect from reduced geometry.

5.4.2 Long Urban Simulation

In longer simulations, the duration of masks were prolonged to over a minute. As the obstructed environments last longer, its impact would sustain more in the processing. Clock coasting became more challenging as well, due to clock drifting. The simulation used the same datasets, however, with a longer mask duration. Clock coasting over longer period is more difficult because of the drifting will become more apparent and the effect from the change of road environments over time will create more uncertainty in processing.

Simulation Using a Smaller Mask

A mask lasting 240 seconds was placed after driving through an underpass on a curvy road from epoch 7850 to 9050. The goal is to challenge processing with some three-satellite situations. The mask was placed in the dataset right after an underpass, with effects shown as in Figure 5.23. The natural underpass caused a spike of errors of several metres.

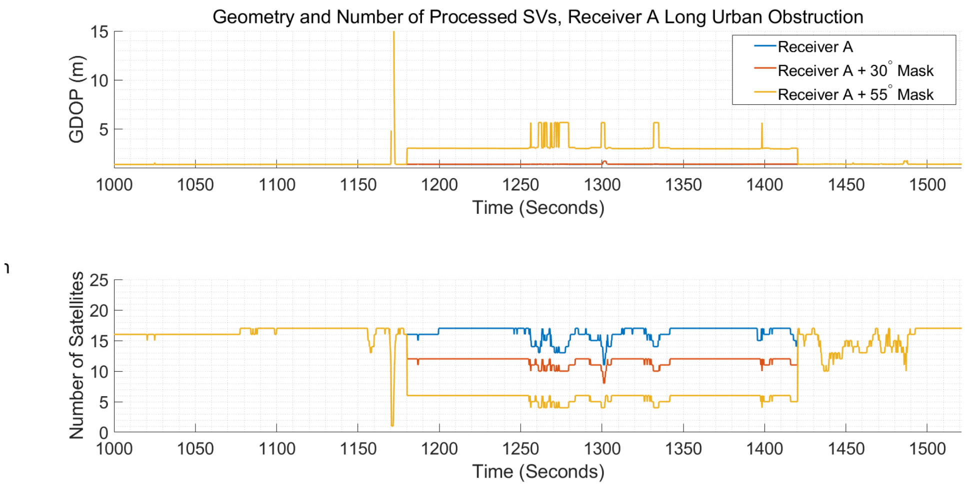

Figure 5.23: Plot of geometric dilution of precision (above) and number of satellites processed through the engine (below) in long , 55° urban simulation

Error statistics for this set of long clock coasting experiment is shown in Table 5.7. Horizontal and vertical plots are shown in Figure 5.24, Figure 5.25, Figure 5.26 and Figure 5.27. Despite a longer period of clock coasting from 30 s to 240 s, horizontal errors with Receiver A did not show clear accumulation. However, Figure 5.26 shows clear increasing vertical errors with time. This corresponds to the clock drifting effect of CSAC over a few minutes. The result indicate that the additional errors from clock coasting affect less in the horizontal direction over a few minutes of intervals than that in the vertical direction. The dataset was not long enough to support longer clock coasting after the initial convergence. However, it can be cautiously estimated that using the current interfacing and setup, clock coasting can last 40 minutes before horizontal errors reach a metre even without addressing the clock drift.

Receiver/Errors in cm	rmse (horizontal)	$\sigma_{horizontal}$	rmse (vertical)	$\sigma_{vertical}$
Receiver A	53	25	30	13
Receiver A + CC	53	25	62	43
Receiver B	53	24	27	12
Receiver B + CC	67	34	180	180

Table 5.7: Error statistics for Receiver A and B in the 240 s, 30° mask, epoch 8000-9200

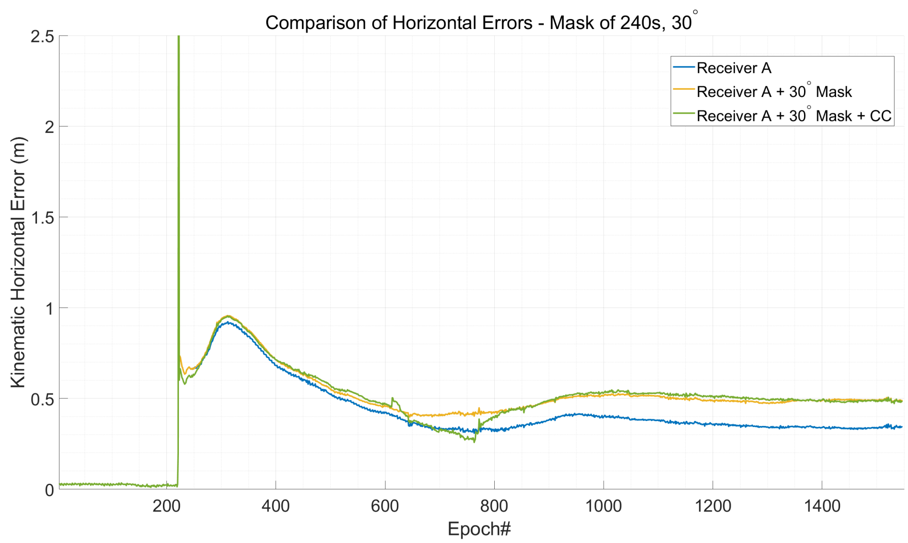

Figure 5.24: Horizontal errors with a long, 30° mask, Receiver A

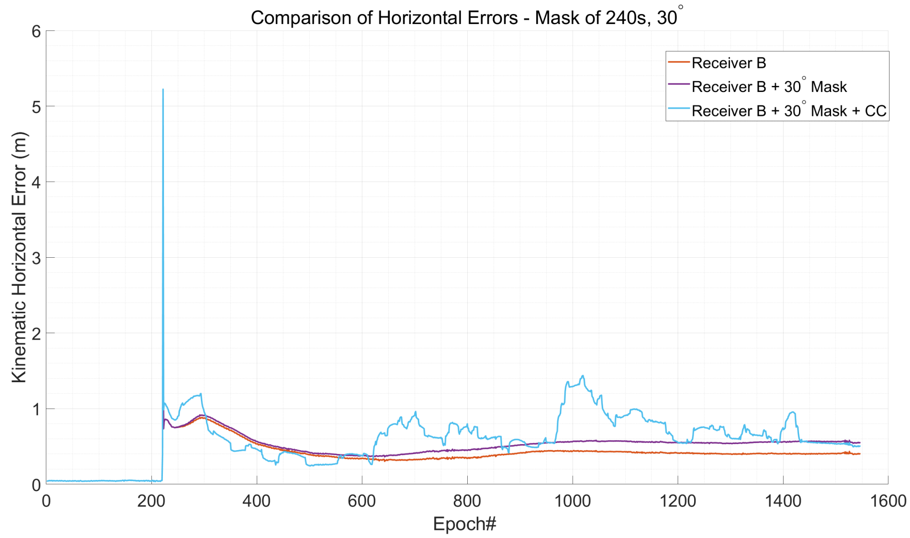

Figure 5.25: Horizontal errors with a long, 30° mask, Receiver B

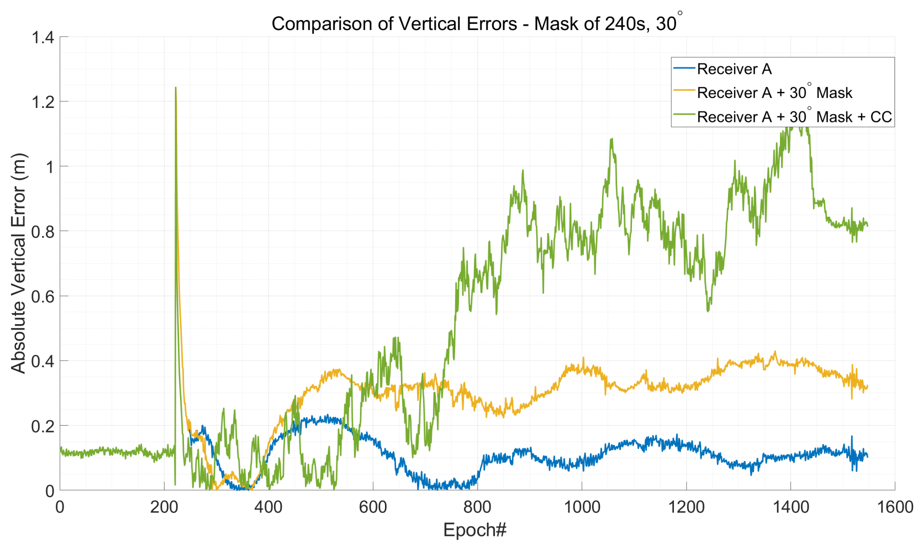

Figure 5.26: Absolute vertical errors with a long, 30° mask, Receiver A

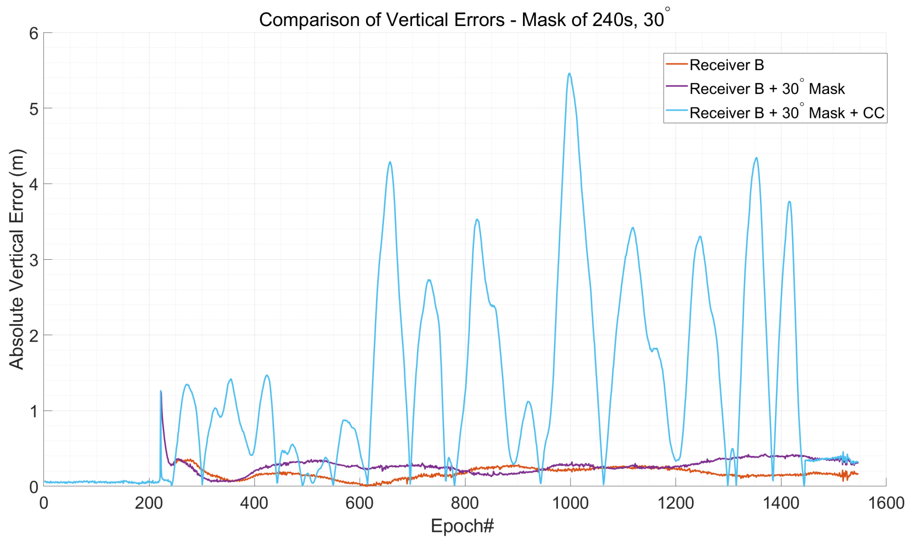

Figure 5.27: Absolute vertical errors with a long, 30° mask, Receiver B

The extended masked periods produced similar result to the shorter one, where the horizontal errors were very similar with or without clock coasting when CSAC was used. Following a similar procedure as the 30-second mask, the 240-second mask was made larger to cover satellites below 55°. A table of error statistics is presented in 5.8. Horizontal errors are plotted in Figure 5.28 and Figure 5.29. Vertical errors are plotted in Figure 5.30 and Figure 5.31. Both receivers showed spikes of errors due to poor geometry as the number of processable satellites dwindled around 5. Clock coasting appeared to be able reduce the effect and therefore producing a more stable solution. With the CSAC, the solution was able to maintain horizontal errors below sub-metre level with clock coasting. Most notably, the spikes of errors due to losing track of the fifth or fourth satellite were eliminated, greatly improving the stability of the solution. However, the effect of clock drifting became more apparent later in the dataset, as an upwards trend could be observed for errors both vertically and horizontally.

Receiver/Errors in cm	rmse (horizontal)	$\sigma_{horizontal}$	rmse (vertical)	$\sigma_{vertical}$
Receiver A	61	35	153	138
Receiver A + CC	58	30	51	38
Receiver B	87	53	279	259
Receiver B + CC	98	56	161	98

Table 5.8: Error statistics for Receiver A and B in the 240 s, 55° mask, epoch 8000-9200

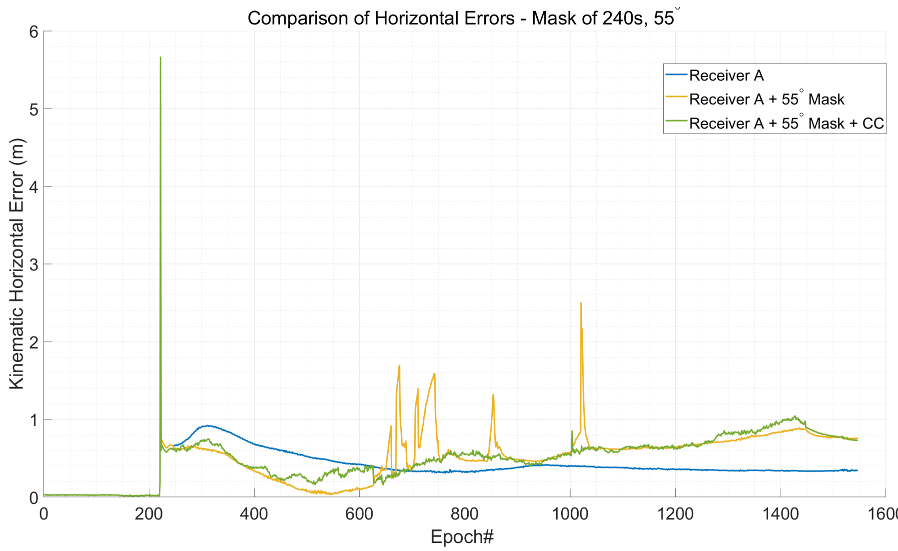

Figure 5.28: Horizontal errors with a long, 55° mask, Receiver A

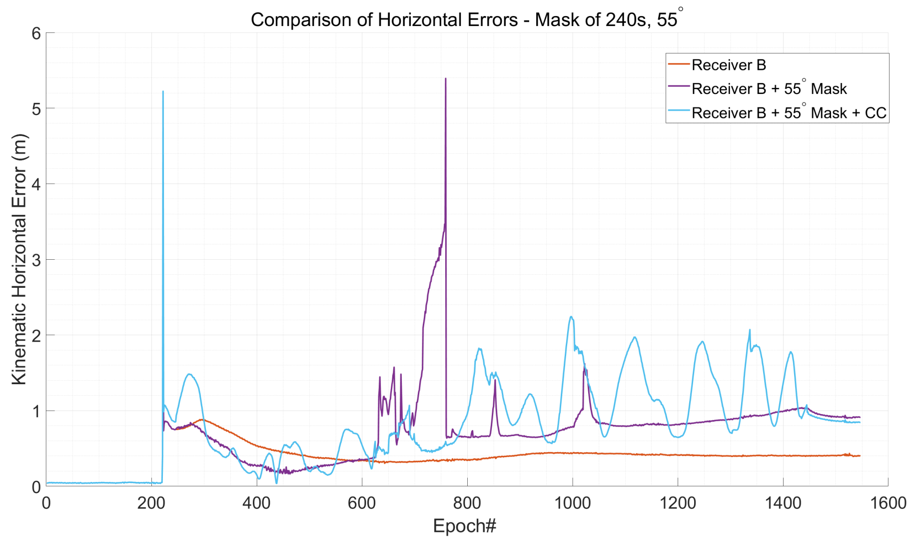

Figure 5.29: Horizontal errors with a long, 55° mask, Receiver B

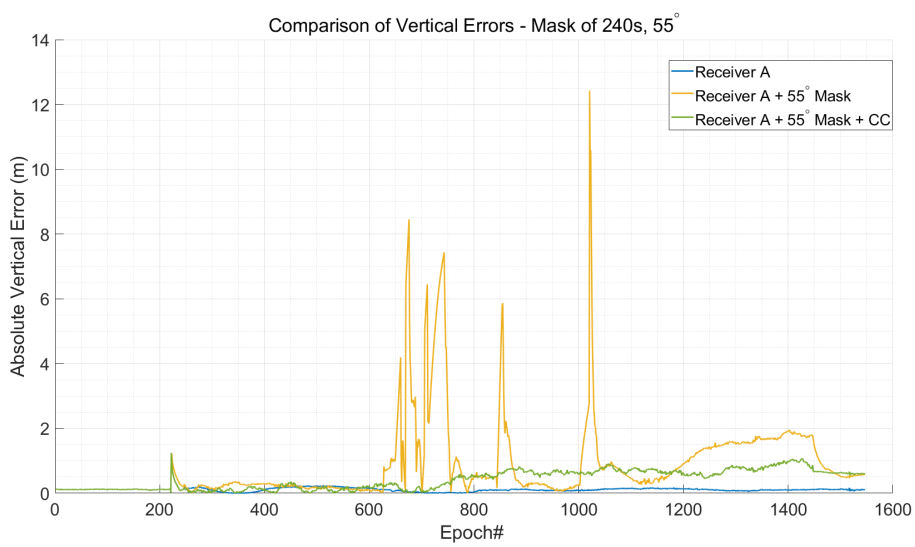

Figure 5.30: Absolute vertical errors with a long, 55° mask, Receiver A

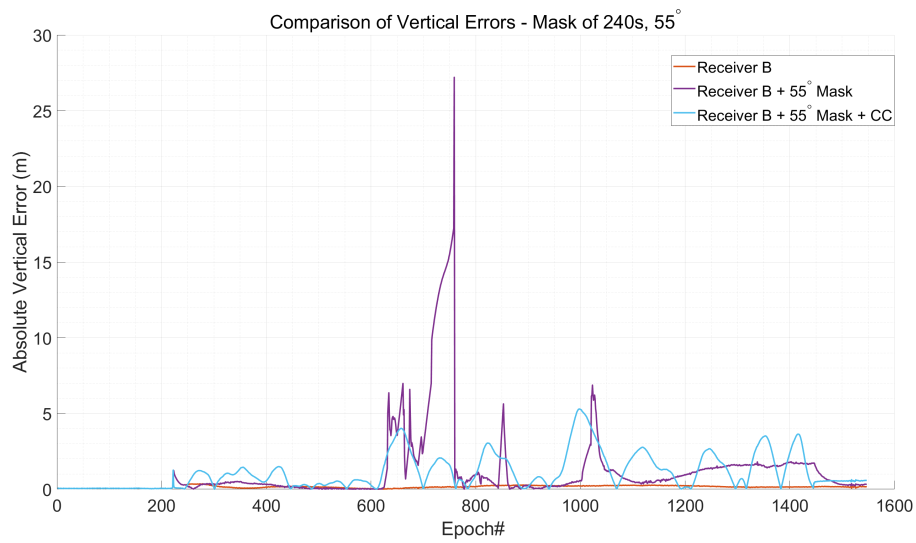

Figure 5.31: Absolute vertical errors with a long, 55° mask, Receiver B

5.4.3 3-Satellite Scenario

A more extreme case is where exactly three satellites are available. Traditional single point positioning processing algorithms requires observations from four satellites to solve the four unknowns but there are always occasions where the fourth satellite may lose track. In this scenario, the previous 240-second mask was altered so that two satellites that were not constantly tracked got removed (E10 and E11), leaving only three constantly tracked satellites (G8, G16 and G23). Horizontal and vertical errors are shown in Figure 5.32 and Figure 5.33. Statistics are shown in Table 5.9. The figures show that errors in both receivers reached tens of metres without clock coasting but stayed within a metre for Receiver A. Statistics for three-satellite solutions without clock coasting are not shown as they are not meaningful for comparison due to errors above tens of metres. Both receivers showed no degradation in horizontal errors compared to the previous scenario. Some statistics are in fact showing a bit of improvement primarily due to the same three satellites were being tracked, without sudden addition or loss of other satellites whose measurement may suffer more from multipath or attenuation. The upwards trend of errors for Receiver A was still visible and could be addressed in future work using some simple models to predict the drifting behaviour.

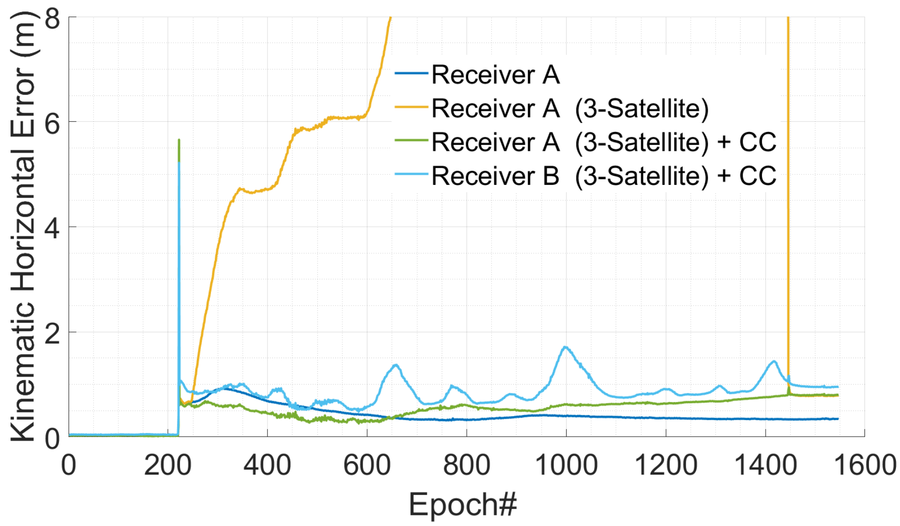

Figure 5.32: Horizontal errors with three satellites

Receiver/Errors in cm	rmse (horizontal)	$\sigma_{horizontal}$	rmse(vertical)	$\sigma_{vertical}$
Receiver A (no mask)	53	24	30	13
Receiver A (3-sat) + CC	56	27	54	38
Receiver B (no mask)	45	22	19	18
Receiver B (3-sat) + CC	85	38	156	156

Table 5.9: Error statistics for Receiver A and B in the 3-satellite scenario, epoch 8000-9200

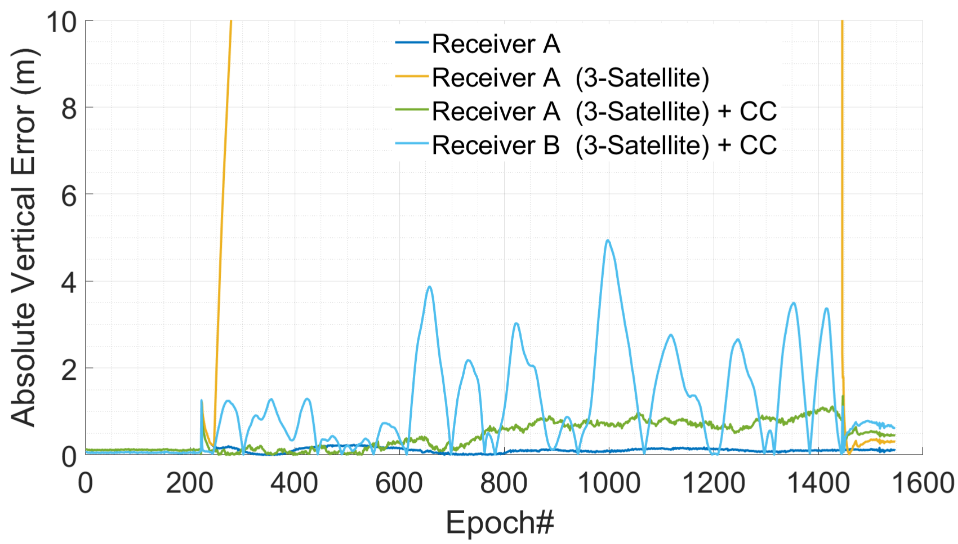

Figure 5.33: Vertical errors with three satellites

5.4.4 Cliff Simulation

In this simulation, a mask was implemented in the dataset to block most of satellites on one side of the user, while a 30-degree elevation mask was implemented all around the user. The scenario was used to simulate a pedestrian or car next to high-rises in urban area, and is referred to as 'cliff' in the study. The all-around urban mask lasted 100 s, and the 70° cliff mask covered 60 s right within. The cliff mask affected satellites between 90° to 270° of azimuth angle, and will therefore greatly affect northing errors more.

The effect on geometry and number of satellite processed is shown in Figure 5.34. The mask leaved 5 satellites for the PPP processor, as shown in earlier scenarios, the induced horizontal errors are expected to be less than a few decimetres.

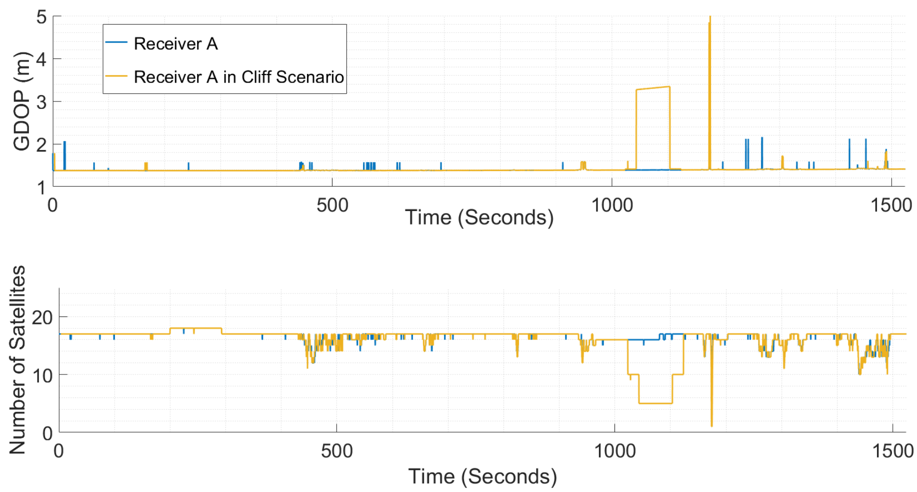

Figure 5.34: Plot of geometric dilution of precision (above) and number of satellites processed through the engine (below) in cliff simulation

However, the effect of the cliff-like mask severely impacted the positioning performance in the north direction, as shown in Figure 5.35 and Figure 5.36. For both receivers, the errors in the north direction were brought to near-metre level later in the simulation. In the east direction, the errors were within centimetre level. Notice the quality of performance in this part of the dataset was much superior to other datasets shown in the study, as the section for the cliff simulation was set on a long and undisturbed intersection with little obstructions. Clock coasting began when one side of the satellites are blocked, and was able to bring down errors in the north direction back to less than a metre for Receiver A. For Receiver B, the clock coasting introduced errors too high that overshadowed the impact from simulated scenario.

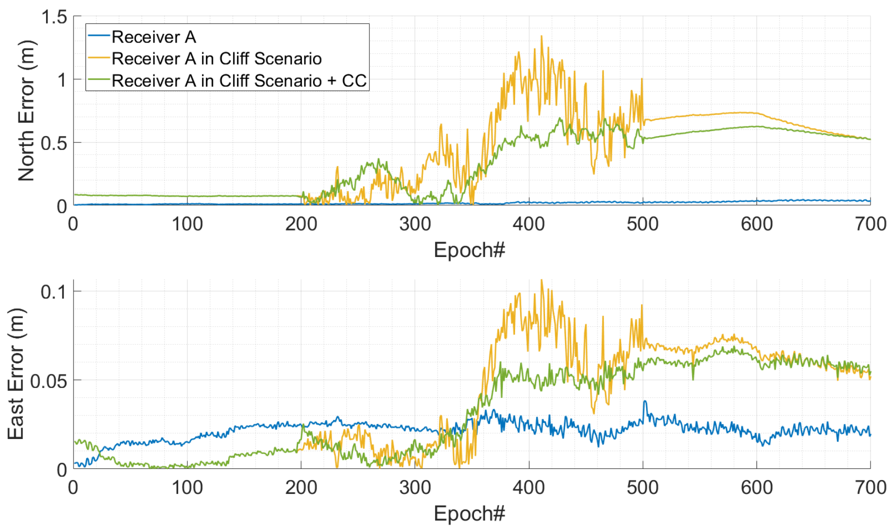

Figure 5.35: North and east errors in cliff scenario, Receiver A

Receiver/Errors in cm	rmse (horizontal)	$\sigma_{horizontal}$	rmse (vertical)	$\sigma_{vertical}$
Receiver A	52	33	39	24
Receiver A + CC	41	24	36	20
Receiver B	53	35	31	23
Receiver B + CC	139	101	76	57

Table 5.10: Error statistics for Receiver A and B in the one-sided 60 s, 70° mask, epoch 5325-5625

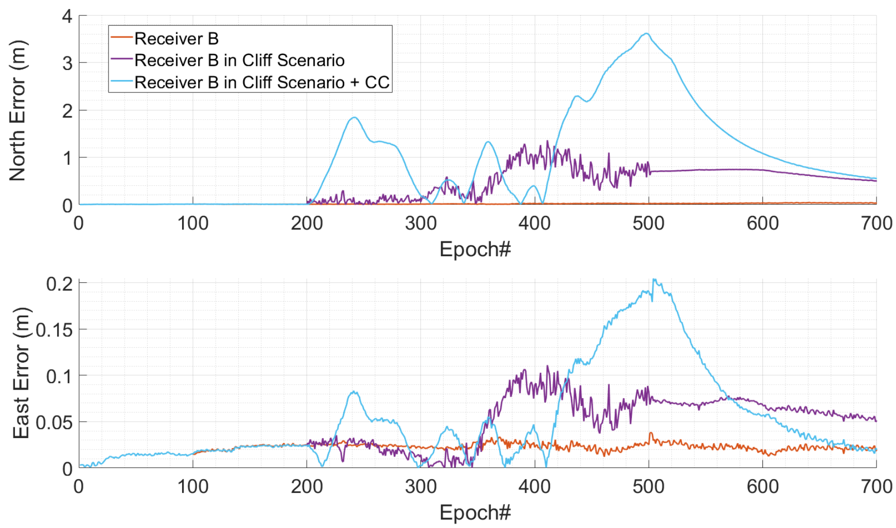

Figure 5.36: North and east errors in cliff scenario, Receiver B

More detailed statistics is shown in Table 5.10. Plots for horizontal and vertical errors are shown in Figure 5.37 and Figure 5.39 for receiver A, and Figure 5.38 and Figure 5.40 for receiver B. The statistics show an improvement of positioning performance in the cliff scenario when a CSAC was used, but a degradation when the internal TCXO was used instead.

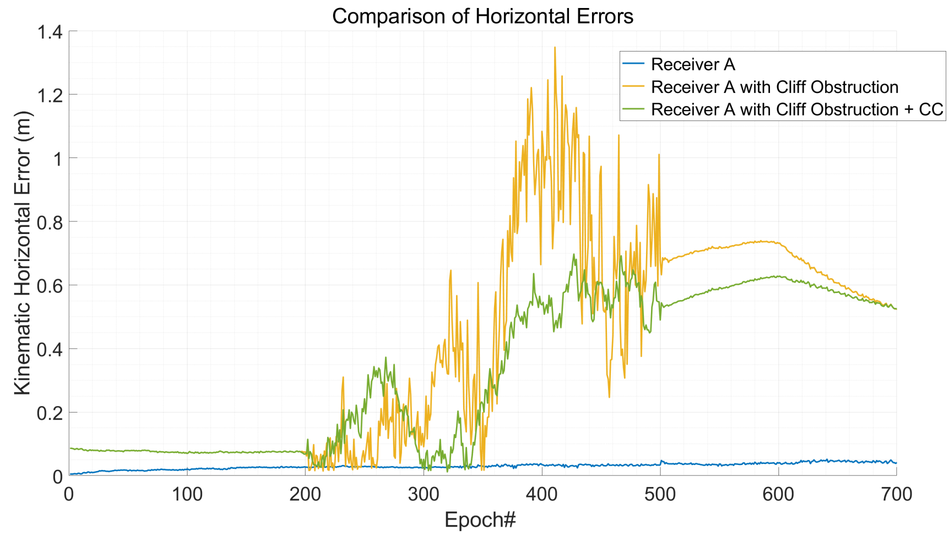

Figure 5.37: Horizontal errors in cliff simulation, Receiver A

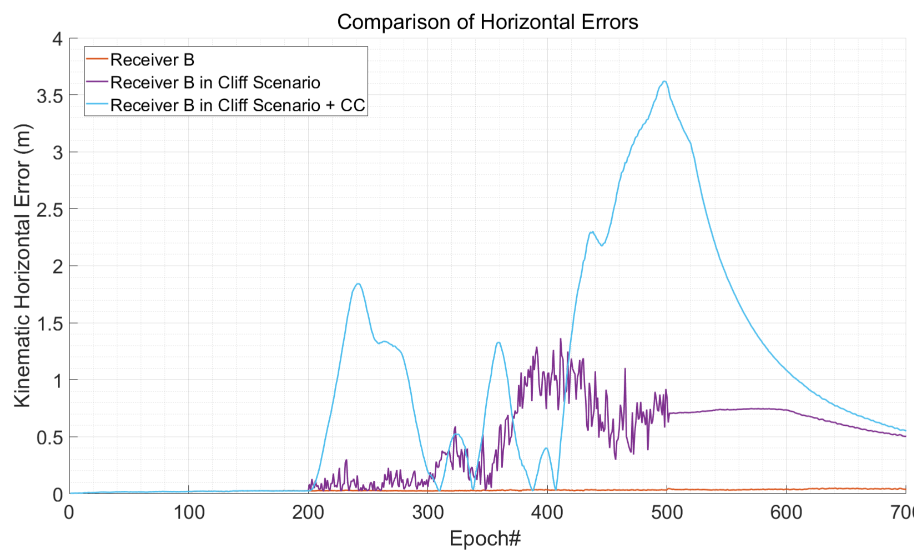

Figure 5.38: Horizontal errors in cliff simulation, Receiver B

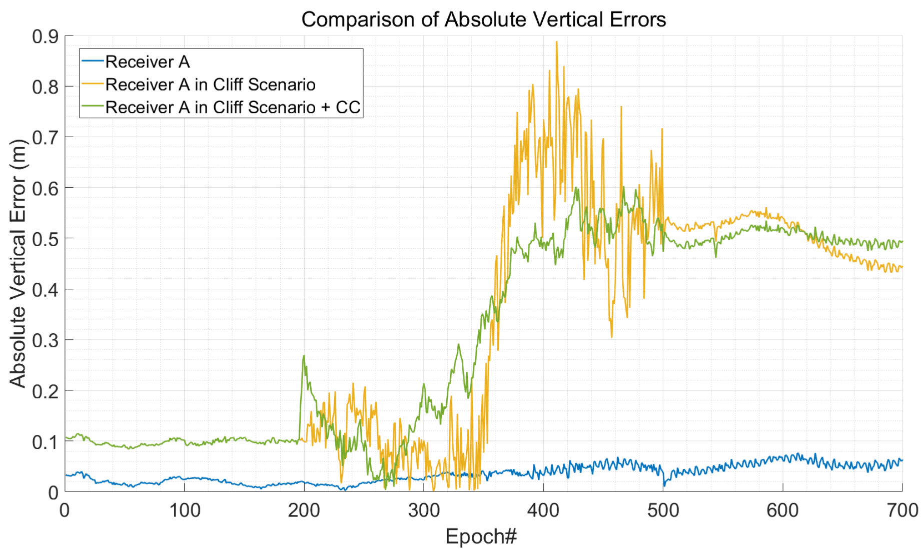

Figure 5.39: Absolute vertical errors in cliff simulation, Receiver A

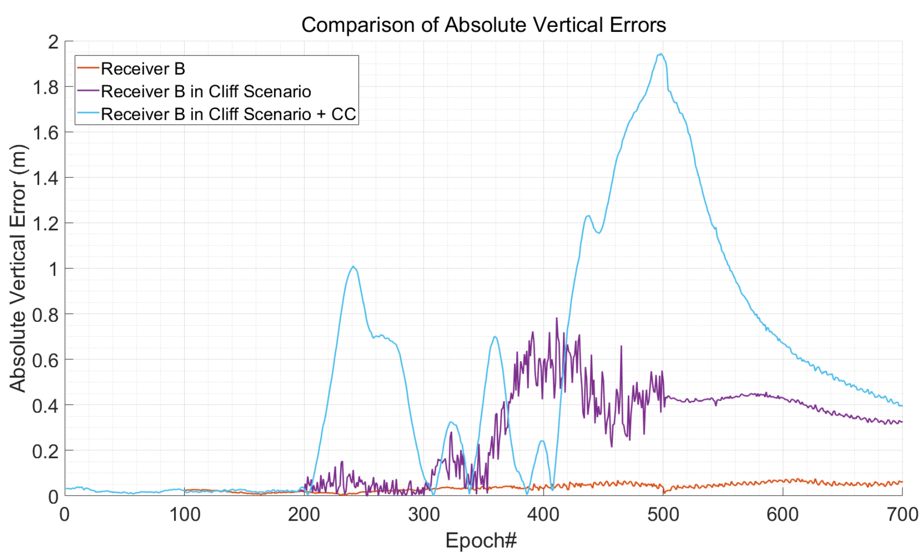

Figure 5.40: Absolute vertical errors in cliff simulation, Receiver B

The cliff scenario simulated a realistically challenging situation for all GNSS processing. It is expected that an improved 'geometry' with an addition sensor based on previous research. The result indeed showed an improved positioning performance in such scenario with a precise clock, and reduces horizontal errors by about one decimetre. Using a TCXO does not bring benefit in this situation. However, the improvement from the CSAC is also limited as a clear bias is observed in the north direction due to geometry.

5.4.5 Discussion

GNSS data was collected in the real world by driving in a suburban area for 30 minutes. Simulation of urban environments was accomplished using a set of elevation masks with various sizes and duration. For Receiver A with CSAC, the smaller 30° masks lead to slight degradation of positioning performance. Clock coasting was not able to make improvement in such scenario, as the geometry was not severely impacted. However, errors were only introduced in the vertical direction, signalling that the negative effect on positioning accuracy due to clock coasting can be constrained in the vertical direction. In the simulations involving a larger mask of 55°, the geometry became degraded and satellite counts dropped to around 5. Clock coasting showed general improvements in the situation, and in particular, prevented spikes of errors due to loss-of-track. Three-satellite scenarios over four minutes were tested and resulted in accuracy lost in the centimetre-level in the horizontal direction, and decimetre-level in the vertical direction. The result shows a clear improvement over previous work on CSAC-aided GNSS receivers, whereas 3-satellites scenarios often gave errors at metre-level, even if clock modelling or other integration methods were employed. A 'cliff' scenario where a 70° one-sided mask was implemented was also tested. The scenario represents a practical situation where the user is located next to a tall building in an urban area. Clock coasting successfully mitigated geometrical effect on the solution by reducing errors in the cross-street direction by several decimetres. On the other hand, Receiver B, using its native TCXO clock as a mean for clock coasting demonstrated greater errors at some metre-level in both horizontal and vertical direction whenever clock coasting was turned on. The result shows it is not realistic for the clock coasting algorithm to work using a clock at such level of stability. However, during the three-satellite scenario where traditional PPP failed to produce a meaningful solution, the TCXO clock managed to provide a PPP solution of a few metres of errors nonetheless.

5.5 Limits and Caveats

Using the selected dataset, a number of experiments were performed by simulating obstructed scenarios using actual measurements. The result showed an improvement of navigation solution with CSAC in most cases, and more obviously when the number of satellites dropped lower. However, the experiments also presented a number of limits and caveats in the approach.

Firstly, the quality of the measurements reduced the quality of clock coasting. Clock coasting relies on an assumption that the receiver clock bias estimation prior to coasting is accurate. When the solution itself degraded, so did the estimation. Receiver clock modelling should be able to address the problem more elegantly. However, clock coasting can also be further optimized to address the situation by incorporating a more sophisticated extrapolation using clock bias estimation and some clock modelling without requiring expensive spectrum anaylser hardware.

Secondly, in most cases a worse performance in the vertical direction was observed for both receivers. This is expected as the receiver clock error dictates more on the quality of vertical positioning, and clock coasting brings error to receiver clock. This limit of clock coasting restricts the solution's usage when vertical positioning is essential, such as for UAV applications, and additional sensors should be used in such applications.

Thirdly, clock coasting only secured solution availability with 3 satellites. As we have seen in the natural underpass where the number of satellites is reduced below 3, the PPP engine fails as it would traditionally with 3 satellites. In this case, clock coasting was not able to show any benefit compared to other alternatives such as integrated inertial navigation.

Chapter 6

Conclusions and Recommendations for Future Research

GNSS technology has become ubiquitous in daily life, and more recent day-to-day applications such as delivery tracking, bike/car sharing, and contact tracing, as well as emerging applications such as autonomous driving and augmented realities are being developed. Many, if not most of these applications will take place in urban and obstructed environments, where GNSS is not initially designed for, and yet provides the most cost-effective PNT solution. The demand leaves research communities in search of improving robust GNSS solutions in obstructed environments, making the solution more resilient to obstructions, and preferably, continue to be low-cost and available for mass-market.

This study proposed a solution to improve kinematic positioning in such difficult environments in general, and maintained the sub-metre level of accuracy of PPP, even if the user was in an obstructed environments with a potentially low-cost and methodologically simplistic approach. Compared to existing studies in incorporating CSACs and GNSS receivers, this work leaned more on the practical side of the technology and aims to provide a viable and composite approach to bring GNSS PNT solutions to the next level of resilience. The combination GNSS technology, the PPP technique, and a precise external clock provided greater PNT availability, and stronger resilience.

6.1 Conclusions

The research began as an investigation of the use of CSAC in GNSS processing to improve the solution in PPP processing. A two-way augmentation where the CSAC serves as a timing sensor to the GNSS receiver and disciplined by the receiver in the long term is proposed. The study laid the base as a practical system for the research ahead. It was found that the use of PPP does not directly benefit from the external CSAC, as in many cases the solution, either static or kinematic can already be within decimetre or centimetre level. However, the most essential element was the accompanying upgrades in the processing algorithm, leading to greater accuracy in many scenarios, greater availability of solution as 3-satellite solutions are now within sub-metre-level. The CSAC-aided GNSS receiver shows a promising performance when geometry is poor and number of satellites low as PPP is achieved with 3 satellites. The findings expand PPP's usage in emerging urban applications, and improve the accuracy and availability of the PNT solution. To answer the research questions propose early in the thesis:

- How good was the static GNSS-PPP solution with CSAC (with no obstructions)? The experimented recorded no obvious improvement/degradation in static performance. The result differed from other works using single point positioning. Therefore, it is most likely that the PPP processing eliminated enough errors that the clock did not provide an advantage.

- How good was the solution in an 'open-sky' environment with CSAC? Experiments were conducted in suburban scenarios by driving around campus. Similar to the static scenario, the results were largely similar to the solution without CSAC. However, in one dataset where the car was taken to a residential area with substantial foliage coverage, a greater positioning accuracy was observed in Receiver A. The finding requires more validation and may open opportunities for future work.

- How much error was introduced when clock coasting is applied? Several interfacing modes were tested. Using the selected mode, the clock coasting algorithm produced an rms error of 3 cm horizontally and 24 cm vertically with CSAC over 240 seconds (based on the 3-satellite scenario). A linear drift pattern was observed in estimated clock errors over hours. However, the pattern seems to fit a linear model and can be roughly modelled simply.

- How effective was clock coasting in obstructed environments? Datasets collected in real-world is used to simulate short and long urban obstructions, cliffs, or underpasses. The scenarios were designed based on real-world applications and in each scenario the system was tested. In urban obstructions of various duration as well as in the cliff scenario, we observed an improvement of accuracy with the CSAC-aided GNSS receiver. In the cliff scenario, solution downgrades in the north direction as a bias is produced from poor geometry. The study showed an improved solution to mitigate the effect so that the solution becomes more accurate and more trustworthy. Navigation solution without clock coasting experience gaps in availability if number of satellites drops to three or less. With clock coasting algorithm the availability of solution was improved as 3-satellite solutions were available. In urban applications, this translates into improvement of continuity as well. Using a CSAC, the clock coasting approach keeps the solution accuracy at sub-metre level in 3-satellite periods as well.

- What were the limits of the current CSAC-aided GNSS receiver prototype? This is addressed in the end of chapter 5. The selection of clock bias candidates requires accurate clock bias estimations prior to clock coasting. Vertical accuracy is usually poorer. The availability of solution only expands to 3-satellite scenarios and does not help 2-satellite situations or less.

6.2 Recommendations for Future Research

The research also presented limits and caveats of the current prototype of the CSAC-aided GNSS receiver. In light of these problems, future research topics can be proposed.

- The study highlighted the practicality and potentially low-cost approach of the CSAC-aided receiver by using PPP where additional infrastructures are not needed, and clock coasting where individual characterisation of clock is skipped. However, a CSAC is worth a few thousands dollars and the research employed geodetic level receiver hardware. CSACs are expected to become cheaper as the technology evolves, but it is unrealistic to assume it will soon become a mass-market option. This solution benefits from CSAC's timing stability over short terms of at most a few hundreds of seconds for clock coasting. However the CSACs can be replaced by new OCXOs as cheaper alternatives, that may provide better stability in 100 s intervals. OCXOs tend to be more power-consuming and larger in size. The drawback may not be a problem as we are not looking for hand-held sized navigation system, but one that is expected to be used in vehicles. The use of geodetic hardware in this research is a result of the highly customisable features of the receivers. As validation tests using low-cost receivers have shown, the interfacing options are usually more limited for them and the full potential of the approach cannot be revealed.

- The analysis of CSAC timing errors over time showed clear linear trend. This finding explained the increasing positioning errors, especially in the vertical direction when clock coasting was used for a longer period. While this study refrained from the RCM approach due to its requirement for spectrum analysis of the clock's behaviour, it should not be too difficult to find a simpler modelling method for the existing SLS algorithm in PPP to compensate for the drift. Also, as mentioned, the quality of clock coasting approach also depends on the accuracy of clock bias estimation prior to clock coasting. A more accurate extrapolation of clock error could be devised in challenging environments where previous estimates were less accurate.

- The CSAC-aided GNSS receiver with PPP shows an improvement in the PNT performance criteria of accuracy, continuity and availability in tested obstructed scenarios. However, only simulations are used. Future work should include real-world testing of the system in the scenarios where a trustworthy reference solution can be produced, such as one from a high-quality GNSS + () solution.

- The CSAC-aided GNSS receiver improved availability of solution by offering 3-satellite GNSS solution. And yet what is its advantage over many of the available GNSS + IMU solutions, which can be more low-cost? While spared from some of the IMU's problem such as accumulative errors, the system also suffers from inability to provide a solution with 2 or less satellites. In light of this, it is more meaningful to consider the use of a precise clock in filling the gap between having few satellites and no satellites in a system that also incorporates some forms of inertial navigation. The future of the approach most likely relies on a mass-market combination of a low-cost receiver, a low-cost precise clock such as newer OCXOs, and an IMU. With clock coasting, PPP and integration with IMU, the most use of the potential from the three low-cost components for a resilient PNT solution may be possible for emerging PNT applications in obstructed environments.

References

Aggrey, John Egyir (2014). “Multi-GNSS Precise Point Positioning Software Architecture And Analysis Of GLONASS Pseudorange Biases”. PhD thesis. York University.

Aggrey, John Egyir et al. (Sept. 2019). “Accuracy Trend Analysis of Low-cost GNSS Chips: The Case of Multi-constellation GNSS PPP”. In: *Proceedings of the 32nd International Technical Meeting of the Satellite Division of The Institute of Navigation (ION GNSS+ 2019)*, pp. 3618–3635.

Banville, Simon et al. (2014). “Global and Regional Ionospheric Corrections for Faster PPP Convergence”. In: *NAVIGATION* 61.2, pp. 115–124.

Barnes, J. A. and D. W. Allan (1966). “A Statistical Model of Flicker Noise”. In: *Proceedings of the IEEE* 54.2, pp. 176–178.

Barnes, J. A. et al. (1971). “Characterization of Frequency Stability”. In: *IEEE Transactions on Instrumentation and Measurement* IM-20.2, pp. 105–120.

Beard, R. and K. Senior (2017). “Clocks”. In: *Springer Handbook of Global Navigation Satellite Systems*. Ed. by Peter J.G. Teunissen and Oliver Montenbruck. Cham: Springer International Publishing, pp. 121–164.

Bisnath, S. and Y. Gao (2009). “Current State of Precise Point Positioning and Future Prospects and Limitations”. In: *Observing our Changing Earth*. Ed. by Michael G. Sideris. Berlin, Heidelberg: Springer Berlin Heidelberg, pp. 615–623.

Bullock, J.B. and M. King (2017). “Integration of GNSS with Other Sensors and Network Assistance”. In: *Understanding GPS/GNSS: Principles and Applications, Third Edition*. Ed. by Elliott Kaplan and Christopher J. Hegarty. 3rd. USA: Artech House, Inc. Chap. 13.

Calero, D. and E. Fernandez (2015). “Characterization of Chip-Scale Atomic Clock for GNSS navigation solutions”. In: *2015 International Association of Institutes of Navigation World Congress (IAIN)*, pp. 1–8.

Choy, S (2009). “Investigation Into the Accuracy of Single Frequency Precise Point Positioning (PPP)”. PhD thesis. RMIT University.

Davis, J. L. et al. (Nov. 1985). “Geodesy by Radio Interferometry: Effects of Atmospheric Modeling Errors on Estimates of Baseline Length”. In: *Radio Science* 20.6, pp. 1593–1607.

Fei, Lu et al. (Mar. 2010). “Effect of Vehicle Speed on Shock and Vibration Levels in Truck Transport”. In: *Packaging Technology and Science* 23, pp. 101–109.

Fernandez, E., D. Calero, and M. Eulia Pares (Feb. 2016). “CSAC Temperature Calibration for Improving GNSS Positioning Performance”. In: *Proceedings of the 47th Annual Precise Time and Time Interval Systems and Applications Meeting*. Monterey, California, pp. 36–44.

— (Feb. 2017). “CSAC Characterization and Its Impact on GNSS Clock Augmentation Performance”. In: *Sensors* 17, p. 370.

Griffiths, D. J. and D. F. Schroeter (2018). “Symmetries Conservation Laws”. In: *Introduction to Quantum Mechanics*. 3rd ed. Cambridge University Press, pp. 232–276.

Groves, Paul et al. (Sept. 2013). “A Portfolio Approach to NLOS and Multipath Mitigation in Dense Urban Areas”. In: *26th International Technical Meeting of the Satellite Division of the Institute of Navigation, ION GNSS 2013*. Vol. 4.

Hegarty, Chris et al. (2017). “Performance of Stand-Alone GNSS”. In: *Understanding GPS/GNSS: Principles and Applications, Third Edition*. Ed. by Elliott Kaplan and Christopher J. Hegarty. 3rd. USA: Artech House, Inc. Chap. 11.

Hobiger, T. and N. Jakowski (2017). “Atmospheric Signal Propagation”. In: *Springer Handbook of Global Navigation Satellite Systems*. Ed. by Peter J.G. Teunissen and Oliver Montenbruck. Cham: Springer International Publishing, pp. 165–193.

Knable, N. and R. M. Kalafus (1984). “Clock Coasting and Altimeter Error Analysis for GPS”. In: *NAVIGATION* 31.4, pp. 289–302.

Kouba, Jan (2009). *A guide to using International GNSS Service (IGS) products*.

Kouba, Jan and Pierre Héroux (Oct. 2001). “Precise Point Positioning Using IGS Orbit and Clock Products”. In: *GPS Solutions* 5, pp. 12–28.

Krawinkel, Thomas (2018). “Improved GNSS Navigation with Chip-scale Atomic Clock”. PhD thesis. Gottfried Wilhelm Leibniz Universität Hannover.

Langley, R., P. Teunissen, and O. Montenbruck (Jan. 2017). *Introduction to GNSS*.

Lutwak, Robert et al. (Dec. 2002). “The Chip-Scale Atomic Clock – Coherent Population Trapping vs. Conventional Interrogation”. In: *Proceedings of the 34th Annual Precise Time and Time Interval Systems and Applications Meeting*. Reston, Virginia, USA.

— (Dec. 2004). “The Chip-Scale Atomic Clock – Low-Power Physics Package”. In: *Proceedings of the 36th Annual Precise Time and Time Interval Systems and Applications Meeting*. Washington, D.C, USA.

Ma, Lin et al. (Sept. 2015). “Deep coupled integration of CSAC and GNSS for robust PNT”. In: *Sensors* 15, pp. 23050–70.

Mader, Gerald (July 1999). “GPS Antenna Calibration at the National Geodetic Survey”. In: *GPS Solutions* 3, pp. 50–58.

Microsemi (2014). *White Paper - Shock and Vibration Testing of the SA.45s Chip Scale Atomic Clock (CSAC) Validation Units*.

— (2016). *White Paper - Leading-Edge Technology Enables a Chip Scale Atomic Clock*.

— (2017a). *User Guide - SA.45s Chip-Scale Atomic Clock*.

— (2017b). *White Paper - Thermally-Improved Microsemi Chip Scale Atomic Clock (CSAC)*.

— (2018). “White Paper - Chip-Scale Atomic Clock (CSAC) Performance During Rapid Temperature Change”. In:

Montenbruck, O., A. Hauschild, and P. Steigenberger (2014). “Differential Code Bias Estimation using Multi-GNSS Observations and Global Ionosphere Maps”. In: *NAVIGATION* 61.3, pp. 191–201.

Musso, Maristella et al. (Sept. 2005). “GNSS Multifrequency Receivers in Urban Environment: Theoretical Analysis”. In: *Proceedings of the 18th International Technical Meeting of the Satellite Division of The Institute of Navigation (ION GNSS 2005)*. Long Beach, CA, pp. 2661–2669.

NovAtel (2019). *User Guide - OEM7 GNSS Receivers*.

Preston, S.E. and D.M. Bevly (Jan. 2014). “CSAC-Aided GPS Multipath Mitigation”. In: 2014, pp. 228–234.

Ramlall, R, J Streeter, and J.F. Schnecker (Sept. 2011). “Three Satellite Navigation in an Urban Canyon Using a Chip-scale Atomic Clock”. In: *Proceedings of the 24th International Technical Meeting of the Satellite Division of The Institute of Navigation (ION GNSS 2011)*. Vol. 4, pp. 2937–2945.

Schaer, S. and W. Gurtner (Feb. 1998). *IONEX: The IONosphere Map EXchange Format Version 1.1*. Darmstadt, German.

Sturza, Mark A. (1983). “GPS Navigation Using Three Satellites and a Precise Clock”. In: *Navigation* 30.2, pp. 146–156.

Teunissen, Peter J.G. (2017). “Carrier Phase Integer Ambiguity Resolution”. In: *Springer Handbook of Global Navigation Satellite Systems*. Ed. by Peter J.G. Teunissen and Oliver Montenbruck. Cham: Springer International Publishing, pp. 661–685.

Wang, Lei, Paul D Groves, and Marek K Ziebart (2012). “Multi-Constellation GNSS Performance Evaluation for Urban Canyons Using Large Virtual Reality City Models”. In: *Journal of Navigation* 65.3, pp. 459–476.

Ward, P. W., J. W. Betz, and C. Hegarty (2017). “GNSS Disruptions”. In: *Understanding GPS/GNSS: Principles and Applications, Third Edition*. Ed. by Elliott Kaplan and Christopher J. Hegarty. 3rd. USA: Artech House, Inc. Chap. 9.

Weinbach, U. and S. Schön (Jan. 2011). “GNSS Receiver Clock Modeling When Using High-precision Oscillators and Its Impact on PPP”. In: *Advances in Space Research* 47.2, pp. 229–238.

Wells, Dave et al. (Apr. 1986). *Guide to GPS Positioning*.

Yang, S. and S. Bisnath (Jan. 2020). “GNSS PPP Navigation in Obstructed Environments Using Clock Coasting”. In: *Proceedings of the 2020 International Technical Meeting of The Institute of Navigation*. San Diego, California, pp. 521–537.

Zhu, N. et al. (2018). “GNSS Position Integrity in Urban Environments: A Review of Literature”. In: *IEEE Transactions on Intelligent Transportation Systems* 19.9, pp. 2762–2778.